Lehrstuhl für Leichtbau

# Thermomechanics of Fibre Reinforced Epoxies for Cryogenic Pressurized Containment

**Leonardo Raffaelli**

Vollständiger Abdruck der von der Fakultät für Maschinenwesen der Technischen Universität München zur Erlangung des akademischen Grades eines

**Doktor-Ingenieurs (Dr.-Ing.)**

genehmigten Dissertation.

Vorsitzender: Univ.- Prof. Dr. mont. habil. Ewald Werner

Prüfer der Dissertation:

1. Univ.- Prof. Dr.-Ing. Horst Baier

2. Hon.-Prof. Dr.-Ing., Dr. Eng.(Japan) Hans-Harald Bolt

Die Dissertation wurde am 12.01.2006 bei der Technischen Universität München eingereicht und durch die Fakultät für Maschinenwesen am 23.05.2006 angenommen.

# Contents

# List of Figures

# List of Tables

## List of abbreviations

| | | | |
|---|---|---|---|
| A | Area | $LH_2$ | Liquid Hydrogen |
| CFRPs | Carbon Fibre Reinforced Plastics | $LH_e$ | Liquid Helium |
| | | $LN_2$ | Liquid Nitrogen |
| CT | Cryogenic Temperature | LR | Leak Rate |
| CTE | Thermal Expansion Coefficient | MLI | MultiLayer Insulation |
| DLS | Double Lap Shear | MPa | Megapascal |
| E | Stiffness Modulus | OL | Overlapping Length |
| $E_P$ | Activation Energy | P | Pressure or Permeability |
| FF | Fibre Failure | PAN | Polyacrylonitrile |
| FRPs | Fibre reinforced Plastics | R | Universal gas constant |
| FPF | First Ply Failure | RLV | Reusable Launch Vehicle |
| G | Shear Molulus or Fracture Toughness | RT | Room Temperature |
| | | SLS | Single Lap Shear |
| GFRPs | Glass Fibre Reinforced Plastics | T | Temperature [Kelvin] |
| | | U | Strain Energy |
| HM | High Modulus | UD | unidirectional |
| I | Strain tensor invariant | ULR | Unitary Leak Rate |
| IF | Inter Fibre | V | Volume |
| IFF | Inter Fibre Failure | W | Work |
| IM | Intermediate Modulus | $\alpha$ | Coefficient of thermal expansion |
| J | Stress tensor invariant | $\Delta$ | Variation or difference |
| K | Constant value | $\epsilon$ | Strain tensor component |
| L | Length | $\sigma$ | Stress tensor component |
| LAr | Liquid Argon | $\tau$ | Shear component of the strain tensor |
| $LCH_4$ | Liquid Methane | | |

## List of used indexes

| | |
|---|---|
| ADM | Admissible |
| C | Compressive |
| eff | Effective |
| f | Fibre |
| i | Integer Number (1, 2 or 3) |
| M | Matrix |
| m | Integer number or average |
| n | Integer number |
| PAR | Parallel |
| PER | Perpendicular |
| S | Symmetric or Strength |
| T | Tensile |
| U | Ultimate |
| I, II, and III | Crack opening mode |
| 0 | General or Laminate referred |

## Coordinate systems

$$\left.\begin{matrix} X \\ Y \\ Z \end{matrix}\right\} = \text{Laminate CS} \qquad \left.\begin{matrix} 1 \\ 2 \\ 3 \end{matrix}\right\} \text{ or } \left.\begin{matrix} \parallel \\ \perp \\ \# \end{matrix}\right\} = \text{Ply CS}$$

# 1 Introduction and overview

Fibre reinforced plastics have found their first applications in aerospace structures at the beginning of the '60s. First applications in military and commercial aircraft concerned secondary structures, i.e. control surfaces, where one of the first examples is given by boron- epoxy rudder in the F-4 Phantom. If at the beginning glass fibres (and boron fibres for high strength applications) have been adopted, carbon fibre composites have progressively replaced them because of better strength and stiffness which new developed CFRPs achieved and significant cost reduction in comparison to boron. Since these first applications, and contemporary to the development of fibres and matrix systems, the need for enhancing aircraft performances has promoted an increasing use of these materials for aerospace structures. The importance of composites has grown early in the military field and these materials have been applied to primary parts, like for the wing box of the BAe Harrier, already at the end of the seventies, to culminate with extensive use of non metallic materials in new generation fighters. Civil aviation has resorted to extensive application of FRPs only in the eighties and nineties when confidence with these materials had grown enough after many years of application in military structures. The application of CFRP to commercial aeroplanes has been particularly pursued within the Airbus family in Europe, as early as the first A-300 model came into service and progressively extended into all new types. At the same time an extensive measurement campaign has been carried out in the eighties to understand the behaviour of non metallic materials and particularly CFRPs at cryogenic temperatures with the aim to exploit their favourable strength to weight ratio for structures which shall work at temperatures far below zero degree Celsius. These researches showed that strength and elastic modules of CFRPs increase and thermal conductivity decreases as temperature is lowered (see Haberle [32]), making them an attractive choice for cryogenic pressure vessels.
Application of CFRPs for Manufacturing cryogenic pressure vessels is a challenging task because it implies dealing with the overall behaviour of these materials on a component level in cryogenic environment. Nevertheless many research programs are running or are going to be started with this aim. Hydrogen integral tanks are foreseen for the future versions of the european Ariane 5 launcher, as well as for future reusable launchers (Haberle, [32] and Pfeffer, [60]). In the first case composites are seen as viable means to improve performances and thus increase payload of the european launcher. The goal of achieving a reusable space vehicle capable to put a payload into orbit, has been pursued for more then ten years and gave the first push to the research in the field of composite cryogenic tanks. While today expendable launchers

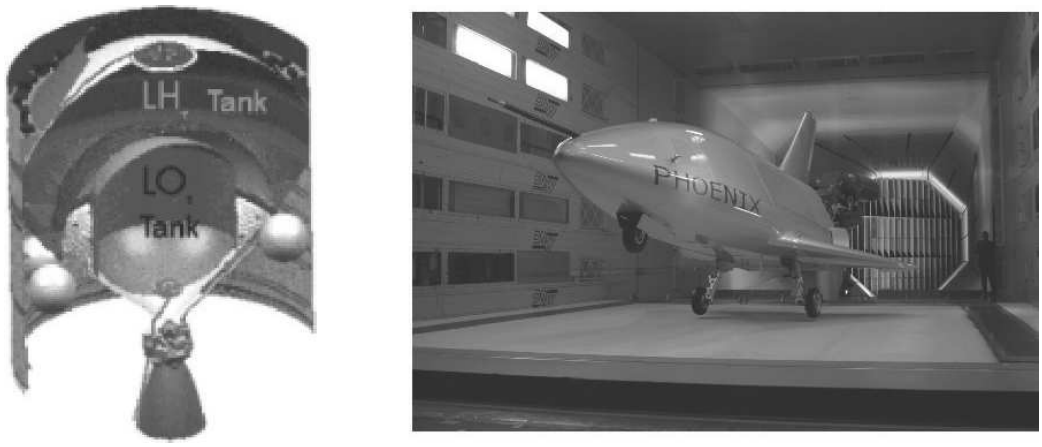


Figure 1: Ariane second stage (left) and "Phoenix" test vehicle, precursor of the european next generation launcher

achieve a structural to gross take off mass ratio of about 10%, the requirement for reusable launchers lies considerably under this value. Beyond that, reusable launchers must fulfil more stringent structural requirements than expendable rockets, deriving from the need to stress the structure for repeated use, and carry additional provisions for recovery and reuse. If consistent helps are expected from enhancements in propulsion technology, structural improvements are mandatory and must rely upon the use of CFRPs for primary structures, like in the case of cryogenic tanks (Pfeffer [60]).
The aircraft and automotive industries are responding to the demand for environmental friendly means of transports by considering hydrogen as fuel for future passenger aircraft and cars. Additionally to the issue of pollution, a second concern arises from the expectation of increase in fossil fuel price in the next future, because of the increasing demand from the Asiatic market and of the running out world reserves. For these reasons the European Airbus has carried out studies on the so called "Cryoplane" under commission of the European Union. If research is active in the aerospace field, progressive efforts for achieving economically competitive terrestrial hydrogen vehicles have been running already for decades. In this case requirements are very different from those typical for the aerospace field. Boil off rate and tank integration in the vehicle are topics where major efforts have been directed. Because of liquid hydrogen low density compared to fossil fuel, a hydrogen fuelled aircraft or vehicle will need a four time bigger tank volume at parity of consumed energy. At the same time cryogenic liquids need to be stored in pressurized vessels which need to have as lowest surface to volume ratio

as possible in order to minimize heating of the fluid. Thus application of carbon fibre composites seem to be an efficient measure to keep tank empty weight reasonably low: they not only offer better strength to density ratio, but may have synergetic effects in that their thermal conductivity, far lower than that of metallic alloys, positively affects insulation mass. Directly connected with these applications are basic questions about long time material Behaviour, and hydrogen permeability. If most matrix systems seem to have inadequate oxygen compatibility characteristics (see A. Denaro, D. Dosio, J. Antonenko [10]) no drawbacks have been reported until now in applications of CFRPs for hydrogen containment except for an insufficient permeability characteristics. Anyway available data are limited because of the novelty of the topic.

# 2 State of the art - literature review

## 2.1 Composite cryogenic tank examples and testing

Materials used for cryogenic pressure vessels are today mainly metallic alloys, like austenitic stainless steels or aluminium alloys. Some limited examples of GFRP-steel hybrid tanks exist, but the full potential of reinforced plastics is not yet exploited, because the metallic liner also carries a major percentage of the structural loads and glass fibre stiffness is far from satisfying for structural applications. Metallic construction provides a high fracture toughness even at liquid hydrogen and helium temperatures, the possibility to weld the tank parts in order to manufacture a vessel which is impermeable to the small hydrogen molecules and to apply well proofed manufacturing techniques. The technology of metallic hydrogen tanks has been developed in the United States starting from the fifties and in Europe some years later for the respective space programs in which hydrogen is the standard propellant. Outstanding examples of metal hydrogen tanks from the present generation of launchers are those of the european Ariane and the Space Shuttle main tank, for which an Aluminium- Lithium alloy has recently replaced the more conventional 2219 Aluminium- Copper alloy, accomplishing 5% weight saving. Applications of hydrogen as fuel for atmospheric flight are very few: an experimental program was conducted by NASA in the fifties, during which a B-57 Camberra flew with a modified engine and a liquid hydrogen tank, also of metallic construction (Brewer, [59]). A contemporary study (Reynolds, [6]) stated the possibility to manufacture a metallic cylindrical tank for an hydrogen fuelled aircraft. The tank would have weighted less than 15% of the fuel weight and had a boil off rate less than 30% of the cruise fuel flow. Despite several studies, the second and last test bed to be flown followed only in 1988, this time in the former USSR, and since that further research did not lead to the production of any hydrogen fuelled aircraft. European contribution to the research in the field has grown in the last fifteen years and culminated in the "Cryoplane Project", a complete system study for a hydrogen powered commercial aircraft family. The further steps of the projects foresee the conversion of an Airbus A-310 and Dornier 328 into technology demonstrators. Indeed none of them has been manufactured yet.
In the field of terrestrial vehicles most interest is given to boil off rate and tank volume rather than to weight, because performances of road vehicles are not so sensitive to weight as those of aircraft and spacecraft. Hydrogen tanks for road vehicles have a metallic double walled construction with vacuum insulation, which allows boil off rates of about 1.5% per day (Peschka, [57]). This value, related to typical tank volumes of 150 litres and release pressure

of 3.5 bar for gaseous hydrogen, corresponds to a time interval between tank filling and the beginning of fuel losses of approximately 40- 60 hours. Carbon fibre composites offer in that regard a very low thermal conductivity compared to metals which can increase the loss free time. Anyway the application of liquid hydrogen to the automotive transportation has the major drawback of its intrinsic danger: the fuel must be stored as cryogenic fluid under pressure, thus research activities are not closed to other solutions. For aeronautic and space transportation this seems to be the only way to achieve the best compromise among weight and quantity of carried fuel, thus most research effort is directed in the technology of liquid hydrogen tanks. Space transportation in particular has been the motor of the multiple efforts of the last decade to produce composite pressure vessels for cryogenic fluid containment. Aim of those programs was a considerable reduction in structural mass of next generation space vehicles in order to enable single or two stage reusable launchers to carry a reasonable payload. The first composite test tanks to be manufactured have been monolithic pressure vessels, for which it has been made use of intermediate modulus carbon fibres and toughened epoxy systems (see Shimoda and Cantoni, [1] and Murphy, Lake and Wilkerson, [2]). In reference [1] several lay up and filament wound tanks have been manufactured and tested by filling liquid nitrogen and with additional GHe pressurisation up to 0.98 MPa. Tank wall permeability has been measured before and after the filling with liquid nitrogen and small differences in the recorded data indicate a degradation due to thermal and pressure loads. Filament wound test tanks have been manufactured as well in order to check suitability of this manufacturing process with respect to the requirements for a cryogenic tank. Again leaks were detected after filling with $LN_2$ in most parts of the tank, although no pressurisation had been applied to the test article. The thin adhesive layer added at the inner tank wall did not prevent leakage as hoped. Murphy, Lake and Wilkerson report in reference [2] on the production and testing of a similar test bottle. The tank was designed for 12 MPa burst pressure at $LH_2$ temperature. Test pressure was successively lowered to 2,2 MPa, because wrinkles in the composite wall had been found. The test article has been subjected to 18 temperature and pressure cycles and a room temperature leak test revealed no consistent leaks. Results on this test tank are coherent with those achieved in previous works carried out by NASA, as reported by Kessler, Matuszeski and McManus in [24], where some specimen were cryocycled several times. The following room temperature measurement had given the same level of permeability than reference specimens which had not been subjected to thermal loads. At the end of the nineties the NASA decided to manufacture a technology demonstrator for a reusable launch vehicle, the X-33, which had to be equipped with two com-

posite liquid hydrogen main tanks designed to carry the fuel under pressure and contemporarily provide a path for the thrust loads to the above placed liquid oxygen tank as well as to thermal protection system through its attachment sub- structure. The tank was completely of sandwich construction, for which chosen materials were intermediate modulus fibre reinforced epoxy (IM7/977-2) for the facesheets and aramid- phenolic honeycomb core. The design revealed unsatisfactory for the purposes and the tank failed during the first cryogenic ground tests.

## 2.2 Permeability of fibre reinforced epoxies

The Failure of the X-33 hydrogen tank occurred after three fillings with liquid nitrogen and one with liquid hydrogen during which tank pressure had been risen up to 3 bar, corresponding to a tensile strain of 0.2% in the facesheets. As reported in the final report (reference [4]), tank failure was the result of several factors, initiated by penetration of gaseous hydrogen into the sandwich core through the inner facesheet, due to micro cracks developed in the composite facesheet under thermal and mechanical loads. Following researches (Aoki, [14] and Rivers, [19]) came to the conclusion that combined thermal and mechanical loads are responsible for micro cracking in CFRP laminates which provides leak paths for the cryogenic liquid through the laminate. The liquid contained in the tank can penetrate the tank wall through these cracks and reach the outside. In the case of the X-33 hydrogen tank, gaseous hydrogen accumulated in the sandwich core and increased the core pressure causing debonding of the outer facesheet. Thus the main concern related to CFRPs application to cryogenic tanks seems to be their gas permeability at cryogenic but also room temperature: if on one side early and more recent material characterizations (Okada, Nishijma, Fujioka and Kuraoka in [17], Humpenöder in [18] and Kessler, Matuszeski and McManus in [24]) did not point out any material property degradation and in particular increase in permeability after temperature and mechanical load cycles, the X-33 hydrogen tank disaster and successive leakage tests assess the contrary. As more deeply explained in chapter 3 and 5, CFRP permeability to gas may be the result of two distinct phenomena: intrinsic material permeability, due to adsorption, diffusion and desorption phenomena, and occurrence of micro cracks, that is openings in the composite material which may allow the liquid to flow through the material. The first one is a temperature activated phenomenon which can be described by the Arrhenius law (Humpenöder, [18]), thus it decreases as temperature reduces. Despite this favourable trend, it is not yet clear if CFRP permeability suffices for the purpose, that is if

wall thickness resulting from mechanical design is always bigger than that resulting from the permeability requirement. In case it is not, further measurements of the relation between thickness and permeability must be carried out in order to determine when permeability is the compelling requirement. This question brings to the consequence that structural advantages, CFRPs provide against metallic materials, may disappear except if a further gas barrier is used. In this respect the complete thermo- mechanical load cycle must be considered because gaseous rests of the previously contained cryogenic liquid may progressively penetrate the tank wall during those operational phases when the tank is empty and relatively hot.

## 2.3 Microcracks and failure criteria

The second phenomenon, that is micro cracking, may occur as result of the superposition on ply level of thermal and mechanical stresses. In this case inter fibre cracks develop in plies which fibres are place with a rather big angle respect to load direction and provide paths trough which the fluid may escape the tank. The so called micro cracks do not significantly affect fibre dominated laminate stiffnesses (Boniface, Smith and Bader, [29]): degradation of stiffness is often of one or two percent for HT fibres, thus of the same order than measurement uncertainties. For IM and HM fibres this variation must even be under the detectable threshold. Furthermore cracks open when thermal load causes the matrix to contract, thus their effect on permeability may be important especially at cryogenic temperatures (see Okada, reference [17]). The issue of micro cracking is a concern for several aspects of a composite structure in general, and still more important in case of cryogenic applications. Starting from the design phase, adequate models must be available to allow the designer to correctly analyse the new structure and describe the influence of the several design parameters. This is the case for stiffness and stress analysis of laminates, but strength prediction is still hindered by the absence of a theory able to describe the complex behaviour of CFRPs. The several failure criteria which have been developed in the last thirty years, like the Tsai- Hill, Hoffman or Puck, are obtained by testing UD plies under combined loads and can not describe the complex interactions occurring in laminates when plies having different orientation are present. A large number of papers address this issue, starting from the very initial work of Parvizi [50] on GFRPs, but also the more recent contribution of Boniface, Smith and Bader ([29]) on CFRPs, in which first ply failure of cross ply laminates is experimentally determined. All these works investigate the onset of (micro) cracks in the $90^o$ layers of $[0^o_n/90^o_m]_s$ laminates under unidirectional tensile

load. They all assess an influence of the thickness ratio between $0^o$ and $90^o$ plies on the crack onset load. As the $90^o$ ply becomes thinner the crack onset load increases such that for very thin transverse plies it may exceed laminate ultimate failure load. In other words they state that strength perpendicular to fibre direction is not anymore a ply property, but a laminate property. For that reason the very basic principle behind classic failure criteria, that is that strength is an intrinsic ply property, seems not to be valid. According to these authors, crack onset stress is progressively delayed to higher values as $90^o$ ply thickness decreases and may be completely absent when angle plies are very thin. In this case quasi static fibre failure is not preceded by inter fibre cracks. Analytical models developed to describe FPF in cross ply laminates essentially resort to a fracture mechanics approach, in which a crack forms and grows when it is energetically favourable (Boniface, Smith and Bader, [29], Brown, [35] and Parvizi, [50]). This models assume that the forming crack spans the entire ply thickness and width and spreads instantaneously when the total change of elastic energy of the system, due to crack formation, is bigger than the energy release rate. Based on that, an approximated expression of the stress field in the uncracked and cracked laminates is derived and the energy balance is then calculated. Because stress distribution in the cracked laminate depends on the surrounding constraining plies, this approach is able to find a dependence of FPF load on the thickness and stiffness ratios between the $0^o$ and $90^o$ plies. The accuracy of the model depends on the accuracy of the modelled stress state, which is accomplished mainly following either a shear lag model or a variational approach. The first one is more versatile, being able to treat not only cross ply laminates, but leads to less accurate state of stress. On the contrary, the variational approach is able to consider out of plane stresses, but it is limited to cross ply laminates. In both cases the approximation of the state of stress is always limited to few laminate types and external load combinations, that is of little help for laminate design. Secondly, It has been questioned (see Boniface, [29]) that the fracture mechanics approach is really able to model FPF in all cases, because cracks seem to be propagation rather than initiation controlled in very thin plies. Thus assumption of a instantaneous spreading of the crack is not true in this case. Third, theories modelling constraining effects in laminates are based on a failure parameter, the energy release rate, which is still a ply property. Thus a strength approach based on more accurate laminate stress modelling, than the classical laminated plate theory, may also be able to describe such effects. This is the case of the new strain failure criterion proposed by Gosse and Christensen ([52]), who identified a failure surface in the space of the principal strains which may be able to describes matrix crack onset in angle ply laminates. The criterion needs a very precise deter-

mination of the state of strain in the matrix, thus a three dimensional micro and macro mechanics finite element analysis is needed.
Although the effective laminate behaviour in case of two dimensional load, as in a tank, may sensibly differ from the one occurring when unidirectional tensile load is applied, the occurrence of some sort of constraining may cause too conservative predictions when classic failure criteria are used for calculations. Consequently the need for more precise theories describing laminate first ply failure, when it does not coincide with last failure, are of vital importance for the application of CFRP to cryogenic tanks. The problem of micro cracks occurrence must also be seen from the point of view of tank service life. In this case static properties may not be representative of the long time behaviour and even if constraining effects are really effective in the short time, they may no longer be active against repeated thermo- mechanical cycles. This is especially true in case of thin plies: if cracks are propagation controlled when ply thickness is small, they could increase in size at each load cycle until a complete leakage path forms.
Characterization of CFRPs cryogenic fatigue has been carried out both on UD and cross ply laminates. Kessler, Matuszeski and McManus (reference [24]) test some IM7/977-2 samples under limited number of thermal cycles spanning the range 20 up to 400 Kelvin without any detectable property degradation or micro crack formation. A higher number (500 - 2000) of thermal cycles has been carried out by Eggers, Hartung and Knaak in [22] on T300/914C cross ply laminates, subjected to shock cooling in liquid nitrogen. Their result is in contrast with that of Kessler and they report crack occurrence in all layers. In a more recent paper ([21]) Yokozeki, Aoki and Ishikawa test cryogenic permeability of IM6/#133 tubular specimens and find very poor impermeability characteristics even without mechanical strain in the specimen. When they apply a tensile strain to the specimen, they find a direct relation between strain and leak rate. Hübner ([34]) carries out a more thorough investigation of cryogenic fatigue behaviour on several fibre/matrix combinations, among which normal and toughened epoxies and PEEK combined with T300, AS4 and HTA fibres. By testing crack occurrence in cross ply laminates under cycling load he finds that cracks form after the first hundred cycles in all specimens even if cyclic load does not exceed the fatigue limit. Brown ([35]) investigates micro cracking occurrence in cross ply and QI laminates under thermal cycles. He tests several epoxies (Fiberite 934 and ERL 1962) and cyanate ester together with PAN and Pitch based carbon fibres. His conclusions are that the number of cracks grows very rapidly in laminates having thick plies and very slowly in those with thin plies. Nevertheless the final crack density is higher when plyies are thin. From the point of view of material choice, PAN fibres and cyanate

ester show the highest resistance to micro crack formation.
Following researches are trying to solve the problem of permeability principally by means of additional layers which should act as barrier for hydrogen. In reference [11] room temperature permeability of some suitable materials is measured in order to make an adequate choice. Anyway the application of a gas barrier, besides increasing manufacturing costs, presents some other points which have to be considered. Material properties itself must be proper for cryogenic applications, starting from failure behaviour. Compatibility with the cryogenic fluid must also be demonstrated, that is its influence on material properties must be negligible during the whole life of the tank. If the barrier sheet is laminated with the CFRP, thermo- mechanical compatibility must be satisfactory. Again the long time (repeated cycles) behaviour is a major issue. A last point to be introduced concerning composite cryogenic tanks is that of joining and manufacturing techniques. If welding is the natural choice for a metallic tank, because it provides impermeable joints, this technique can not be applied to thermoset composites, for which bonding represents the alternative. In no case normal rubbers or even metallic gaskets, which may find application in metallic tanks, are suitable to be used at such temperatures together with composites because of the huge difference in thermal expansion coefficients. Even when the tank is manufactured by filament winding, fittings and joints to the surrounding structure must be bonded or in- laminated to the tank. In tanks manufactured with prepregs the several parts must also be bonded together, like in case of the X-33 hydrogen tank. Limited data on adhesive joint behaviour and only for temperatures around $0^oC$ or little lower are available in the literature: Adams, Coppendale, Mallick, Hamdan ([63]), Fischer and Schmidt ([66]) report an initial increase in strength as temperature is lowered. At the same time intrinsic material properties, like strength and moduli are known to considerably increase for plastics at cryogenic temperatures (Hartwig, [27]). However as thermal load becomes more important, strength of bonded joints stops increasing. For these reasons measurements of the effects of temperature on bonded joints should be extended to very low temperatures.

**Open questions - research tasks**

The complexity of this topic is underlined in the preceding literature review. All aspects of structural thermo- mechanics, structure design, some of material and cryogenic sciences are of interest for the purpose and need to be investigated. Exhaustive treatment of all them exceeds the possibilities of a single research work, thus attention will be focused on CFRPs failure behaviour at cryogenic temperatures, their permeability and the issue of micro

cracking. A list of points, to which this work tries to find answer, follows.

1. Measurements of material CFRPs intrinsic permeability at cryogenic but also at room temperature are needed to estimate the minimum thickness needed to satisfy permeability requirements

2. The relation among thermal stress, mechanical strain leak rate for CFRP laminates. It is necessary to assess at which mechanical strain cracks begin to form in a laminate under a two- dimensional stress state, like in a real tank. How these cracks influence permeability at cryogenic but also at room temperature

3. In order to accomplish points 1 and 2, a test set up capable of reproducing the cryogenic environment, a bi- dimensional state of stress and allow measurement of permeability must be developed.

4. The question if CFRPs, in case of static load, can provide weight savings compared to metallic construction should be answered

5. The possibility to make numerical predictions on laminate strength based on the new failure theories must be investigated both in case on uni- directional and bi- directional load

6. If point 4 has a negative answer it is necessary to investigate the possibility to increase composites impermeability by means of gas barrier. These can be in the form of a film (liner) or of particular "ad-hoc" layup made of different fibres/matrix combination or other fibre volume percent (Discrete Gradient Material). In case of a liner, it is necessary to understand which materials are suitable and if they can be successfully in- laminated and work at cryogenic temperatures without break or debond under the thermal load

7. If 4 has a positive answer, it is necessary to investigate the behaviour under repeated cycles. When do micro cracks nucleate under thermal fatigue and how does permeability increase with the number of thermomechanical cycles?

8. Concerning bonding techniques, an assessment of the influence of thermal load at very low temperatures must be carried out.

# 3 Discussion of tank requirements

## 3.1 Introduction

Hydrogen is liquid at the temperature of 20,268 Kelvin, at atmospheric pressure, namely a lower temperature than that at which air liquefies. As liquid it exhibits a very low density in comparison to fossil fuel. Its molecule is smaller than any other, with the exception of helium, being but the lightest, having a molecular weight of only 2. In addition hydrogen is very reactive with oxygen, being flammable in concentrations which range from 4 to 76% and it tends to embrittle some metallic materials by penetrating their crystal lattice, although hydrogen embrittlement is a thermally activated phenomenon, which takes place at high temperatures. The following table 1 shows a comparison among several fuels. In comparison to gasoline, hydrogen has a 2.8 times higher heat value, which means that, in order to produce the same

| | LH2 | LCH4 | Gasoline | Synjet |
|---|---|---|---|---|
| Molecular weight | 2,016 | 16,04 | 114 | 168 |
| Liquid density $[g/cm^3]$ | 0,071 | 0,423 | 0,7-0,74 | 0,8 |
| Boiling point $[K]$ | 20,27 | 111,7 | 473 | 440-540 |
| Specific heat at b.p. $[J/Kg]$ | 9,69 | 3,5 | 7 | 1,98 |
| Lower heat value $[Kwh/Kg]$ | 33,3 | 13,8 | 12 | 11,9 |

Table 1: Physical data of several alternative fuels

work produced by a mass M of gasoline, the mass of needed hydrogen is 2.8 times lower. On the contrary, liquid hydrogen density is 10,4 times lower than that of gasoline, that means that the volume of hydrogen is almost 4 times bigger (still at parity of work done). This volume can be only slightly reduced by increasing storage pressure, if structural drawbacks are admissible, because liquid hydrogen compressibility is limited (see table 2 for comparison). In conclusion, if synergetic effects are not considered, a hydrogen car

| T $[K]$ | P $[MPa]$ | $\rho$ $[Kg/m^3]$ |
|---|---|---|
| 20,4 | 0,1013 | 70,784 |
| 22 | 0,1585 | 68,72 |
| 23 | 0,2039 | 67,414 |
| 24 | 0,2579 | 66,01 |
| 27 | 0,48 | 61 |
| 30 | 0,8116 | 53,93 |
| 33,18 | 1,313 | 31,428 |

Table 2: Liquid hydrogen pressure and density at several temperatures from [59] (saturated liquid)

or aeroplane will carry a less weight of fuel but 4 times bigger volume than a conventional one. Actually because of the lower fuel weight, an hydrogen aircraft will weigh less, require smaller wing area than a conventional one, thus affecting again fuel weight. This synergy is probably less visible in a road vehicle, where weight considerations are not of primary importance. On the other side, because hydrogen is a cryogenic liquid, its storage is not easy, being implemented in thermally insulated pressurised containers in order to avoid uneconomical high boil off rates.

## 3.2 Thermomechanical requirements

As seen, storage temperature ranges in the 20-23 Kelvin ($-253^oC : -250^oC$) interval, according to tank pressure. Heat inputs continuously transform liquid into gas, and thus increase inner pressure. Starting from a certain pressure, which is design chosen, gas begins to flow out through opening overpressure valves. The leak free time is the time elapsing between the filling and the moment at which overpressure valves open. Beyond this moment, the amount of hydrogen lost per day is called boil off rate and is solely function of insulation effectiveness. In case of leak free time, maximum operating pressure and insulation effectiveness are the interacting variables in determining its value: the more efficient the insulation, the longer leak free time is at a given operating pressure. Their allowable values are function of the application, materials and applied technologies. Typical design values are shown in table 3, and briefly discussed here. Insulation efficiency will be taken as fixed value, being discussion on insulation technology out of scope in this work.

| Vehicle type | Leak free time [$hrs.$] | Lower pressure [$bar$] | Upper pressure [$bar$] |
|---|---|---|---|
| Private (car) | 40-60 | 1,5 | 5 |
| Commercial (bus) | 10-20 | 1,5 | 5 |
| Commercial aeroplane | 5-10 | 1,5 | 2 |

Table 3: Comparison among leak free time, upper and lower tank pressures for several categories of vehicles

Tank operating pressure influences leak free time rather than the amount of stored fuel, because, as shown in table 2, liquid hydrogen compressibility is modest. Thus operating pressure should be higher where a high leak free time is desired. This is the case of private road vehicles, which generally undergo an irregular use. A leak free time of about 40 - 60 hours is desired in this case [57], for there is the eventuality for a private vehicle to remain long time parked in poorly ventilated environment. Today vapour cooled super insulation is capable of limiting pressure build up to 0,03 bar/h, this means that operating pressure should be not smaller than 3,5 bar (if initial pressure is 1,5 bar after filling up the tank), but with 4 -5 bar as usual goal, due to safety reasons. Higher operating pressures increase leak free time, but they are not chosen again because of safety reasons, particularly in case of accident. The requirement for commercial vehicles is less stringent, because their use is much more regular, thus after filling, hydrogen is consumed over the 24 hours. Same considerations can be applied to commercial aircraft, which after tank filling, are not expected to wait long time on the ground and, anyway, not without running engines.
Tank pressure requirements are defined by the two limiting pressure values. Requirements concerning the lower pressure value are determined by the need of preventing air from flowing into the tank, where it would freeze as soon as in contact to liquid hydrogen. In doing that, it could plug tank feed or outlet lines. As consequence lower pressure value must lie enough above atmospheric pressure. A value of 1,5 bar is considered as sufficient.
The upper pressure extreme is more application dependent. As already seen, leak free time is an important issue in road vehicles, while tank weight is of secondary importance, thus pressure can be risen up to 5 bar. From that point of view a high pressure tank, having operating pressures in the order of 500 bar, is also an alternative because it may allow a considerable increase in leak free time. Nevertheless the aspect of passengers' safety in case of accident banish it to a second choice and thus it will not be considered here. Leak free time is less important in aerospace applications, because aircraft

undergo a more regular employment, but structural weight is to be minimised. Thus upper pressure boundary should not exceed 2 bar ([57] and [58]), being a 0,5 bar margin between the two extremes a mean to prevent vent valves from immediately opening after tank has been filled.
Concerning fatigue life requirements, cyclic loads have to be evaluated. Two sources for repeated loads are present: thermal shocks due to cooling and re-heating as tank is empty, and hydrogen storage pressure (structural loads, as occurring in an aircraft integral structure are not considered here). The occurrence and combination of these two load cases is strongly dependent on the application.

| Vehicle type | Mechanical (*pressure*) cycles | Thermal cycles | Life (*years*) |
|---|---|---|---|
| Private car | 5500 | 5500 | 15 |
| Commercial aeroplane | 10000 | / | 25 |
| Reusable launch vehicle | 700-1500 | 700-1500 | 25 |

Table 4: Comparison among cyclic loads/fatigue life for several categories of vehicles

Pressure cycles depend exclusively on the number of years and frequency of use of the vehicle under consideration. Table 4 shows typical life requirements for several means of transport, concerning number of mechanical (pressure) and thermal cycles.
In case of road vehicles the same number of thermal as pressure cycles must be assumed, because of the irregular use they would undergo. This assumption, backed up by the relatively small thermal mass of a automotive tank, implies a complete heating up to room temperature between two successive fillings. Service modality for a commercial aeroplane are different. First, it will fly nearly every day, in order to maximise profit, and thus the number of tank filling is of the order shown in table 4. Nevertheless, because of the much bigger thermal mass, allowing the tank to heat up to room temperature could not be operationally and economically efficient (see functional requirements). For these reasons a smaller number of thermal cycles is expected. This measure further spares the structure and reduces filling time for the huge tank volume. A mean to accomplish it is by leaving some liquid hydrogen in the tanks, which would not be emptied and thus heat to room temperature unless for maintenance purposes. The same expedient could be applied to automotive vehicles for commercial use, i.e. busses, at least partially by

filling it with liquid nitrogen, in order to reduce filling costs, although the effectiveness of the procedure is to be evaluated, as the mass to cool down (tank mass) and thus expended liquid is sensibly smaller than for an aircraft tank. The requirement for a space launcher is, in this respect, of an order of magnitude less stringent. A time interval of one-two weeks between two successive launches is expected ([4], [57]), therefore number of thermal and mechanical cycles will be equal, being such a procedure of keeping tanks at cryogenic temperature, as for a commercial aircraft, meaningless because of the long time elapsing between two consecutive flights.

## 3.3 Permeability requirements

### 3.3.1 Leak rate

Tank wall shall be impermeable to hydrogen molecules, in order not to let fuel escape. For the purpose of the present section, leak rate will be introduced as physical quantity and a requirement for a hydrogen tank will be derived in dependence of its life requirement in number of years. For further comments on material permeability refer to chapter seven.
Impermeability of a material may be determined by measuring the leak rate flowing through a specimen made of that material. Leak rate is defined as the quantity of fluid (in number of molecules) flowing through the material per unit time. Taking figure 2 as reference, let $V_1$ be the volume where all gas molecules, flowing through the tank wall, are collected.

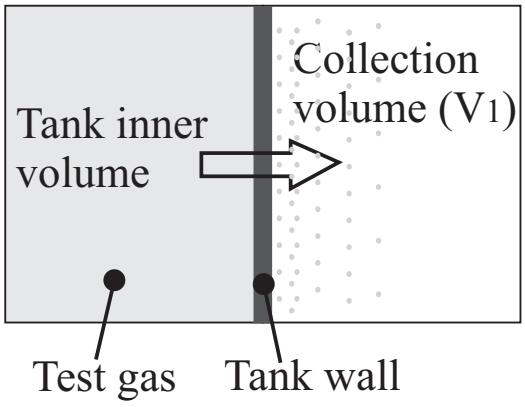


Figure 2: Molecules flowing through the tank wall are collected in a reference volume, $V_1$. The slope with which pressure increases in the collection volume is a measure of the leak rate

These molecules cause pressure in volume $V_1$ to increase. The slope with

which pressure increases in a volume is a measure of the leak rate through the wall delimiting it. Thus dimensions for leak rate (LR) are:

$$LR = \frac{Pressure * Volume}{Time} \tag{1}$$

Because of the very low values with which one has generally to deal, pressure is measured in millibar, time in seconds and the reference volume is in litres, giving the $\frac{mbar*litre}{sec}$ as leak rate unit. It follows that a unitary leak will produce in a one litre volume a pressure increase amounting to one millibar every second. Because leak rate is a function of pressure difference between the tank inner volume and collection volume, it tends to decrease with time as pressure in the collection volume builds up. Anyway, measurement is limited to time intervals during which pressure in the collection volume is negligible in comparison to that in the vessel, that is to very small leaks, for long time, or very small time periods for big initial leaks.
Leak is also a function of total surface through which the fluid can flow. Thus material permeability must be referred to a unitary surface.

### 3.3.2 Leak rate requirements

**Automotive**

In case of a double walled super insulated tank for automotive application, leaked hydrogen collects in the volume between inner and outer vessels, where the insulation is placed, and affects insulation effectiveness by degrading vacuum. Because tank replacement or some kind of extraordinary maintenance, like half life vacuum pumping, are not expected during the whole service life, vacuum has to be kept for the whole life of the pressure vessel.

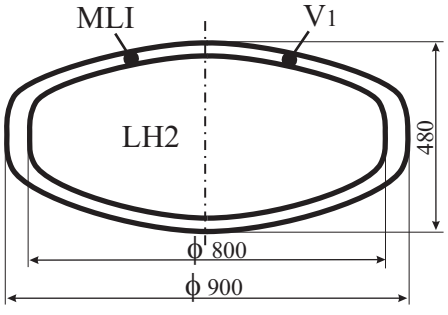


Figure 3: DLR automotive flat cylinder tank scheme

| | |
|---|---|
| Tank collection volume, $V_1$ $[Litre]$ | 117 |
| Inner wall area, A $[m^2]$ | 2 |
| Admissible $\Delta$ P $[mbar]$ | $1,33 * 10^{-4}$ |

Figure 4: Approximate geometric data for the inner tank wall, inter wall volume and admissible pressure rise

A representative automotive tank section is shown in figure 3 and taken from [57]. Its approximate dimensions are used to calculate the admissible leak rate through the material, and summarised in figure 4. Volume $V_1$ is that between inner and outer tank wall, which is partially occupied by the multilayer insulation, wound onto the inner tank. Tank service life is shown in table 4, while the admissible pressure rise is taken from reference [57] as well and corresponds to the threshold pressure for efficient multilayer insulation functioning: for pressures above that value, heat leaks begin to sensibly rise. The admissible leak rate is calculated as follows:

$$LR_{ADM} = \frac{\Delta P \cdot V_1}{Time} = \frac{1,33 \cdot 10^{-4} \cdot 117}{236 \cdot 10^6} = 6,6 \cdot 10^{-11} \qquad \frac{mbar \cdot litre}{second} \tag{2}$$

This value corresponds to the total leak through the inner tank wall, which surface is A. The correspondent value for unitary material surface is:

$$ULR_{ADM} = \frac{LR_{ADM}}{A} = 3,3 \cdot 10^{-11} \qquad \frac{mbar \cdot litre}{second} \tag{3}$$

This value is only indicative of the acceptable order of magnitude. Several possible methods could help increasing allowable leak rate: for example volume $V_1$ may be (slightly) increased and/or some adsorbing material may be placed between the two walls in order to keep vacuum even if gas molecules are flowing through the tank wall.

**Aerospace application**

As in the case of automotive vehicle, leak rate requirement depends on the insulation concept. In fact the gaseous hydrogen flowing through the tank wall will be collected into the available space between tank inner wall and insulation (tank) outer wall. Because of maintainability reasons, MLI insulation is not to be used in aeronautic application, thus the two more promising insulation concepts are microspheres - vacuum insulation and closed cell foam insulation [59]. With reference to the first solution a leak rate requirement can be derived, by the same procedure used in the previous section. The considered tank geometry is a 2,3 m radius, 8 metre long cylinder, which well represents a commercial aircraft hydrogen tank. Insulation properties and representative tank size are taken from [57] and [59] and shown in table 5 together with the leak rate allowables. Calculation are carried out by the same procedure as in previous section. For computation of total lifetime a 12 hour flight per day and 250 day/years have been considered.

| Application | Commercial aeroplane | RLV (X-33) |
|---|---|---|
| Insulation type | microspheres | vacuum |
| Collection volume $V_1$ $[Litre]$ | 2700 | 3000 |
| Inner wall area A $[m^2]$ | 148,85 | 132 |
| Admissible $\Delta P$, [mbar] | 0,0133 | 1 |
| Unitary leak rate $[\frac{mbar \cdot litre}{sec}]$ | $9 \cdot 10^{-10}$ | $2,9 \cdot 10^{-8}$ |

Table 5: Approximate geometric data for the inner tank wall, collection volume, $V_1$, admissible Pressure increase and unitary leak, in case of microspheres and evacuated honeycomb core insulation

The liquid hydrogen tank for the X-33 experimental RLV has been chosen as example of aerospace application. In that case the hardware is a sandwich tank, whose evacuated core provides the insulation as well. Tank geometry is taken from [4]. Admissible pressure has been choosen in order to keep hydrogen concentration low enough to be able to neglect its conductivity, being aramid core thermal conductivity the term of comparison. Allowable leak rate is again not stringent in comparison to the other two examples. The reason is the few number of flights and short duration of a flight in comparison to a commercial aeroplane. Furthermore, for such a vehicle like a RLV, vacuum pumping of the sandwich core before a mission start could be a feasible measure, while it could hardly be axcepted for a commercial aeroplane, because of safety reasons and operational costs. In case of rigid foam insulation, vacuum is not required because insulation properties do not depend on it. The allowable leak rate depends on structural behaviour as following. An impermeable sheet must protect the outer insulation in order to avoid moisture penetration, which would solidify and break the foam. As hydrogen penetrates the insulation material it exerts a pressure on the inner side of the outer impermeable sheet. This pressure must lie far below the peel stress. Quantification of this pressure value is dependent on material combination and bonding techniques, thus it can not be generalised.

## 3.4 Functional requirements

Functional requirements are principally driven by the very low temperature at which liquid hydrogen must be stored. This is lower than nitrogen and

oxygen solidification temperature, thus no air can be inside the tank as it is filled, in order to avoid possible obstruction of tank openings through solid nitrogen or oxygen. Presence of oxygen must be avoided also for the reason of possible formation of dangerous mixtures which could ignite. Thus all air must be purged by application of gaseous helium before filling with liquid hydrogen. A mixed procedure in which gaseous helium or nitrogen at first and gaseous hydrogen in a second stage are applied is also possible. The applicability of this requirement is to consider in conjunction with the type of vehicle under consideration. Again, if in case of aerospace applications stepwise filling can be accepted, a road vehicle tank is not suitable for a complicated and long- lasting filling procedure, because operational costs shall be affordable for private customers. In connection to tank fatigue life, the need to inspect and maintain the tank must be considered. In that respect the differences existing among the several type of vehicles are even more pronounced. Fuel tanks must be routinely inspected in commercial aeroplanes, for the duration of the whole service life. Furthermore insulation must be easily reparable, possibly without removing the entire tank from the aircraft. This requirement is less severe for a reusable launcher, because of the smaller number cycles and lower frequency of use. Completely different is the perspective for a road vehicle tank, which is not expected to be replaced or even only checked during the whole life, if maintenance costs have to remain as close to those for gasoline vehicles as possible.

# 4 Tank shape and basic concept

## 4.1 Tank shape

Tank shape is driven by three principal requirements, that is, weight, boil off rate and bulk, the importance of which is also related to the type of vehicle considered. Spherical shape provides the best empty to loaded weight ratio, that is the lowest tank structural mass for a given mass of hydrogen to be carried. Sphere is also optimal for minimising heat loss in that its surface to volume ratio is the smallest among all possible shapes. Drawback is the difficult integration into an aerodynamic profiled geometry, which leads to a low volume efficiency. As consequence, the available volume inside the vehicle is poorly exploited, thus the aerodynamic body must be much bigger than needed for a given hydrogen volume. Cylindrical or truncated conic shapes can be easier integrated in aerodynamic bodies. They still offer good structural efficiency because stresses are still free from bending components except in the regions where the end domes are applied. For these reasons these shapes are usually chosen for application to commercial aeroplanes or reusable launchers, while spheres is used in expendable launchers oxygen tanks. Other shapes lead to heavier tanks because considerable bending stresses occur in them, thus they are not taken into consideration where structural mass is to be minimised. Advantage of a so- called conformal shape is the possibility to better exploit vehicle inner volume to place the tank, when the penalty in term of weight can be borne. In road vehicles, for example, weight is not of primary concern, but tank shape should allow the most efficient exploitation of vehicle inner volume. In case of private vehicles, being the tank often placed in the boot behind the rear seats, it should be profiled in a manner to follow the contour of the rear seats.

## 4.2 Tank basic concepts

Some tank basic concepts are briefly discussed here based on the previous requirements. The principal aim of this paragraph is that of showing the typical features of a liquid hydrogen tank as reference to treat a non metallic or hybrid tank concepts. Cryogenic tanks may consist of one or two vessels, according to the requirements for the insulation. In the single walled tank the unique tank wall bears inner pressure and provides a load path for the inertial loads. The insulation is than applied to the outer side of the tank by direct bonding, when consisting of rigid foam (see figure 5).

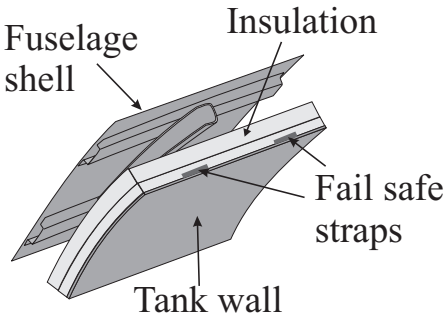


Figure 5: Single walled tank concept for Commercial aeroplane(from [57])

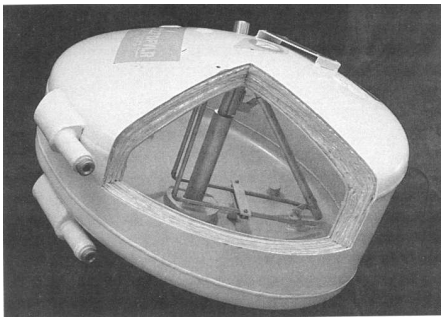

Figure 6: Automotive double walled tank concept (from [56])

A double walled tank is shown in figure 6. It consists of an inner vessel, and outer vessel and an in- between placed insulation. The inner vessel is responsible for the containment of the fluid and provides load paths for the inertial loads acting on the fluid. The outer vessel is mainly responsible for the delimitation of the outer boundary of the vacuum region, in which a multi- layer insulation (MLI) may be placed. Joints between the two vessels represent thermal bridges, but are needed to provide necessary load paths to the outer structure. This type of tank represents the most efficient from a point of view of the insulation, but it is also more expensive.

A variant of the double walled tank is the sandwich tank (see figure 7), in which the space between inner and outer wall is filled by a core. That can be a evacuated honeycomb or a rigid foam, exerting the function of thermal insulation. Like for a non cryogenic structure, the sandwich tank represents an effective mean to reduce weight in case of integral structure, in which the tank wall has the two functions of carrying the fluid and providing load paths for the inertial loads to the rest of the structure, that is the tank is an active part of the load carrying structures.

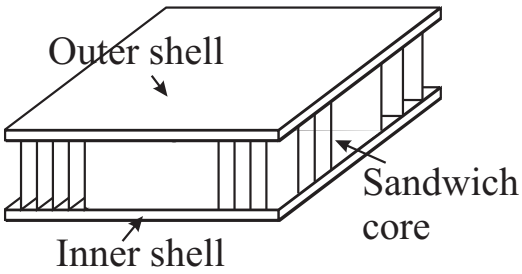


Figure 7: Sandwich tank section

# 5 Tank base materials

## 5.1 Fibre reinforced materials

### 5.1.1 Introduction

The term fibre reinforced plastics (FRPs) identifies a class of materials composed of two constituents: fibres and matrix (identified as plastic). Fibres provide the high strength and stiffness while the matrix fulfil the tasks of protecting fibres, transmitting load through the fibres and fixing the fibres in a given geometry. Reinforcing fibres are available as short (chopped) or long (continuous) fibres, but only the last ones are of interest for high strength applications. Materials for high strength fibres are glass, carbon or polymers (Aramid). Glass fibres, which are composed of quartz, were the first to be applied, but their low stiffness represents a major drawback. Carbon fibres are the type of main interest because of their high specific strength and stiffness and they will be further discussed in this work as candidate for cryogenic tank applications. They are available in several grades which offer high strength or modulus. Aramid fibres are the most successful example of polymeric fibres and are characterized by a very high toughness which make them the material of choice for manufacturing armoured vests, but their lower stiffness than carbon fibres make these latter the preferred in structural applications. Epoxy is the typical and widespread matrix material in aerospace structures. It belongs to the category of thermoset plastics, that is, those polymeric materials available as viscous fluid at room temperature and which develop polymeric links when they are kept at a high temperature for a defined time (curing). The final state is a linked amorphous state. CFRPs are available in several semi-finished forms mainly characterized by fibre direction, weaving, and presence or absence of matrix (in the latter case the fluid matrix is introduced during the lamination process). But the characteristics of the final material also depend on the lay- up parameters, which change according to the needs. Thus the single unidirectional layer is generally taken as reference when material properties are listed. The same will be done in the following paragraphs, where mechanical and thermal properties of typical CFRPs will be illustrated at room and cryogenic environment. These unidirectional sheets are characterized by two in- plane principal directions, namely the fibre and the perpendicular- to- fibre (or transverse) directions, exhibiting very different property values both at room and at cryogenic temperature. In fibre direction fibre properties dominate, while in the perpendicular direction the matrix has a stronger role.
A thorough investigation on CFRP laminates will be carried out in chapters

6 to 8. There, thermomechanical effects on whole laminate strength and permeability will be examined both theoretically and experimentally.

### 5.1.2 Material properties

Tables 6 and 7 show the most important mechanical and thermal material properties at room and cryogenic temperature (respectively RT and CT) for typical CFRPs. Strength and stiffness increase both in and perpendicular to fibre direction as temperature is decreased, although the matrix dominated properties exhibit a stronger temperature dependence than the fibre dominated.

| Material | T300/Epoxy | T700/Epoxy | M40/Epoxy | IM7/8552 |
|---|---|---|---|---|
| $\sigma_{parT}$ RT $[MPa]$ | 1600 | 2140 | 1000 | 2700 |
| $\sigma_{parT}$ CT $[MPa]$ | 1800 | 2460 | 1240 | 2700 |
| $E_{parT}$ RT $[GPa]$ | 124 | 145 | 225 | 176 |
| $E_{parT}$ CT $[GPa]$ | 133 | 144 | 233 | 188 |
| Integral CTE $[10^{-6} \cdot K^{-1}]$ | 0,16 | 0,16 | -0,52 | -0,35 |
| Curing Temperature $[K]$ | 393 | 393 | 393 | 453 |

Table 6: Material properties in fibre direction

Strength and stiffness in fibre direction experience a 5- 10% increase, while for the values in direction perpendicular to fibres the increase amounts to 30-40%. Despite that the difference in material properties between the two directions remains remarkable.
The integral thermal coefficient (CTE) is calculated by the following relation and takes into account the total thermal strain from curing down to operating temperature

$$\alpha_{eff} = \frac{1}{\Delta T} \int_{T_0}^{T_1} \alpha(T) dT \tag{4}$$

The remarkable difference in CTE in and perpendicular to fibre direction cause in typical laminates pronounced thermal stresses already at room tem-

peratures, and becomes very important in cryogenic environment. The topic of thermal stresses will be discussed in the following paragraph.

| Material | T300/Epoxy | T700/Epoxy | M40/Epoxy | IM7/8552 |
|---|---|---|---|---|
| $\sigma_{perT}$ RT $[MPa]$ | 42 | 45 | 30 | 51 |
| $\sigma_{perT}$ CT $[MPa]$ | 58 | 56 | 50 | / |
| $E_{perT}$ RT $[GPa]$ | 7,9 | 8 | 7,5 | 8,6 |
| $E_{perT}$ CT $[GPa]$ | 10 | 10 | 11 | / |
| Integral CTE $[10^{-6} \cdot K^{-1}]$ | 24,5 | 25 | 33 | 19 |

Table 7: Material properties in direction perpendicular to fibres

### 5.1.3 Thermal stresses in composite materials

Unidirectional fire reinforced laminas have an orthotropic behaviour. As previously seen stiffnesses and CTEs in the two principal directions are extremely different. Let now consider a cross ply laminate such as shown in figure 8. Because of difference in CTE the $0^o$ and $90^o$ layers have different thermal strains and, if free, would differently contract under negative thermal load.

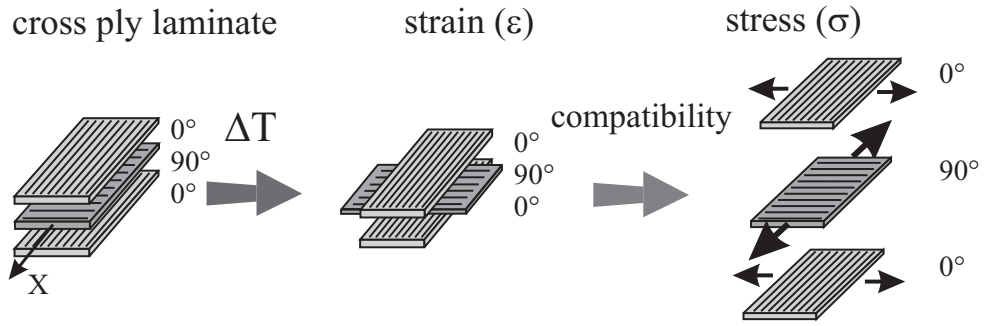


Figure 8: Onset of thermal stresses due to material orthotropy in CFRP laminates

Namely, the $90^o$ layer, which has a far bigger CTE, would experience a more pronounced dimensional reduction in X direction than the $0^o$ layers. Yet, being all laminas bonded together in the laminate, this contraction is impeded and the final laminate strain will lie between the that of the $0^o$ and that of the $90^o$ layer. The $0^o$ layers will experience a compression while the $90^o$ a tension stress. These stresses become extreme in case of high intermediate or high modulus fibres, which exhibit negative CTE in fibre directions. Thermal stresses together with further mechanical tension, like that occurring in a tank, may cause inter- fibre failure and subsequent micro cracks as shown in figure 9.

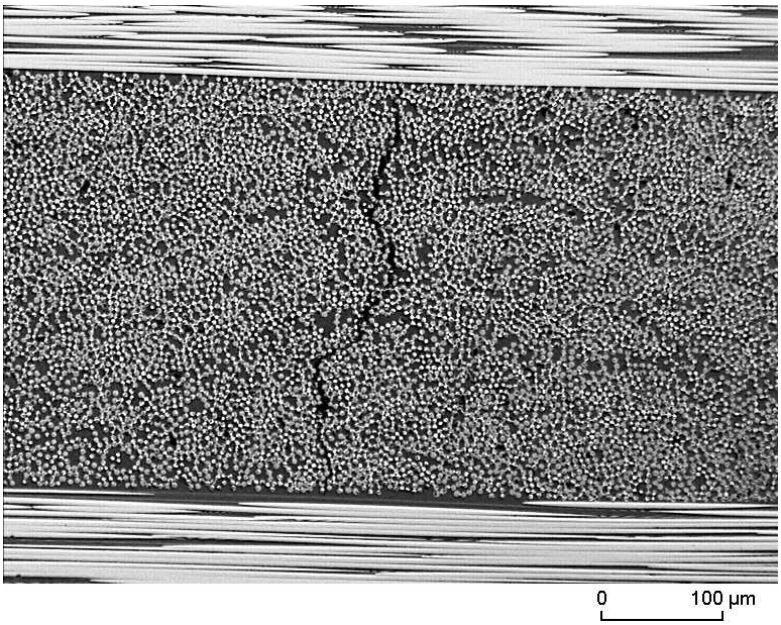


Figure 9: Example of a typical microcrack in CFRP angle ply laminates

These ones have generally only a negligible effect on laminate stiffness and static strength. Anyway occurrence of micro cracks is usually the first in a chain of events which leads to final laminate failure under cyclic loads (Reifsnider, [40]). The process of crack nucleation under repeated load covers about one third of the whole room temperature fatigue life of the laminate. If cracks appear during the first cycle in cryogenic environment, a significant reduction in fatigue life is to be expected at this temperatures. The second main concern with micro cracks is due to leakage through the tank wall: micro cracks provide leak paths through which the cryogenic liquid may diffuse and leave the tank. This is the case when all laminate layers are cracked, but in

case only a portion has developed cracks, the effective laminate thickness is anyway reduced and permeability increases due to diffusion phenomena.

## 5.2 Adhesive materials

### 5.2.1 Introduction

Bonding techniques present many important advantages compared to conventional joining techniques (riveting, welding, soldering) from manufacturing and performance points of view. Bonding is a simpler technology than welding and soldering of metals / metallic alloys because its needs for fixtures and infrastructures are more limited. It allows joining different materials which, for different melting temperatures, surface structures etc., cannot be welded or soldered. It does not require heating metallic parts up to temperatures which may alter their microscopic structure. It avoids direct contact of metals with different electric properties, thus preventing metal to metal corrosion, allows joining very thin sheets, or parts with very different thickness. Bonding, like welding, allows to achieve impermeable joints at cryogenic temperatures. From a point of view of the mechanical performances, bonding offers a more uniform stress distribution than conventional techniques because of the absence of weakening points like holes for rivets or screws or thermal altered zones. Bonded joints have better responses under dynamic load than riveted ones, allow higher loads and have a higher damping. These features lead to lighter joints than by conventional techniques. For the same reason it represents an adequate choice for joining fibre reinforced plastics, where fibre breaking holes should be avoided if possible. Furthermore the adhesive may be an epoxy as well as the composite matrix, thus warranting best adhesion and compatibility. From a point of view of the stress and strength calculation, bonding is a much more complicated joining technique than conventional ones, because the weakest part of the joint, where failure occurs, may be either the adherend, the adhesive or the interface between them. This complexity is worsened by the lack of successful analytical and numeric methods to calculate stress and strength (See chapter 8), thus most of the job of determining joint strength must be accomplished experimentally. In that, the choice of specimen geometry should be driven by two main needs. First, it should resemble that of the part to be manufactured in order to produce useful results for design purposes. Second, it should give quantitative predictions on the influence of the several geometric and process parameters, as well as operational conditions on joint strength. This obviously leads to an extreme increase in number of specimens and effort needed. In the application of bonding techniques to cryogenic structures the magni-

tude of thermal loads rises to higher order than in near- room temperature applications, which deeply influences the joint behaviour. Investigations on the effects of thermal loads on bonding strength has been carried out only for limited temperature differences between curing and operating condition, related to room temperature structures (see [63], [66] and [67]). Both reference [63] and [66] report a marked influence of temperature on joint strength. General trends are an initial increase of strength in single lap joints as temperature decreases starting from the glass transition temperature. At lower temperatures strength remains constant or decreases because of the effects of thermal stresses. In ref. [64] torsion specimens are tested to compare their behaviour to that of single lap joints and a significant difference is reported due to the absence of peel stresses at the joint ends: shear strength of all tested adhesives increases almost linearly as temperature decreases. This observation implies that there could be an interaction between peel and thermal stresses, which does not occur in the torsion specimen because of the absence of peel stresses. Measurements of the shear modulus also report its almost linear increase as temperature decreases, but, like investigations on strength, they are limited to the near - room temperature environment, thus an extension of the temperature range must be provided.

### 5.2.2 Test program and specimen geometry

A typical cryogenic structural adhesive, the HYSOL EA9361 epoxy adhesive, has been chosen for investigations at the Chair for Lightweight Structures. Its mechanical properties has been established under several temperatures and influence of geometric parameters has been investigated as following illustrated. The adhesive is described by the Hysol Company, which commercialises it, as a high elongation, two components room temperature curing adhesive, suitable for cryogenic applications (EA9361 Data sheets, [68]). The suggested curing cycle is one week at room temperature, but accelerated curing is possible up to 1 hour at $82^oC$. The chosen procedure was a one day room temperature plus 2 hours $65^oC$, in order to reduce curing time without increasing the thermal loads by adding further temperature difference to the already big difference between curing and operating temperatures. The test program is articulated in two parts. In the first one pure adhesive tension specimen have been tested and the stress strain tensile curve has been measured as well as the failure and stiffness data. In the second part bonded joints have been tested, whereas several geometric dimensions and joint characteristics have been treated as parameters and subjected to changes inside a range as later shown. Purposes of the test program are the following.
Pure adhesive tests:

- Measurement of tensile strength at several temperatures
- Measurement of material stiffness at several temperatures
- Acquisition of the tensile stress/strain relation for the pure adhesive at several temperatures

The acquired material stress/strain tension curves are to be used for numeric simulation of the adhesive behaviour (see chapter 8).

Bonded joint tests:

- Measurements of bonding strength at several temperatures
- Characterisation of the influence of overlapping length on the bonding strength
- Characterisation of the influence of the specimen geometry (single lap shear / double lap shear) and adherend thickness on the joint strength
- Characterisation of the influence of the adherend preparation (application / absence of a primer to the adherends) on the joint strength
- Verification of the possibility to exploit a single lap shear tensile specimen to measure the adhesive shear stress/strain curve without resorting to a torsion specimen

Table 8 summarises the adhesive test program. Five temperatures have been chosen in order to provide the widest range from moderate high down to liquid helium temperature (4.2 Kelvin) and be able to establish the influence of temperature in the whole range. The number of specimens has also been limited by the need to keep the test program as constrained as possible, but be able to provide reliable data for each temperature. Further comparison to other adhesive types has been carried out both by resorting the literature data and by limited testing of a second non cryogenic adhesive, namely the EA9321 of the same company, which is designed for higher temperatures as well as for moderate low ones.

| Specimen type | Overlapping length (OL) $[mm]$ | Test temperature $[^oK]$ | | | | |
|---|---|---|---|---|---|---|
| | | 313 | 293 | 203 | 77 | 4,2 |
| Pure adhesive tension specimens | | | 3 | 3 | 3 | |
| Single lap shear (SLS) | 5 | | 3 | 4 | 3 | 3 |
| | 12,5 | 3 | 3 | 3 | 3 | 3 |
| | 25 | | 3 | 3 | 3 | |
| Double lap shear (DLS) | 5 | | | | 3 | |

Table 8: Test matrix for adhesive test program. Number of specimens per temperature and overlapping length are provided

Specimen geometries for the bonded joints are shown in figure 10. Material chosen for the adherends was an aerospace aluminium alloy, the 2024-T6, which was primered by a standard primer, the EC 3980. Two adherend thicknesses have been chosen according to the purposes of the test program: thick adherends and short overlapping length has been chosen to reduce peel stress and gain a quasi pure shear stress state. According to [69], thick adherends and short overlapping length provide best adhesive strength because, on one side, thick adherends reduce peel stresses at the bonding ends and, on the other, short overlapping length allow a more uniform stress distribution. Additionally, double lap shear specimens have been also tested at 77 Kelvin, being the purpose the investigation the real possibility to further increase joint strength in comparison to single lap shear (SLS) configuration. If on one side double lap shear (DLS) reduce peel stresses because of the symmetric load paths, on the other side asymmetries, caused by tolerances in the manufacturing process, could contribute in the opposite direction, leading to an overall reduction in strength. Thin adherends and longer overlapping lengths have been adopted to approximate real structural joints and thus determine more realistic failure values. Load application occurs through round bolts, inserted into the holes of the adherends. This allows testing at very low temperatures where friction coefficient is too low to provide efficient load transfer.
Adhesive thickness has been chosen 0,1 mm. This represents a typical value, which is commonly used in structural applications and at which most epoxy adhesives show the best resistance to cohesion failure ([69]). Despite that, an interesting assessment of the influence of adhesive thickness on strength, though initially in program, had to be abandoned because of the extremely high effort in term of number of specimens.

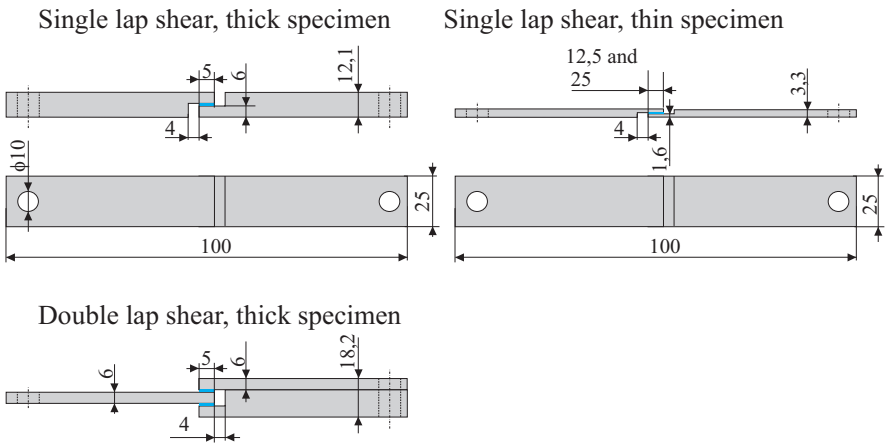


Figure 10: Single and double lap shear specimens geometries

### 5.2.3 Cryogenic test setup

The Chair for Lightweight Structures is provided with a set of test facilities which allows testing in a temperature range between 4.2 and 423 Kelvin. A conditioned chamber can be applied together with an INSTRON universal machine for testing in a $+150^oC : -100^oC$ temperature range. Additionally cryogenic testing can be accomplished at two more temperatures, namely 77 and 4.2 Kelvin, by the liquid nitrogen and liquid helium cryostats shown in figure 11.

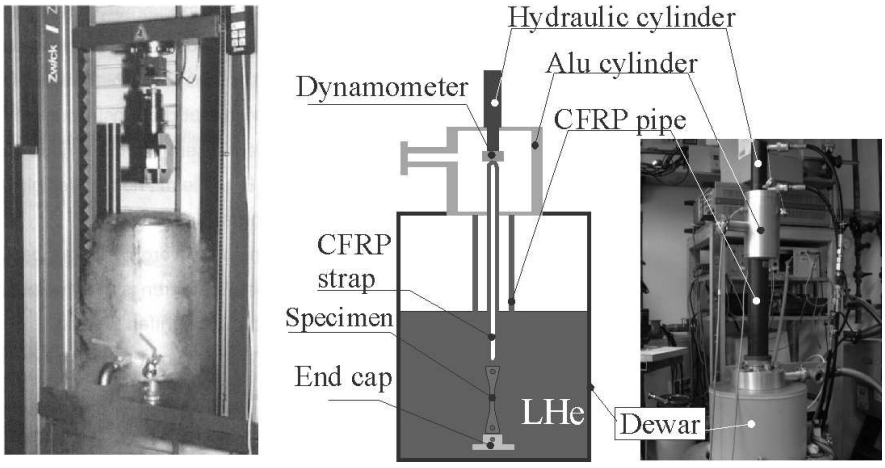


Figure 11: Cryogenic tensile test facilities for tests at liquid nitrogen (left) and liquid helium (right) temperatures

The liquid helium test setup allows to immerse a test specimen into a liquid Helium filled dewar, while tensile force is applied by an hydraulic cylinder which is placed on top of the cryostat and remains at room temperature. A CFRP strap transfers tensile force to the test specimen, but also provides thermal insulation and minimises the heat flux to the cryogenic environment. The test specimen is mounted between the end cap and the CFRP strap by a metal fitting. The whole group is placed inside the CFRP tube, except the end cap which closes the assembly. Temperature and strain sensors are applied to the specimen and connected by cables running trough the CFRP tube and the Aluminium cylinder to a measurement system which records the data strains and the applied force. The CFRP tube has an inner diameter of 70 mm and a length of 1 metre, while the 3 mm thick tube wall, made of high strength T700/epoxy, is composed of a 2 mm thick $0^o$ layer laminated in-between two 0.5 mm thick $90^o$ layers. Tensile force is applied by axial displacement of the hydraulic cylinder and is transferred to the specimen by the CFRP strap, made of the same material than the tube. The end cap holds the specimen and transfers the load to the CFRP tube which is pushed against the Aluminium cylinder and works under compression. The duration of the cooling phase depends on the thermal capacity of the specimen and fittings and lasts approximately ten to twenty minutes for normal tensile specimens, during which the CFRP cylinder is progressively inserted into the cryostat until the test temperature has been reached. After testing, the apparatus is slowly extracted from the Dewar and heated to room temperature. The specimen can be almost immediately replaced and a new test can be performed within a few minutes.

### 5.2.4 Test results: pure adhesive

Figure 12 shows the tensile stress-strain relation for both EA9361 and EA9321 adhesives at the three test temperatures (293K, 203K and 77K). The two adhesives show very different tensile curves at room temperature, where the EA9361 fails at strains around 13% and experiences a pronounced yielding, while the EA9321 at around 2%, with poor signs of plastic behaviour. Failure stresses are very different as well, failing the EA9361 at considerably lower stresses than the EA9321.
At low temperature the behaviour of the two adhesives does not contradict that typical for epoxies and plastics in general: increase in failure stress and stiffness, decrease in failure strain. As Hartwig ([27]) noted, relaxation phenomena due to thermodynamic motion of molecular chains reduce at low temperatures, thus difference among polymers tend to depend only on crystalline content and cross link density, but only secondarily on chemical

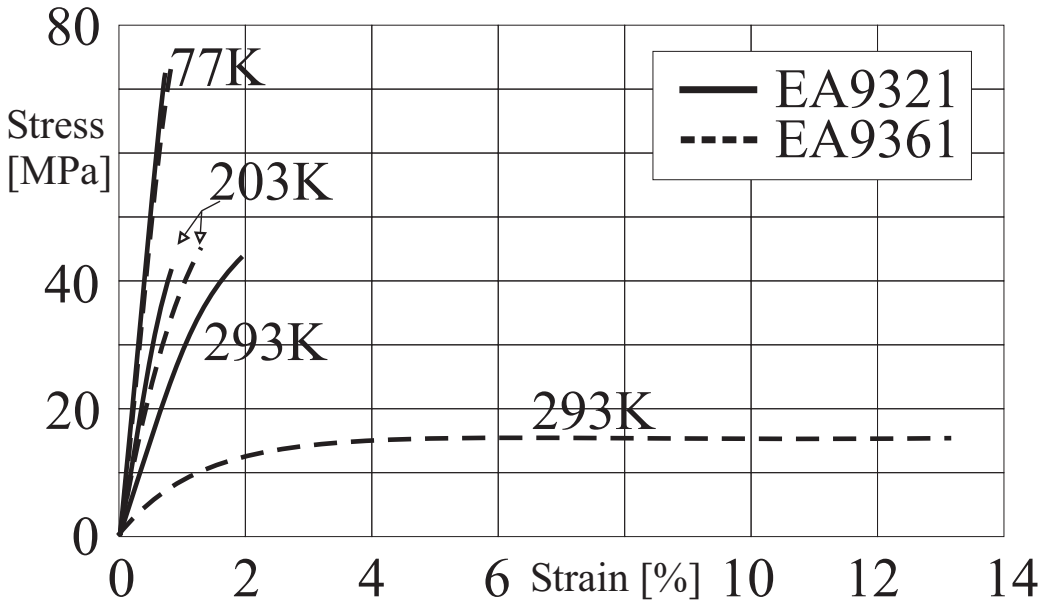


Figure 12: Tensile stress/strain relation for the two tested adhesives at several test temperatures

composition. This dependence on chemical composition completely disappears at lower temperatures, where the so called basic properties become evident. Thus differences in failure stress and strain between the two adhesives progressively reduce as test temperature is lowered and the two materials become more brittle and strong. Being the EA9321 a non cryogenic adhesive this very brittle behaviour does not surprise. The steep fall in failure strain experienced by the EA9361 within a 70 degrees temperature range is rather worth of notice. At 203 Kelvin ($-70^oC$) test temperature, both adhesives fail at around 1% strain and 40-45 MPa stress. Plastic behaviour is absent although the EA9361 still shows a slightly higher failure strain. At cryogenic temperatures the two material curves overlap almost perfectly and are linear. Both failure strains are at these temperatures even lower than those of normal epoxies, which lay at about 2-3%.

### 5.2.5 Test results: bonded joints strength

Test results on bonded joints are summarised in figures 13 and 14 for the EA9361 and EA9321 respectively. All specimen types show a marked dependence of joint strength on test temperature, but, in opposition to what happened for the pure adhesive specimens, differences in behaviour become

more marked as test temperature is reduced. Three temperature ranges (two for the EA9321), with three distinctive trends, can be identified: the first spacing from room down to 203 Kelvin temperature, the second from 203 down to 77 Kelvin and the third from 77 down to 4.2 Kelvin.

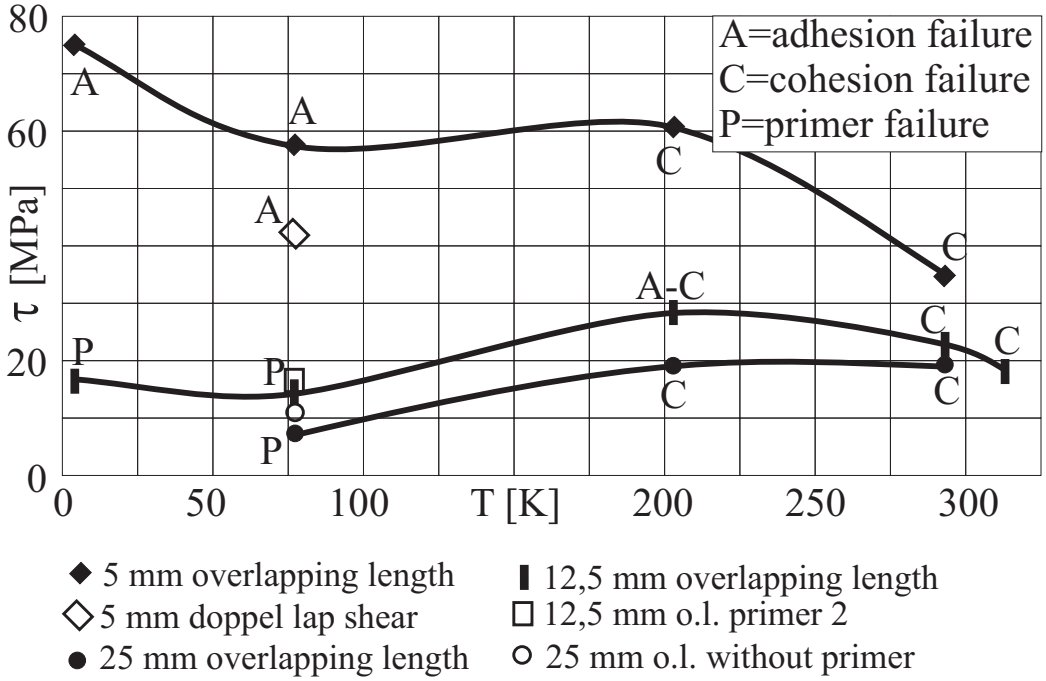


Figure 13: Shear strength function of test temperature and overlapping length for EA9361 bonded joints

Starting from room and moving towards cryogenic temperatures, a first range down to 203 Kelvin can be identified in which strength of all specimen increases. This increase is more pronounced for the short overlapping length and almost absent for the longer one. Behaviour of both adhesives is in this range partially opposite to what stated in [63], where strength of the tested adhesive decreases instead of increase as test temperature was lowered. In the second temperature interval, the two adhesives show opposite failure tendencies. For the EA9361, thick specimens keep approximately the same failure stress, while thin ones experience a marked reduction in strength. On the contrary, for the EA9321 the thin specimen vary only slightly their failure stress, while the thick ones experience a steep decrease in strength. In the last interval, that corresponding to cryogenic temperatures, data are available only for the EA9361. Again a inversion in tendency is noted and joint strength tend to increase again from 77 to 4.2 Kelvin. This increase is

again more pronounced for the short and thick specimen and less, but still visible, for the 12,5 mm overlapping length. The joint strength level for the two adhesives is similar at room temperature down to 203 Kelvin, than a distinction must be done among the thick and the thin specimens. In case of the thick specimens, the EA9361 bonded joints show higher strength than the EA9321 at the last temperature where comparison is possible, that is 77 Kelvin. In the case of the thin ones, strength level is again similar for the two adhesives at 77 Kelvin as well.

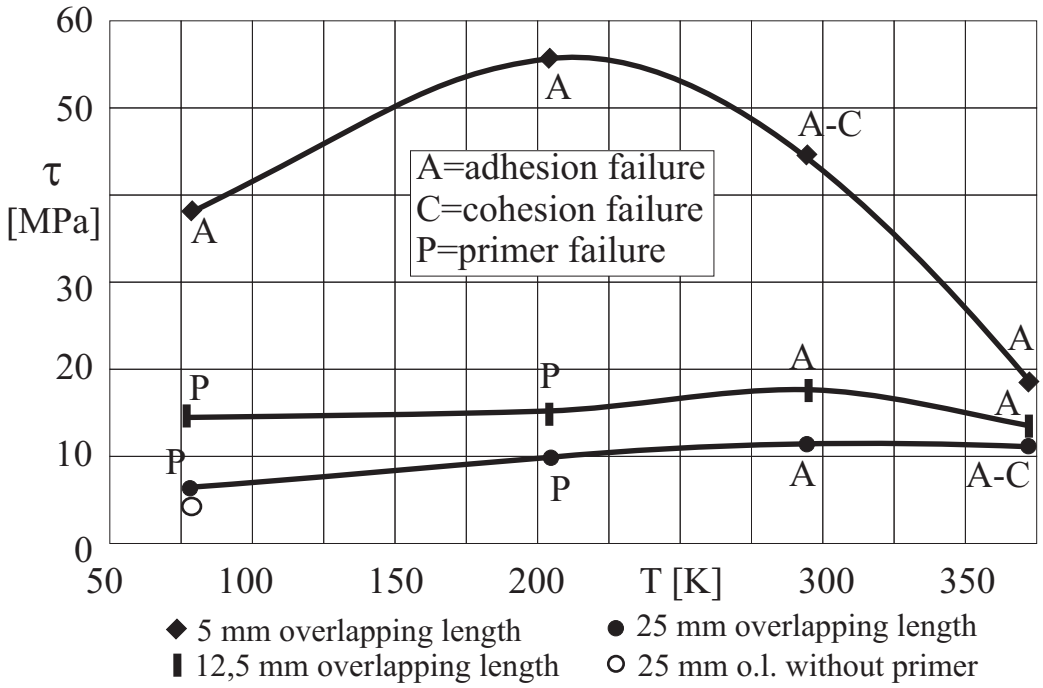


Figure 14: Shear strength function of test temperature and overlapping length for EA9321 bonded joints

This complicated behaviour can be related to the several phenomena which concur to bonded joint failure: adhesive cohesion, adhesive to primer adhesion, primer to adherend adhesion, stress distribution on the bonding length, ratio among stress components. Generally the following phenomena have been observed for the two adhesives.

- At high test temperatures, that is around room temperature, failure is mainly cohesive, while as temperature is lowered it becomes adhesive, either of the adhesive to primer or primer to adherend. Contemporarily to the transition in failure type, joint strength reduces.

- Adhesion failure is more pronounced for thin specimens and longer overlapping lengths or as thermal loads is bigger, that is at lower test temperatures.
- At very low temperatures, thin specimens failure tends to occur between primer and adherend, but not in thick specimens (which also have the shortest overlapping length)
- Together with the primer failure a bigger strength scattering is noticed

This schematisation is valid for both adhesives, but occurs at higher temperatures in the EA9321 and at lower in the EA9361, that is, the same phenomena occur in almost the same succession, but are shifted to higher temperatures for the EA9321. The reduction of joint strength is clearly connected to the failure type. As failure turns from cohesive to adhesive, in the thinner specimens, dependence on temperature is considerably reduced. This is particularly evident in the two figures 13 and 14, for the lower temperature interval, that is 77 - 4.2 Kelvin and 203- 77 Kelvin for the EA9361 and EA9321 respectively, where bonding between primer and adherend represents the weakest part of the chain. Meaning of that is that primer to adherend bonding strength does not depend on temperature in that temperature interval. It simply fails as an average shear of 8 MPa, in case of 25 mm OL, and 14 MPa, in case of 12,5 OL, is reached, independently on the adhesive type. At these temperatures it is not anymore adhesive strength which is measured, but adhesion properties of the primer to the adherend. Because this adhesion is sensitive to surface quality, scatter in measured failure values may directly be a result of the preparation process.

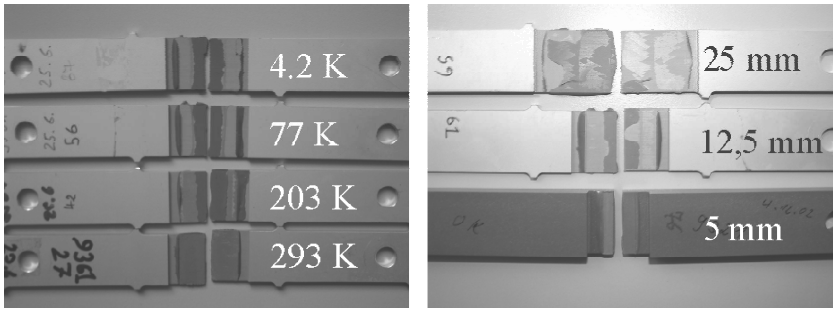


Figure 15: Failure surface for 12,5 mm OL at several temperatures (left) and at 77 Kelvin for several overlapping lengths (right)

Figure 15 shows the progressive occurrence of the phenomenon and its dependence on temperature and overlapping length. Dependence on temperature

is shown on the left for 12,5 mm OL EA9361 bonded joints. Room temperature failure is almost exactly cohesive and progressive appearance of the metal surface demonstrates the increasing proportion of the primer debonding, as test temperature is lowered.
At 77 Kelvin, primer bonding fails on the whole bonding surface. Dependence on overlapping length is shown in the right picture again for the EA9361 bonded joints at 77 Kelvin. The short and stiff 5 mm overlapping lengths (OLs) specimens do not experience this type of failure, but for all other tested OLs it is easily identifiable. The aspect of the failure surface for 25 mm OL specimens is quite remarkable, for its symmetry clearly points out the relation between primer failure and peel stresses (see figure 16). The middle line on the bonding surface is a primer rest in the point where peel stress is zero. Even at that point the adhesive did not fail but separated from primer. Some tests have been carried out without primer in order to investigate joint behaviour when adhesive bonds directly to the adherends. A neat change in joint strength cannot be reported (see figures 13 and 14).

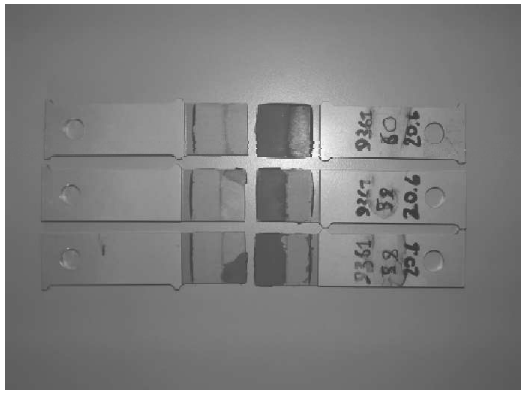

Figure 16: Symmetric failure surface is typical when primer fails

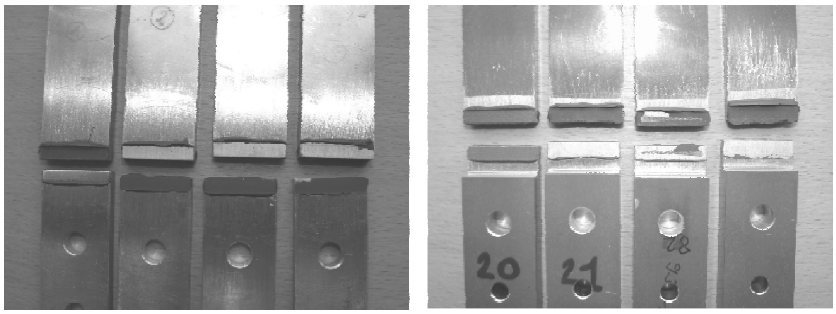


Figure 17: Failure surface of the DLS specimens. Failure is mainly asymmetric.

On the contrary, strength remains on the same level than with primer, while the common type of failure is this time adhesive- adherends debonding. Strength of the DLS specimens is also shown in figure 17. In their case a remarkable reduction in comparison to SLS joints has been noticed. Reason for

this result probably lies in the slight imperfections arising from manufacturing tolerances, which make the achievement of a symmetric joint practically impossible. As in the SLS specimens case, failure occurs at the adhesive - adherend interface, being the primer absent in these specimens. Noticeable is also the asymmetry of the failure mode: the central specimen portion has on one side adhesive, while on the other side adhesive always separated from it. This let again think about the possibility that some sort of bending has caused failure of the specimens, although a more extended test program would be required to take into account all aspects.

### 5.2.6 Adhesive shear stress-strain relation

One of the purposes of the test program was the investigation of the possibility to retrieve the shear stress-strain curve from a tensile test on thick specimens. The common test adopted to measure pure adhesive curves is torsion on thin tubes. This test configuration allows a stress state in the adhesive composed only of a shear component. Anyway, tension of SLS joints represents a much simpler test on the point of view of needed hardware, if not in specimen preparation. Starting point for the whole investigation was the thought that by applying very stiff adherends all average stress and deformation components could be negligible compared to the shear ones and such a specimen should thus be able to provide a good approximation of the adhesive deformation law. The shear stress-strain curve, as measured on the SLS 5 mm OL specimen has been used to calculate the shear modulus at room and 203 K temperatures (see figure 10 for details of the measurement scheme). At the same time the law for isotropic material

$$G = \frac{E}{2 \cdot (1 + \nu)} \tag{5}$$

has been used for the same purpose, where Poisson's ratio has been measured on tensile specimens provided with cross type strain gauges. Results are shown in table 9. The values for the shear module gained by the measurement and by calculation based on isotropic material law have been inserted in a finite element model to re-simulate the linear part of the shear stress-strain experimental curve (for details on the FE model see section 8.4). Results of the simulation are shown in figure 18. It is clearly shown that when shear module from experimental measurement is applied, the simulated curve has a far smaller slope than the experimental one, while, the two slopes are comparable when the value from isotropic material law is applied.
This result can be explained by considering that the extensometer, so as it is applied on the specimen, measures a path deriving not only from adhesive

| | Shear Modulus $[MPa]$ | |
|---|---|---|
| | 293 Kelvin | 203 Kelvin |
| Measured | 64-66 | 97-103 |
| Calculated [FE] | 74 | 96 |
| Isotropic material law | 371 | 1567 |

Table 9: Shear modulus as determined through the relation for isotropic materials and by direct measurement on a SLS 5 mm OL thick specimen (adhesive: EA9361)

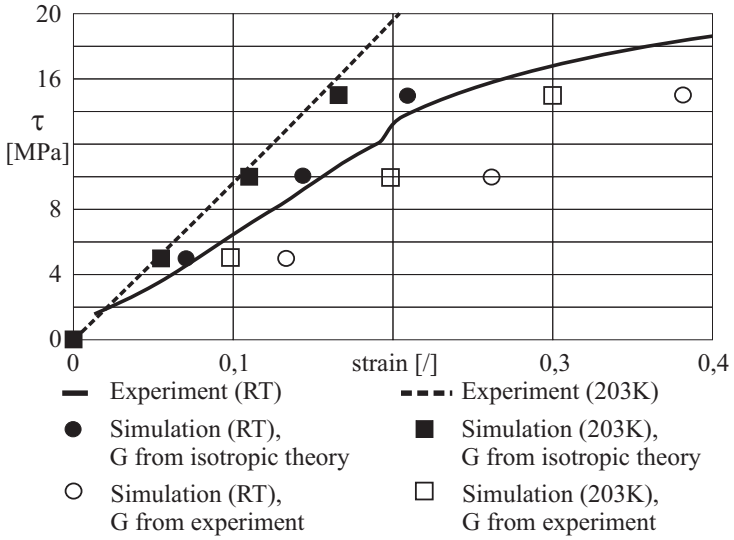


Figure 18: Comparison between experimental and simulated shear stress-strain curve.

shear, but also from adherends deformations. The FE model of the bonded joint has been prepared and used to simulate displacements in load direction of the two points where the extensometer is applied (see figure 19). The results clearly show that the contribution of the adherend is not negligible in comparison to that of the adhesive, thus the measured displacement is totally wrong and much bigger than the actual one. From that a smaller shear module results.

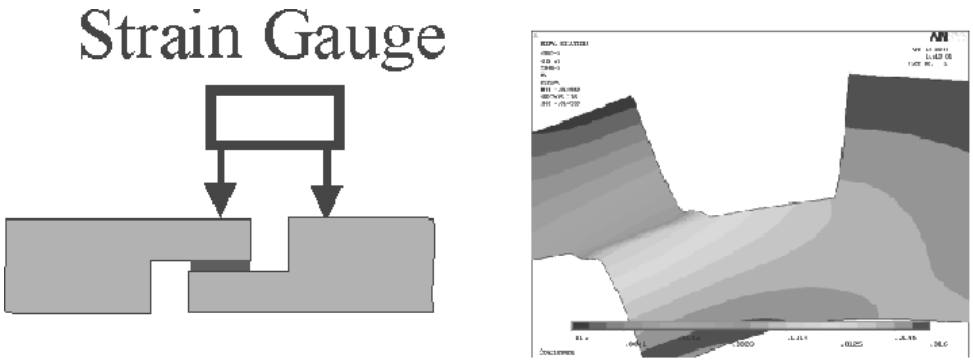


Figure 19: Position of the extensometer for shear module measurements (left) and displacements in the FE simulation (right)

### 5.2.7 Conclusions

The two adhesives have been tested over a wide range of temperatures, from 373 K down to 4.2 K. Strength, stiffness and failure elongation have been recorded for neat adhesives, while strength of single lap shear specimens has been measured in dependence on overlapping length, primer type and test temperature. Neat adhesive specimens show typical characteristics common to epoxies as there are an increase in strength and progressive embrittlement as temperature decreases, while differences between the two adhesives at room temperature disappear starting from 203 K.
Single lap shear specimens show a complex behaviour caused by several phenomena which act together, namely temperature loads, peel stresses, adherends preparation, stress distribution:

- In all cases the dependence of joint strength on temperature is marked due to changes in material properties and the build up of thermal stresses.
- Failure of 12.5 and 25 mm overlapped specimens is determined at cryogenic temperatures by the weak interface between primer and adherends together with the contribution of peel stress due to the low bending stiffness of the thin adherends, which does not allow to exploit the whole potential of the adhesive. At the same time a wider scatter is noticed in test results as consequence of the primer failure.
- Use of a second aerospace certified primer did not produce significant changes in the failure behaviour of the joints, while bonding of rough

aluminium resulted in comparable when not even in slight increase of joint strength for the 25 mm overlapped specimens at cryogenic temperature.

- No occurrence of primer-adherend failure was noticed on the 5 mm overlapped specimens, which may be an indication for a relation between the high peel stresses in joints with low bending stiffness and a long overlapping length.
- Double Lap shear specimen showed smaller strength than the single lap shear type because of manufacturing imperfections which made the specimens unsymmetrical.
- Lap shear specimens are not suitable for measuring shear module in the adhesive because, although stiff adherends are applied, their contribution to the total measured deformation is still comparable to that of the adhesive.

## 5.3 Liner materials

### 5.3.1 Introduction

A barrier material, which prevents the contained liquid from penetrating the tank wall and escaping in the outside, is named "liner". A liner is necessary when the tank material shows poor impermeability to the liquid that has to be stored. This may be due to two factors:

1. The tank material microstructure allows too high diffusion rates
2. Micro cracks in the tank material provide paths to the fluid

The first point represents the usual diffusion phenomenon taking place in all solids. Thus it is influenced by temperature, molecular weight of the fluid, microstructure of the material. The physical formula which describes the permeability of a material is, in this case:

$$P = P_0 \cdot \exp[-\frac{E_p}{RT}] \tag{6}$$

where, $P_0$ is the permeability at a fixed temperature, $E_P$ is the activation energy, which is material dependent, R the universal gas constant and T the absolute temperature. According to this relation, permeation reduces with temperature and disappears completely as 0 Kelvin are reached.
The second point refers more specifically to the fibre reinforced plastic case. Permeation is not more material dependent, but, as soon as there are mechanical paths, the fluid will flow through them, pushed by the pressure gradient. Material dependent is, in this case, micro crack susceptibility, that is the tendency to develop micro cracks in certain physical conditions, like under thermomechanical loads. As seen in section 5.1, thermal stresses arise in carbon fibre laminates when plies are oriented according to different angles. In this case each ply with different orientation has in X and Y directions a different coefficient of thermal expansion which under a temperature gradient cause thermal stresses. At cryogenic temperatures thermal load may be so high that stresses in some or all layers exceed ply

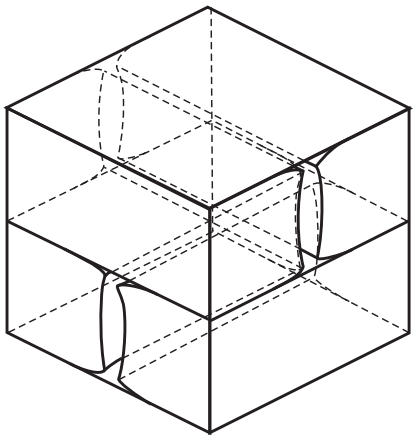

Figure 20: Leak path due to cracks in a Cross ply laminate

strength in direction perpendicular to fibres. Mechanical (pressure originated) stresses superimpose to thermal ones and may also cause inter fibre failure, if thermal stress alone does not suffice. In this case a set of cracks form through laminate thickness (see figure 20), which could either provide the full path to the liquid, or reduce the effective material thickness, so that diffusion takes place faster even at cryogenic temperatures. In both cases tank impermeability is insufficient.

### 5.3.2 Liner concepts

Today's composite tanks have often liners. The reasons for that are CFRPs' insufficient basic permeability at room temperature, chemical characteristics of the contained fluid, which leads to the need of interpose a compatible material, etc. Essentially liners may be classified in load carrying and non load carrying. In the first case the liner carries part of pressure loads and contributes to the tank strength. For that scope material of choice is a structural material, like a metal (typically stainless steal). These kind of liners have primary impact on manufacturing costs, because they are fabricated by cold formed and welded sheets. Secondarily the use of a material like steel implies weight penalties in comparison to a full composite solutions. The non load carrying liner is used only to enhance impermeability. That is it may be thinner and thus have only secondary influence on manufacturing costs because it does not require costly facilities. Liners can also be used as winding core to manufacture the tank. In this case the liner must be pretensioned in order to achieve sufficient stiffness. Thus it must be able to sustain pretension loads, that is its thickness may derive from other consideration than pure impermeability. A second order of concepts is that of membrane liners, that is the liner is partially or completely disconnected from the tank structure, except in those points where fittings and pipes require a fixed connection. As the inner fluid exerts a pressure on it, the liner strains until it gets in touch with the outer tank wall and transfers mechanical loads to that one.

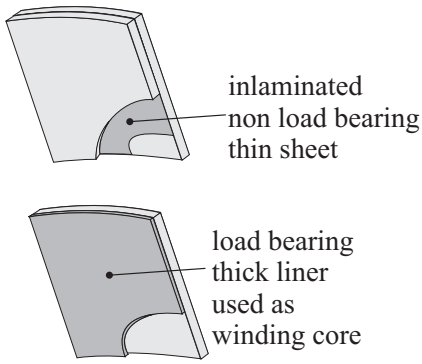


Figure 21: Two type of liner concepts

In this case the CFRP tank is cured separately and the liner is applied in a second step. Thus thermal loads due to the difference in CTE are reduced, because the thermal gradient affecting the liner starts from room instead from

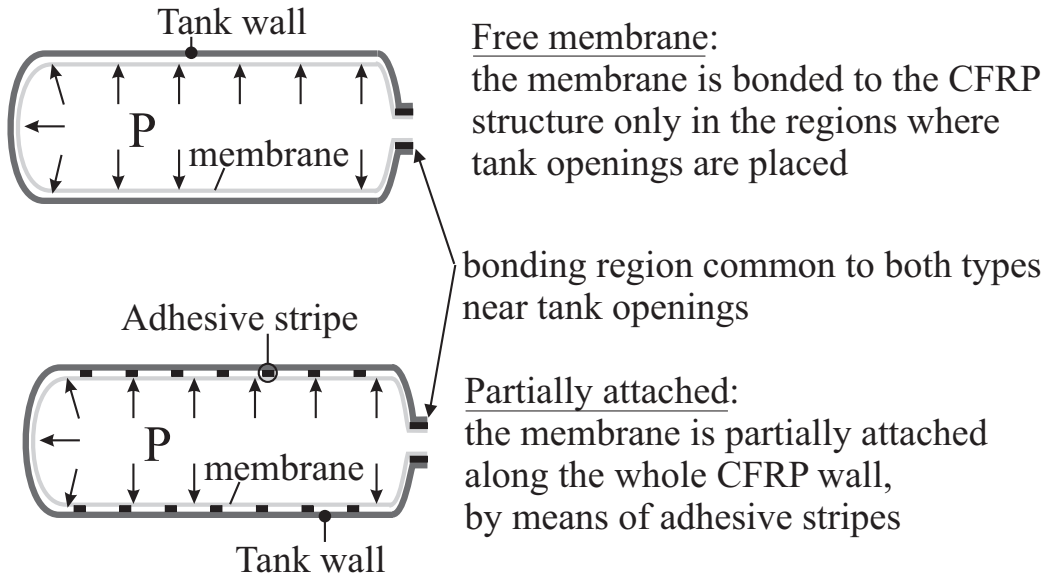


Figure 22: Completely free and partially attached membrane liner concepts

the CFRP curing temperature. Both membrane types can be geometrically dimensioned in such a shape that they exactly reproduce the tank contour at 20 Kelvin, thus completely avoiding the onset of thermal loads. Drawbacks are inherent into manufacturing and assembly difficulties for a thin and big membrane which has to be inserted into the CFRP tank. Moreover dynamic behaviour and fatigue response need to be investigated. This is particularly valid for a liner which is designed to exactly match tank geometry at working temperature. In this case its dimension at room temperature will force it to fold in the tank volume.

### 5.3.3 Materials for liners

Possible material candidates for application as liner in tanks for cryogenic fluids are listed in table 10. The choice ranges from metals, like the usually applied stainless steel, to thermoplastics and thermosets. Metals provide a high impermeability and relatively low CTE. On the other side they also have the highest stiffness among all, thus thermal stresses may be high as well. In order to keep them low, it may be necessary to choose metals with very low yielding stress at CT, and let the liner work in the plastic region of its material curve. In this respect it must be added that the state of stress, an in- laminated liner would experience, is a tensile one only at the first thermal cycle. After yielding, stresses reduce and the liner rather experiences

a compression once the temperature is increased up to room value. Anyway the high stiffness could also be responsible for the onset of delaminations before the yield stress is reached.

| Material | Stiffness at CT $[GPa]$ | $\epsilon_{UTS}$ at CT [%] | CTE (300-20 K) $[10^{-6}K^{-1}]$ | Permeability at RT, $[m^2/sec]$ |
|---|---|---|---|---|
| Al 99.5 | 75 | 50 (0,08) | 15 | $< 10^{-15}$ |
| Stainless steel | 200-220 | 50 (0,32) | 12 | $< 10^{-15}$ |
| Titanium | 120 | 8 (0,7) | 6,4 | $< 10^{-15}$ |
| Epoxy | 6-8 | 2 | 43 | $5 \cdot 10^{-12}$ |
| Kapton® | 5-7 | 5-6 | 22 | / |
| Mylar® | 6,5 | 5-7 | 15-18 | $5 \cdot 10^{-14}$ |
| CFRP | 145 | 1,25 | 0,12 | / |

Table 10: Liner materials and their mechanical properties at cryogenic temperature. T300/epoxy properties are also reported as term of comparison

Plastics have in general far higher CTE than metals, thus the difference in thermal strains with CFRPs is higher than for metals. Furthermore their behaviour at cryogenic temperature is almost completely linear up to failure, without the possibility to exploit a plastic region as in the case of metals. Anyway the total strain they experience when used as liner is for those reported in table 10 acceptably under that at failure. Mylar and Kapton, show from this point of view particularly good properties, because their CTE is comparable to that of aluminium, thus very low for a plastic, while failure strain is still relatively high at cryogenic temperatures. Permeability of plastics is generally much higher than that of metals, with the consequence that the required thickness at parity of permeance is higher. Anyway plastics have a 2-2,5 times lower density than aluminium, thus a thicker sheet does not necessarily mean a drawback in tank weight. Behaviour of plastics is some more complicated than that of metals, because they may experience creep even at cryogenic temperature.

## 5.4 Discussion and selection criteria

### 5.4.1 Composite materials

Because CFRPs are available as semi- finished materials in the form of prepreg, a first attempt choice could be based on prepreg properties, shown in section 5.1. This approach, although it could be of some help in identifying

general criteria the basic material shall satisfy, risks to be misleading. In fact the finished laminate is a different material and its characteristics or suitability are influenced by many parameters. Most of these parameters are considerably different from the very basic prepreg properties and can indeed be estimated starting from them by applying adequate theory, when available. This is for example the case of stiffness and coefficient of thermal expansion. For other properties, like laminate strength, theory itself only provides very approximative results. This consideration is also valid when the laminate is to be a hybrid of two or more materials, in case a liner is imbedded into the laminate. Thus thermal compatibility, micro crack susceptibility, long term behaviour, to mention only some issues, may be understood in detail only by means of numeric analysis and / or by testing. Nevertheless some indications of very general validity can be done. The first characteristic that can be discussed is curing temperature. In order to minimize thermal stresses, curing temperature should be as low as possible. Unfortunately, this requirement is generally contrary to the present tendency in the field of toughened epoxies for aeronautic use, most of which are high temperature systems. Secondly, the difference among thermal expansion coefficients in the two in plane directions should be as small as possible. Yet the qualitative law "the smaller the difference in CTEs the better it is" is false, because final stress to failure ratio also depends on stiffnesses and failure strains. For example, at parity of CTE and failure strain, a higher modulus in fibre direction is desired, because it reduces the mechanical strain in the laminate and thus that in angle plies, allowing higher pressure loads in the tank. Stiffness is also an important characteristic as far as deformation under load is concerned, because the total strain experienced by a laminate is dominated by the fibre. This is exactly the major negative aspect of glass fibre reinforced epoxies. Although being the material with the smallest difference in CTE in the two directions, it also has very low stiffness in fibre direction, thus mechanical loads cause pronounced strains which lead to precocious crack onset in the angle plies. Carbon fibres are in this respect better because, although the difference between CTEs in the two directions is bigger, they are much stiffer. Unfortunately carbon fibre CTE and stiffness do not assume their highest value in the same material, but where stiffness is at its maximum, CTE is at its minimum. Thus, as seen in section 5.1, PAN based fibres having positive CTE in fibre direction also have the lowest stiffness among carbon fibres. High stiffness fibres, like M40J, which also have very high strength, have negative CTE in fibre direction which worsen the problem of thermal mismatch. Between these two categories lie intermediate modulus fibres (IM). They are characterized by intermediate stiffness and slight negative CTE. Thermal mismatch is influenced by transverse properties as well, although

these do not show the same relative variation as in fibre direction (where, for example, the difference in CTE between PAN and high modulus fibres amounts to approximately -300%). Anyway CTE and stiffness distributions are also in direction perpendicular to fibres far from those which would allow best tank performances. For example high modulus fibres also have higher CTE in direction perpendicular to fibre. Thus UD plies made of high modulus fibres show in that direction the highest CTE of the whole category.
The possibility to successfully apply CFRPs to manufacture lighter cryogenic tanks than by aluminium or steel will further be discussed in chapter 9, where a more thorough analysis is carried out by means of numeric tools.

### 5.4.2 Liner selection criteria

Two are the principal requirements for liner materials to be applied to cryogenic tanks: Impermeability and compatibility with CFRPs. None of the available materials shows perfect suitability from this point of view. Metals are generally impermeable but have too high stiffness, while plastics have low stiffness but generally to high CTE to be compatible to CFRPs. No possibility exists to investigate the issue of permeability apart from direct experiment at cryogenic temperature. On the contrary a finite element analysis can provide useful information on thermomechanical compatibility among liner and carbon fibre laminate.

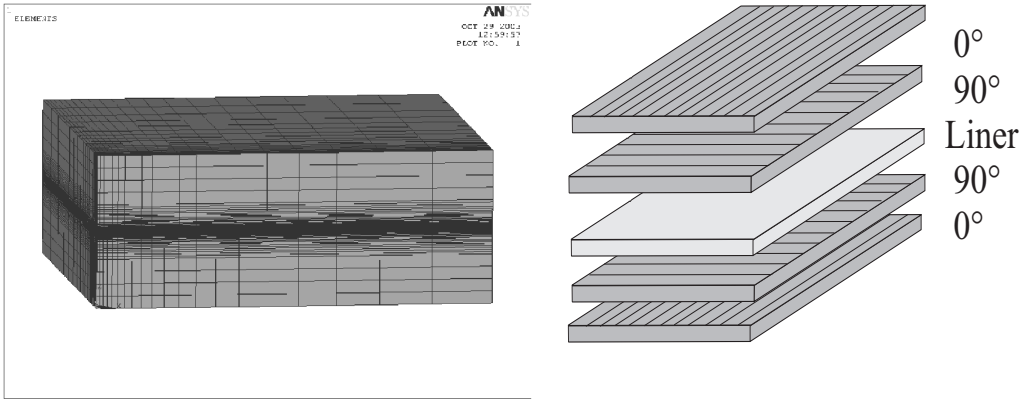


Figure 23: FE model and schematic representation of the laminate layup

To that purpose a finite element model has been implemented, consisting in a 1.5 mm CFRP cross ply laminate, in the middle of which a thin (0.05 mm) liner is inserted (figure 23). The modelled material is IM7/8552 prepreg

because it represents the standard aerospace system. Applied loads consisted in thermal gradient due to cooling down to 20 Kelvin from a 453 Kelvin (180°C) curing temperature and a mechanical strain up to 0,6% in the two in-plane perpendicular directions. Liner equivalent strain and stress has been calculated for several implemented liner materials, as listed in section 5.3, and is shown in figure 24. The strain ratio graph of figure 24 shows the ratio between liner actual equivalent (von Mises) strain and its failure equivalent strain at CT when a mechanical strain is applied to the laminate. Liner stress due to the same applied mechanical strain and thermal load is shown on the right diagram. From the analysis of the figure some considerations can be derived.

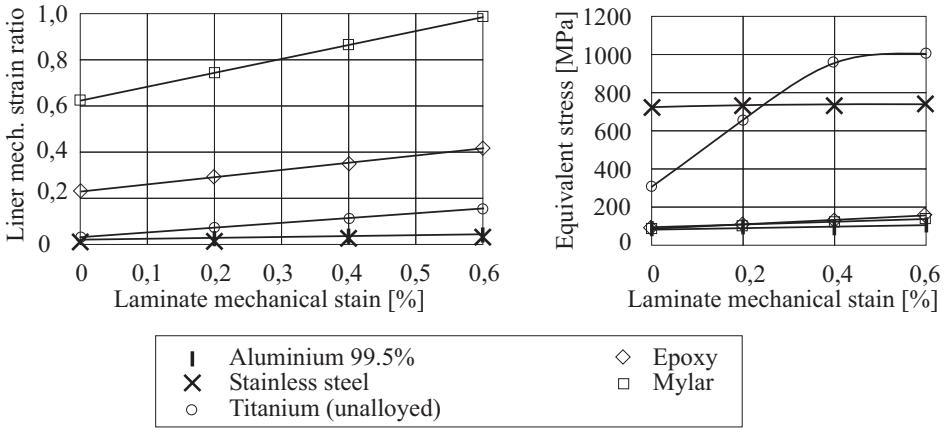


Figure 24: FE analysis results. Liner equivalent stain ratio (left) and stress (right) as function of laminate mechanical strain

First, all metallic liners, namely steel, titanium and aluminium, are forced to work in plastic range. Titanium, because of its relatively low CTE, behaves elastically up to 0.4% laminate mechanical strain, while aluminium and steel reach the yielding point already during cooling down. At the same time titanium experiences the highest stresses, because it has the highest yield stress among the candidate metals. Among metals, unalloyed aluminium is the one which possesses the lowest yield stress, thus it also experiences one order of magnitude lower stresses than the other two materials. All three metals work at strain levels which are far from failure, because their cryogenic behaviour is characterised by a wide plastic range (see table 10 for reference). Plastics have been modelled as linear materials, because their behaviour at 20 Kelvin shows negligible yielding. All plastics develop smaller stresses than metals, with the exception of unalloyed aluminium, because their stiffness

is one order of magnitude smaller than that of metals. The fact that they do not yield up to failure forces them to work in elastic range. For that reason the ratio among liner actual and failure strain is higher than that for metals. Particularly sensitive to this problem is epoxy: it has a very high CTE and low failure strain at cryogenic temperatures and for that reason it is forced to work at strains close to failure. Mylar is not affected by this problem in the same extent than epoxy because its coefficient of thermal expansion is sensibly lower than that of epoxy and because its failure strain at cryogenic temperature is considerably higher. Anyway the very basic difference between the behaviour of plastics and metals, that is the fact that metal yields at the first thermal cycle while plastic do not, may be reason for poorer performance of plastic materials as liner when several cycles are considered during total tank life time.

# 6 Measurement of composites strength

## 6.1 Introduction

As there is a general lack of failure data for FRPs laminates in cryogenic applications an investigation on the reliability of failure predictions with respect to the real behaviour has been carried out. Together with the fundamental question if failure mechanism at cryogenic temperatures is driven by the same phenomena which control the behaviour at room temperature, and thus if prediction for the UD laminate are correct, the question if so called "constraining effects" still have considerable influence on ply failure at these temperatures is of primary importance for permeability of laminates. Cross ply laminates show at room temperature a dependence of inter fibre crack onset in $90^o$ ply on its thickness and stiffness compared to $0^o$ ply stiffness

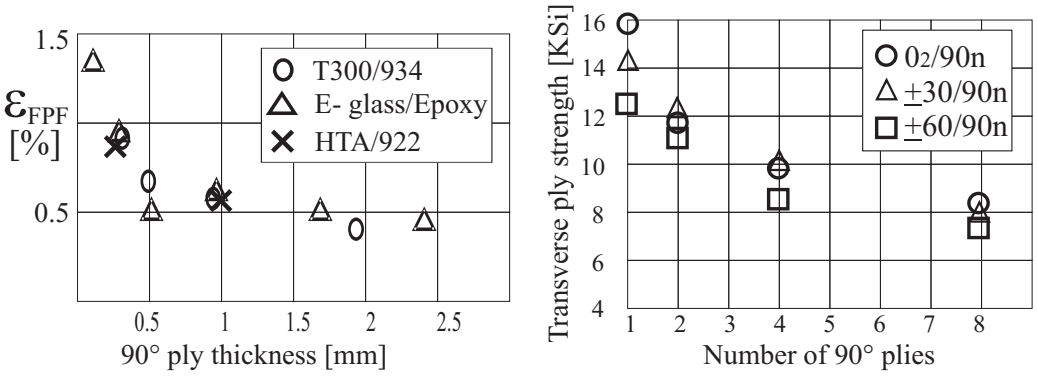


Figure 25: Constraining effect in symmetric cross ply laminates (from [50] and [51]). Dependence on $90^o$ ply thickness (left) and on stiffness ratio between constraining and constrained plies (right).

Such an interaction leads to first ply failure strains approaching 1% for CFRP cross ply laminates with very thin $90^o$ plies, while the failure strain reduces and reaches that of unconstrained plies as $90^o$ ply thickness increases, as figure 25 (left) shows. Constraining effects also depend on the stiffness ratio between constraining and cross plies: thus the effect of $\pm 30^o$ plies on the inlaminated cross plies is lower than that of $0^o$ because their stiffness in X direction is also lower (whereas X represents the direction of load). Successful modelling of these phenomena has been reported in the literature only for laminates having $90^o$ plies respect to load direction. These theoretical models resort to a simplified stress analysis and a fracture mechanics approach. The application of conventional failure criteria together with a two dimensional

stress analysis is reported to underestimate crack onset load. Nevertheless these increase of cross ply crack onset stress may play a crucial role for the impermeability of composite laminates under two- dimensional tensile loads. Haberle ([32]) claims a general similitude of failure behaviour at room and cryogenic environment, which can be due to marked constraining effects in cross ply laminates, but his tests are affected by several sources of objective difficulties arising at very low temperatures (i.e. very low friction coefficients, brittleness of most materials) and he applies a degradation model which needs an inverse procedure to derive the "apparent" stiffness of the degraded (cracked) ply from global laminate stiffness. These uncertainties put the results shown in that work into question. Moreover, as experimentally assessed in [29], transverse ply cracks affect mainly laminate Poisson's ratio, while their influence on laminate stiffness is negligible, thus their detection based on measurements on laminate stiffness may be unreliable. Despite these considerations, some works, like [49], report a substantial constraining effect in transverse cracks onset on $[0/90_2]_S$ IM7/977-3 cross ply laminates in liquid nitrogen. According to these works, transverse crack onset at cryogenic temperature is initiation controlled, even for thin laminates, while propagation along specimen width occurs without arrest when tensile load is kept constant. Results for the investigated material show a crack onset strain reaching 1% in the $90^o$ plies, which is substantially more than the failure strain of unconstrained material. In [33] a fracture mechanics approach has been used to calculate room and cryogenic temperature energy release rates of several FRPs materials and thus make predictions on their load carrying capability under cryogenic conditions. Experimental results, which validated the analytical approach showed a considerable increase in energy release rate at cryogenic conditions, which can explain why fracture propagates without arresting. Yet, results shown in that work are opposite to those reported in [49], and, according to [33] load carrying capability dramatically reduces down to almost zero at liquid hydrogen temperature. This important difference may partly arise from the different laminate layup and used material, which is quasi isotropic in the latter paper, but this rises concerns on the possibility to exploit constraining effects in order to enable higher pressure load in the tank without degradation of impermeability, as quasi isotropic laminate is likely to be chosen due to its much higher shear stiffness than a cross ply one. Two final points of primary importance for cryogenic unlinered tanks must be addressed: first all assertions on constraining effects are essentially based on unidirectional tests, while stress state in a tank structure is mainly bidirectional. Effects of a tensile component in perpendicular direction (t.i. fibre direction of the $90^o$ ply) have not yet been investigated. Second, when service life is considered, micro crack formation is load cycle

dependent and the issue must be faced from a load history point of view.

## 6.2 Test laminates

A test program has been conceived in order to investigate the following points:

- CFRPs effective failure behaviour at room and cryogenic temperatures and to gain failure data
- to investigate failure models and test the reliability of their predictions. Here classic (max stress), quadratic (Tsai- Hill, Tsai-Wu), physical based (Puck) failure criteria have been considered together with fracture mechanics models (comparison is carried out in chapter 8).

Definition of suitable test laminates is driven by the need to reproduce a state of stress similar to that of a real tank wall. this is generally characterized by positive principal mechanical load components which generate a plane state of stress in the regions of the laminate not close to openings or connections to other structures. This state of stress induces on the UD lamina positive $\sigma_1$ and $\sigma_2$, together with a in- plane shear $\tau_{12}$ component (see also chapter 8). Most failure models describe IFF and crack onset as effect of $\sigma_2$ and $\tau_{12}$, while fibre stress has an important effect only when it is close to the failure value.

| Laminate | Lay-up |
|---|---|
| 1 | [90/0/90/0]s |
| 2 | [60/0/-60/0]s |
| 3 | [40/0/40/0]s |
| 4 | [90/0/90$_3$/0]s |
| 5 | [$\pm$35/90/$\pm$35]s |

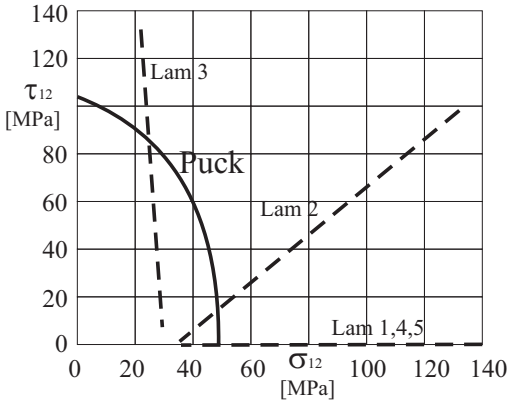


Figure 26: Laminate layup and projection on $\sigma_2$ - $\tau_{12}$ plane of their load paths for increasing tensile laminate strain.

In typical applications, when strain in fibre direction is under 0,5%, $\sigma_1$ has limited or no influence on static IFF, thus unidirectional tensile tests can

be conducted in which only a relevant $\sigma_2$ and $\tau_{12}$ are generated by means of a universal test machine. After numerical analysis five laminates have been chosen. Figure 26 shows projection on $\sigma_2$ - $\tau_{12}$ plane of the load paths for the chosen laminates. Puck's criterion is also reported as representative for classic failure criteria. In fact differences among failure criteria in the considered portion of the stress space are only minor, so that the Tsai-Hill or Tsai-Wu failure curves overlay quite precisely Puck's one and do not need to be further considered. Laminates 1, 2 and 3 have been chosen in order to generate three different load paths and investigate the behaviour under pure $\sigma_2$ (laminate 1) and a progressive bigger shear component (in laminates 2 and 3). Laminate 4 has been conceived to investigate the effect of the thickness of the $90^o$ layer on crack onset load. Laminate 5 has no $0^o$ layers which are replaced by angle plies having lower stiffness in X direction, thus it is suitable for the investigation of the effect of the stiffness of longitudinal plies. All laminates, except number 5, are characterized by unconstrained facesheet plies and constrained plies laminated with the same angle. In this way it is possible to compare constrained to unconstrained outer plies on the same specimen and thus reduce experimental effort and measurement uncertainties.

## 6.3 Test program and procedure

The search for micro cracks has been carried out by application of micrography to tested specimens. Because it is not possible to know a priori at which strain cracks form, a two-step test program has been defined as shown in figure 27.

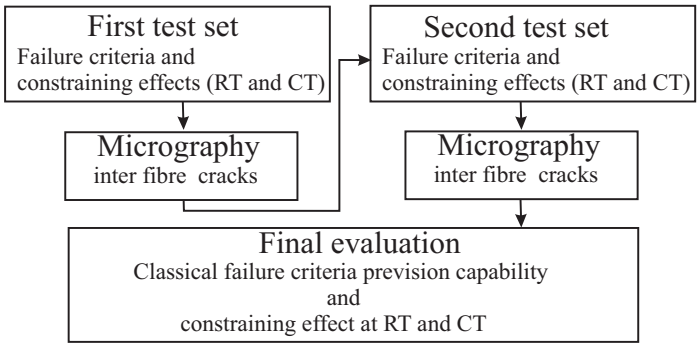


Figure 27: Schematic test procedure for micro crack detection

In the first step a set of test strains has been calculated for each laminate starting from values immediately below those given by failure criteria and

increasing them up to whole laminate failure in 0,2% steps. By means of this first test array the critical strain intervals for each laminate could be identified and a second set of tests could be defined in order to better delimit actual IFF failure strain. Tests have been conducted in an INSTRON universal test machine by clamping the specimen ends in the jaws and immersing the setup into liquid nitrogen which provided a test temperature of 77 Kelvin (CT tests). Strain is applied at constant slope up to the foreseen level and than kept for 60 seconds before unloading with the same slope. Three segments from the specimens central portion are cut after testing and prepared for micrography (see figure 28).

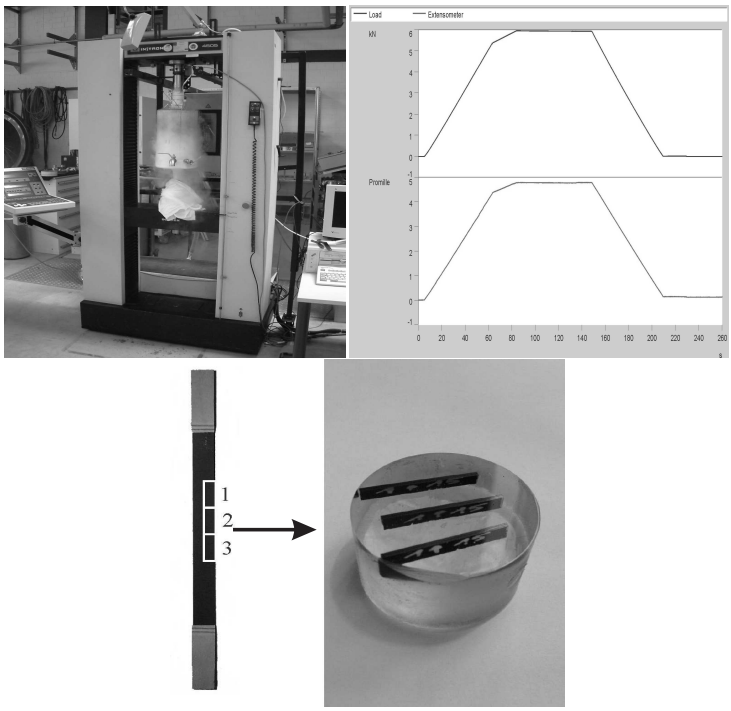


Figure 28: Test procedure for micro cracks research: specimen test, cut and imbedding of three central specimen sections

## 6.4 Experimentally measured crack onset strains

Experimental results show a complicate failure behaviour dependence on geometric parameters and physical test conditions. Among geometric parameters considerable influence on IF onset strain is exerted by:

- Constraining effect: presence or absence of constraining plies

- Constrained ply lamination angle
- Constraining ply stiffness
- Thickness of the constrained ply

Crack onset strain is also dependent on test temperature, because the much greater thermal load, affecting the laminate in cryogenic environment, sensibly reduces the crack onset strain at cryogenic temperature respect to room temperature (see following figure 11).
Test results and single effects will be more thoroughly discussed in the following sections.

### 6.4.1 Constraining effect

A significant difference among crack onset strain has been measured between the constrained and the surface angle plies of a laminate. Table 11 shows a comparison of the applied mechanical strain ("laminate tensile strain $\epsilon_0$" in the table) at which inter fibre cracks have been detected for the inner and outer plies of laminates one and two. The lower and upper boundaries delimit laminate mechanical strain intervals for crack formation as measured during tests.

| | Laminate tensile strain $\epsilon_0$ [%] | | | |
|---|---|---|---|---|
| | RT | | CT | |
| | lower boundary | upper boundary | lower boundary | upper boundary |
| Lam 1 facesheet | 0,588 | 0,688 | 0,128 | 0,228 |
| Lam 1 inner ply | 0,988 | 1,218 | 0,478 | 0,628 |
| Lam 2 facesheet | 0,719 | 0,868 | 0,176 | 0,326 |
| Lam 2 inner ply | 0,868 | 1,016 | 0,623 | 0,772 |

Table 11: Crack onset laminate strain in dependence on ply position. Crack onset is delayed to higher mechanical strains in inner plies

The difference among outer and inner (constrained) plies is clearly visible in both laminates 1 and 2: cracks develop at considerably higher laminate strains in constrained than in unconstrained plies.
From a point of view of the physics behind this phenomenon of crack onset and propagation, a possible explanation of the different failure strains between constrained and unconstrained plies can be sought in the interference

exerted by constraining plies on crack growth. In UD 90 laminates no constraining takes place and a the microscopic flaws (for example fibre matrix debondings or edge defects) grow in an instable manner as soon as the UD strength is reached. In laminates where angle plies are surrounded by constraining plies, these influence the rate of growth of initial flaws, thus cracks propagation is stable. Second, stress initially carried by the matrix in the crack region must be transferred to the adjacent material. From this point of view a facesheet ply can be seen as a constrained ply of double thickness. Thus cracks initially start growing far from the constraining ply (on the laminate surface) and do not experience its influence.

### 6.4.2 Effect of lamination angle

Lamination angle has two important and opposite effects: at low lamination angles thermal mismatch between the $0^o$ and the constrained ply is smaller, thus constrained plies experiences smaller thermal strains in laminate 2 than in laminate 1. Constrained plies are subjected to shear together with tension strains when laminated at angles different from $0^o$ and $90^o$. For this reasons, constrained plies in laminate 2 experience a more complex state of stress than those of laminate 1. The shear component tends to open cracks according to opening mode 2, which superimposes to mode one and may produce significative cracks at lower laminate strains than when shear is not present. Results in table 11 show a reduction in crack onset strain at RT when lamination angle changes from $90^o$ to $60^o$, confirming the importance of additional stress components (namely shear). At CT the situation is opposed because of the far higher thermal load in the angle plies of laminate 1 ($90^o$ plies) respect to those of laminate 2 ($60^o$ plies).

### 6.4.3 Effect of stiffness of the constraining ply

Crack onset laminate strain for two different laminates having constraining plies with different stiffness are shown in table 12. Constraining plies are laminated at a $\pm 35^o$ angle in laminate 5 while at $0^o$ in laminate 1. The difference among their stiffness amounts to -82% at CT. This results in a 18% reduction of crack onset laminate strain in laminate 5 respect to the stiffer laminate 1. RT tests did not find cracks at strains under 0.8%, which represents a strain above the material allowable values and close to fibre failure strains. Thus it was decided not seek for the upper value delimiting the interval.

| | Laminate tensile strain $\epsilon_0$ [%] | |
|---|---|---|
| | lower boundary | upper boundary |
| Lam 1 RT | 0,988 | / |
| Lam 5 RT | 0,781 | / |
| Lam 1 CT | 0,478 | 0,628 |
| Lam 5 CT | 0,413 | 0,513 |

Table 12: Crack onset laminate strain in dependence on constraining ply stiffness. Stiffer constraining plies in laminate one force crack to occur at higher mechanical strains

### 6.4.4 Effect of thickness of the constrained ply

Laminate 4, having three $90^o$ layer laminated between two $0^o$ plies, has been tested in order to analyse the effect of a thicker constrained ply in comparison to laminate 1. A marked reduction in crack onset laminate strain has been measured both at room and cryogenic temperature and reported in table 13. Laminate 4 presents the interesting feature of the same crack onset strain for inner and outer ply, both at room and cryogenic temperature (see table 14).

| | Laminate tensile strain $\epsilon_0$ [%] | |
|---|---|---|
| | lower boundary | upper boundary |
| Lam 1 RT | 0,988 | / |
| Lam 4 RT | 0,607 | 0,707 |
| Lam 1 CT | 0,478 | 0,628 |
| Lam 4 CT | 0,265 | 0,365 |

Table 13: Crack onset laminate strain in dependence on constrained ply thickness. Cracks appear at lower mechanical strains in thicker constrained plies

This result may be explained in terms of load redistribution from the crack region to the adjacent material. When angle plies are thin, the load will be transferred to the constraining ply already when flaws in the angle ply have small size. In thick angle plies the crack must reach a considerable size before its ends are enough close to the constraining plies to experience its discharging effect and thus reduce or stop growing.

### 6.4.5 Effect of test temperature

Test temperature affects crack onset strains both directly and indirectly by influencing the effect of constraining parameters. Direct influence consists in a general reduction of crack onset strain when test temperature is lowered from room to cryogenic. Reason for that is the enormous thermal load charging specimens in liquid nitrogen at $-200^oC$. This load alone produces apparent strain components perpendicular to fibres up to 0.6% in all plies of laminate 1 (value above the UD ply strength). Because of that there is a general flattening effect which reduces relative differences in failure strain at CT respect to RT. Thus failure strain in inner plies, with the exception of the thick inner plies of laminate 4, tend to accumulate around the value 0,4-0,5%, while in outer plies around 0,15-0,35% (see table 14).
In laminate 4, where the $90^o$ inner plies are thick, there is no difference both at RT and CT between the crack onset laminate strain of the inner and outer plies.

| Laminate | Laminate strain $\epsilon_0$ [%] | | | |
|---|---|---|---|---|
| | Experimental results (RT) | | Experimental results (CT) | |
| | Outer ply | inner ply | Outer ply | inner ply |
| 1 | 0,588-0,688 | $> 0,988$ | 0,128-0,228 | 0,478-0,628 |
| 2 | 0,719-0,868 | 0,868-1,016 | 0,176-0,326 | 0,623-0,772 |
| 3 | $> 0,85$ | $> 0,85$ | | |
| 4 | 0,607-0,707 | 0,607-0,707 | 0,265-0,365 | 0,265-0,365 |
| 5 | | $> 0,781$ | | 0,413-0,513 |

Table 14: Effect of test temperature on first ply failure strains in the inner and outer plies

The indirect effect lies on slight modification of stiffness ratios among constraining and constrained plies: increase in stiffness is much more pronounced in direction perpendicular to fibre than in fibre direction. Thus the stiffness ratio diminishes at CT.

# 7 Measurement of composites permeability

## 7.1 Cryogenic permeability test setup

### 7.1.1 Purpose of test facility and program

The experimental activity at the Chair for Lightweight Structures (LLB) has been mainly characterized by the development of a cryogenic permeability test setup, within the MFOS project, financed by the European Space Agency (ESA). The several purposes, which have driven the activities and hinged on cryogenic tank and tank sensors topics. Among them, those relevant for the present work are summarized in the following list:

1. Provide a low cost device to reproduce and apply cryogenic tank loads, that is those due to pressure of contained fluid and cryogenic temperature, to a tank- shaped specimen of relatively low size and bulk

2. Investigate FRPs behaviour under cryogenic environment and mechanical loads occurring in tanks, as at point 1. In particular the effect of gas pressure and tank characteristic dimensions (i.e. tank radius) on permeability has to be clarified

3. Assess possible onset of micro- cracks in laminated structures due to thermo-mechanical loads

4. Investigate the correspondence among analytical models and simulation to real FRPs behaviour under thermal and mechanical conditions which occur in a cryogenic tank.

5. Investigate FRPs capability to carry a cryogenic fuel under inner pressure and compare it to that of metals, to asses the real FRPs potential in allowing weight savings in cryogenic liquid storage systems

6. Investigate FRPs behaviour under repeated thermo- mechanical loads, like those occurring in a non spendable structure. Degrading of FRP load capability, that is increase of permeability, has to be related to number of cycles and mechanical load

### 7.1.2 State of the art in permeability testing

Experimental activity in permeability measurements has increased in the last years, after application of CFRPs to cryogenic tanks has revealed the only mean to achieve sufficient weight savings necessary for a SSTO vehicle. Despite that, until now there are no reports assessing successfully operation of a

cryogenic permeability test facility conceived to test specimens of moderate dimensions and still representative of a tank wall. NASA Langley Research Centre designed the first cryogenic permeability test setup with the aim to test a hemispheric composite specimen at $LN_2$ and $LH_2$ temperature [15]. The developed concept consists in sandwiching the test article in between two hemispheric metal shells in order to create two volumes. On one side a pressure is generated by a cryogenic liquid, which contemporarily provides the cooling mean for the specimen. Test article and metal shells are provided with flanges where two ring gaskets are applied in order to seal the junction. If leakage occurs through the CFRP wall, gaseous molecules accumulate on the other side of the specimen and are detected by a mass spectrometer. No results have been ever published in which the test setup is successfully applied and the following permeability facilities used by NASA at Langley is not designed for a cryogenic environment at all. In [13] a room temperature permeability test facility is far more modest in capability and purposes, being composed of two simple flat metallic plates through which a flat specimen is sandwiched. A gas line introduces the test gas on one side of the specimen and again a vacuum pipe conducts from the second plate to a mass spectrometer for helium permeability assessments. This apparatus was developed with the aim to assess room temperature polymers permeability as pre- investigation o the possibility to exploit them as barrier materials. In [14] a room temperature permeability test setup is used to compare permeability measurements to an analytical model. No cryogenic environment is realized, but a two axial tensile stress state is generated in the specimen by mechanically stretching the specimen in two directions. Again the cross shaped CFRP laminated specimen is used as wall to separate a volume into two parts, one of which is filled by the test gas and the other is the vacuum chamber where the mass spectrometer is attached. No details are given on the sealing method but, even in this case as in [15], there is a relative displacement between specimen and the two metallic walls in the area where the sealing or gasket shall be applied. In [18] a more complicated permeability test facility has been developed for cryogenic testing of FRPs. A flat CFRP circular specimen is placed between the flanges of two steel tubes in order to generate two volumes. The specimen is sealed by means of two indium circular rings placed between each flange and the CFRP specimen. Indium is used, despite its difficult handling and cost, because of the need to provide sealing at very low temperatures. The whole assembly is placed in a cryostat, whose temperature is regulated by liquid helium flowing in a heat exchanger inside it (vaporization cryostat). By regulating helium mass flow it is possible to cool down to and keep a desired temperature between RT and 4.2 Kelvin. This represents the most flexible solution among all, because it

allows testing by several temperatures, but it also imply a very high financial effort, both for the hardware and for the cooling mean. Furthermore it relies upon the availability of liquid helium and a liquefaction facility in order to keep helium cost low. Again, despite the available hardware, only few test results at temperatures under 203 Kelvin ($-70^oC$) have been published.

### 7.1.3 Test setup concepts evaluation

As sum up of the available literature, all permeability test facilities are characterized by clamping the CFRP specimen between two flanges and sealing it by metallic or plastic gaskets. Where a two axial stress state is needed, it is achieved either by gas pressure acting onto a specimen of apposite cambered form, or by directly applying a tensile load in two directions to the specimen. Third, the cryogenic temperature is achieved either by the test gas itself, or by a cooling mean which circulate in a heat exchanger inside the conditioned chamber. These concepts have been the base and starting point for the development of an enhanced permeability test setup at LLB. Since one of the goal is to reproduce a test temperature which is as close as possible to liquid hydrogen temperature, but also to minimise costs, a vaporization cryostat, in which a cooling liquid circulates, has been discarded. The only remaining possibility is to use a bath cryostat in which the test setup is immersed. Cooling liquid has to be chosen among $LH_2$, $LN_2$ and LAr. Gas properties of the three candidates are listed in table 15. Both hydrogen and Argon have been discarded because of costs considerations, whereas handling and hazard problems arise for hydrogen as well. Nitrogen represents a good compromise because it is relatively safe gas, cheap to achieve in liquid form and have a very high cooling capability per unitary volume. Furthermore liquefaction temperature for nitrogen is not that higher than that of hydrogen, namely 77 Kelvin against 20 Kelvin for liquid hydrogen.

| Name | Liquid density $[Kg/m^3]$ | Normal boiling point $[K]$ | Latent heat $[KJ/Kg]$ | Gas type |
|---|---|---|---|---|
| Argon | 1392 | 87 | 160,81 | inert |
| Helium | 124,96 | 4,2 | 20,3 | inert |
| Hydrogen | 70,97 | 20 | 454,3 | flammable |
| Nitrogen | 808,67 | 77 | 198,38 | inert |

Table 15: Cryogenic liquids, their boiling point and latent heat of vaporization. Because of a favorable liquid density and latent heat combination, $LN_2$ is the most effective cooling mean.

Sealing has to be assured down to very low temperature and because of that only a Indium wire, which is the standard demountable sealing used for cryogenic purposes, is suitable to be applied. Despite its high purchase cost, Indium wire offers the possibility to be regained after proper cleaning, thus a relative modest supply reaches even for a high number of tests. Nevertheless no relative displacements between specimen and metallic fixtures in the sealing area can be allowed, because it may provide leak paths and thus affect permeability measurements. This consideration also affects the way to produce a two axial stress state on the specimen: in no way an external mechanical tension shall be applied to specimen ends, again to avoid any relative displacement in the region where the sealing is applied. Consequently specimen has to be spherically shaped and a pressure must be exerted on one of its surfaces. This choice introduces manufacturing complications for the specimen, but it reduces the complexity of the test setup and thus costs. Gaseous helium has been chosen as permeation mean because of several main advantages: it is an inert gas, thus eliminating any major handling hazard. It is an atomic gas which molecules are smaller than molecular hydrogen. As result helium permeability is higher than that of hydrogen, leading to conservative results, thus it may be applied at the place of hydrogen with a high confidence to achieve representative results. Helium liquefaction temperature is far below that of liquid nitrogen and even liquid hydrogen, thus allowing its exploitation as permeation mean even at very low temperatures. Last, but not least, helium gas is commonly available on the market.

### 7.1.4 Test setup schematics and general description

A schematic drawing representing the basic components and functional groups of the test facility is shown in the following figure 29. Functional principle of the device is, as in almost all examined cases, the generation of a gas pressure into a pressure chamber of which CFRP specimen materializes one wall. The specimen also separates the pressure chamber from the vacuum chamber in which possible leaking particles are collected to be sucked by the helium leakage detector. Three main groups may be identified in the scheme:

- Gas feed and dosage unit, which feeds the pressure chamber with gaseous helium and allow pressure cycles from 0 to 10 bar.
- Cryogenic chamber and specimen fitting, where a test article is clamped and cooled down to 77 Kelvin.
- Leak detection unit, to collect leaked particles and measure permeability.

A detailed description of the three main parts of the test setup follows.

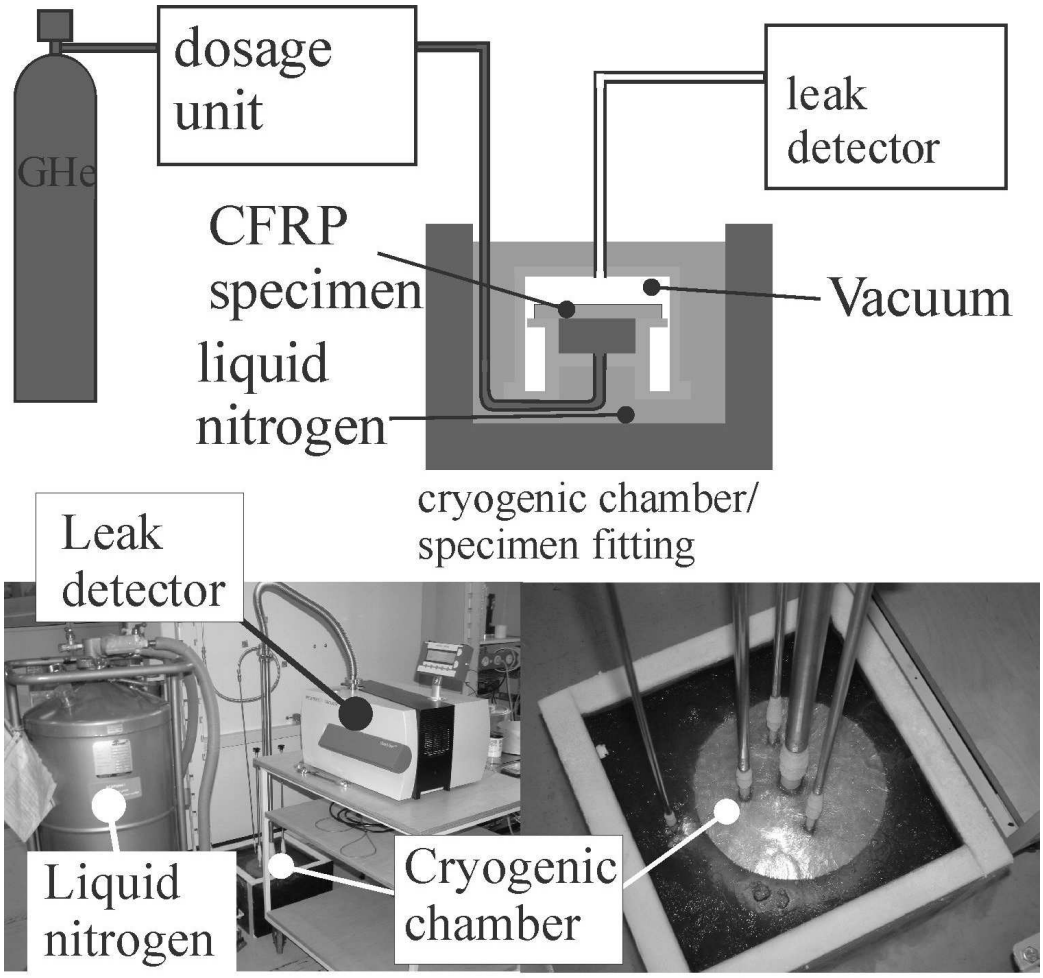


Figure 29: Permeability test setup schematic drawing (simplified) and picture. Three functional groups are helium feed and dosage unit, cryogenic chambers and specimen fitting and leak detection unit

### 7.1.5 Gas feed and dosage system

The gas feed line and valves are shown in figure 30 together with the vacuum side of the feed unit. Their task is to supply gaseous helium to a pressure up to 10 bar into the pressure chamber and allow emptying at the end of the experiment. Gas is stored at room temperature in a gas bottle at 200 bar pressure. The high pressure line directly conducts to the pressure chamber

and is provided with a pressure reducer, a pressure controller and a fine regulation valve, provided by Messer Grissheim, which allow setting pressure with a precision of 1/100 bar. Pressure in the high pressure pipes is monitored by a pressure sensor and through a computer program but setting is manual. A overpressure valve prevents pressure loads in the pipes from exceeding the design value of 12 bar. Furthermore an outlet valve is available in order to allow pressure cycles and reduce pressure at the end of the test. Gas feed can be interrupted by a shut off valve placed forward the outlet valve, if necessary. All pipes are 6 millimeter diameter stainless steel tubes, compatible with liquid hydrogen and very low temperatures and are joined together and to the valves by Swagelok high pressure fittings.

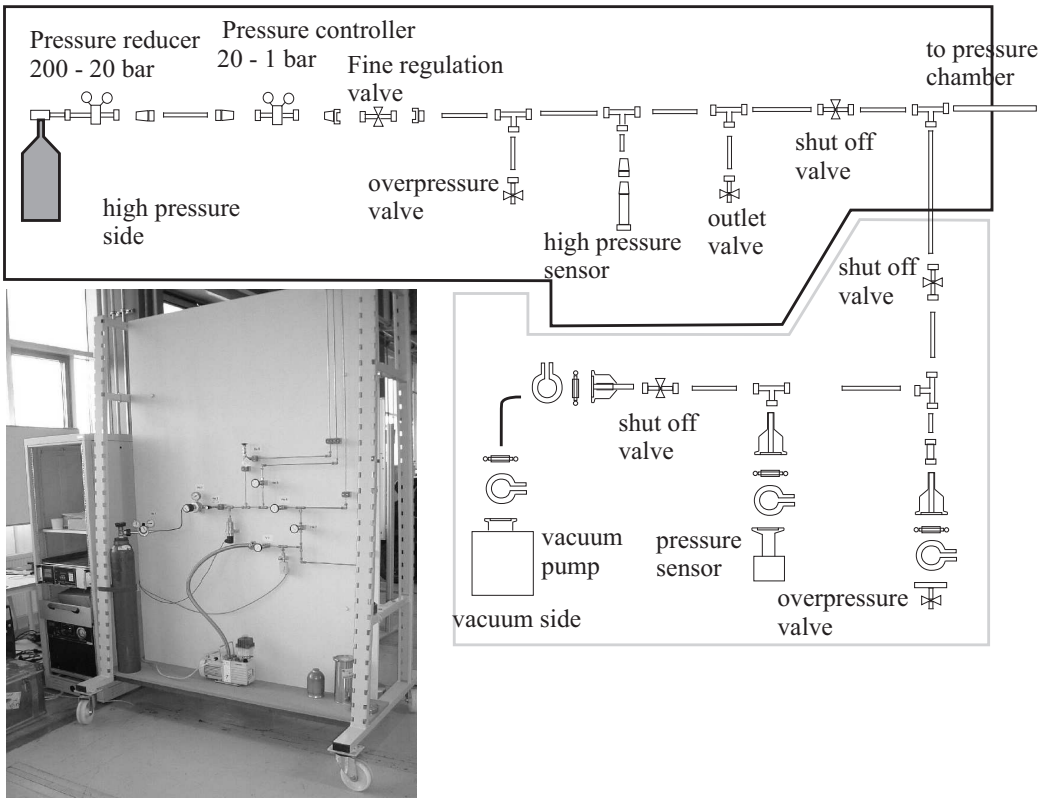


Figure 30: Helium gas feed line and vacuum side of the test setup.

Air in the pipes and pressure chamber must be pumped out before the temperature is lowered because at liquid nitrogen temperature a liquid phase could accumulate into the pressure chamber and disturb the test. To this purpose the system has been provided with a vacuum pump driven side. This pump is able to reduce inner pressure down to a fraction of millibar, which

is measured by a low pressure sensor. The low pressure shut off valve is used to separate the vacuum part of the system from the high pressure part when helium is introduced into the pressure chamber. Anyway even this part of the system is provided with an overpressure valve, which opens if 1.2 bar are reached.

### 7.1.6 Cryogenic chamber and specimen fitting

The task of holding a CFRP specimen in a cryogenic environment under a gas pressure is accomplished by pressure chamber of which the specimen materializes the upper wall. A detailed picture of the specimen fitting is shown in figure 31

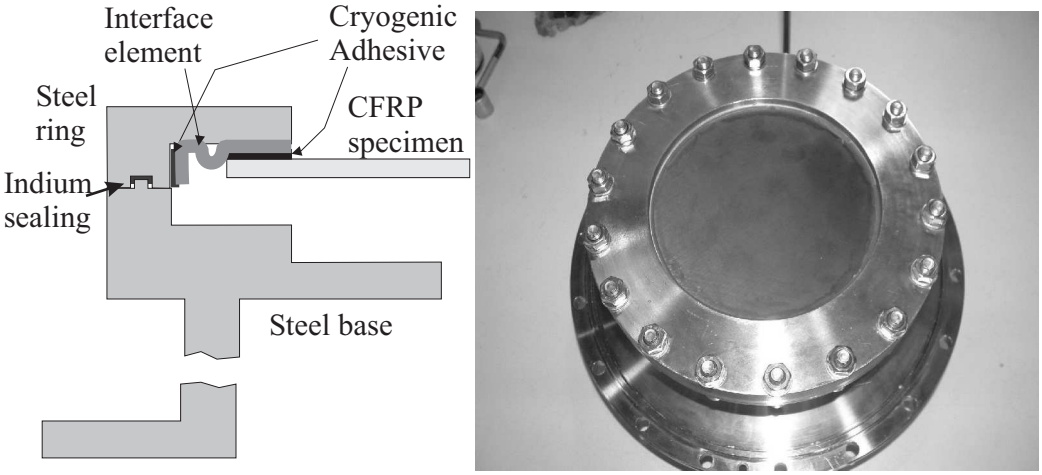


Figure 31: Schematic drawing and picture of the pressure chamber and specimen fitting.

Pressure chamber made of AISI 316-Ti austenitic stainless steel, which is suitable for cryogenic applications. It provides mechanical properties (fracture toughness and failure strain) compatible with cryogenic environment and is a material relatively cheap and available on the market. The chamber is designed to be disassembled in two parts in order to remove and replace the specimen. The lower part is entirely made of steel and connected to the helium bottle through a 3 millimeter tube. The upper part is composed of a steel ring of the same material, to whom the test article is joined. Steel ring and steel base are joined together by 18 bolts and sealed by an Indium wire, which is placed in a circular groove having rectangular section. The working principle of the indium seal is based on local micro- welding of the wire to

the two parts to be sealed. Pressure generated when the bolts are tightened is transferred to the wire through a feather in the steel base and plastically deforms it to occupy the free volume between groove and feather. Thus microweldings occur among indium wire and steel which keep the joint tight. If relative displacement between the two flanges occurs, these microweldings are broken and the bonding is no more tight. For that reason preventing relative displacement between the flanges is an issue of primarily importance. Under the very high thermal loads occurring during cooling down to cryogenic temperatures, these issue can be fulfilled only if materials have compatible CTE.

### 7.1.7 Specimen to steel ring - joint

The joint between test article and steel ring must fulfil two tasks: be impermeable and carry tensile loads which occur due to difference in CTE of the two materials. Adhesive bonding is the only joining technique which can provide an impermeable joint between metals and CFRPs, but from the point of view of thermal loads it does not represent the optimal choice. Thus it has been necessary to place an interface element between specimen and steel ring with the aim to comply with the two different thermal deformations without overloading the adhesive bonding. This purpose has been achieved by choosing a suitable material and forming the element into an appropriate shape. Unalloyed aluminium revealed a good choice because of its very high failure strain at cryogenic temperatures and low yield stress, summarized in the following table 16, because it is an impermeable material and can easily be formed into complicated shapes

| | Temperature$[Kelvin]$ | | |
|---|---|---|---|
| | 293 | 77 | 4,2 |
| Yield stress $[MPa]$ | 48 | 120 | 137 |
| Failure strain [%] | 46 | 56 | 54 |

Table 16: Typical yield stress and tensile elongation for unalloyed aluminium at several cryogenic temperatures.

The interface element is showed in figure 32. The vertical wall is bonded to the steel ring, while the horizontal one to the CFRP specimen (see also figure 3). These two parts experience the high relative displacement during cooling down. The central bulged section acts as load damper insofar it allows such a displacement without causing high forces. Despite the form, strains occurring on the interface element reach 2.6% in the bulged section, thus requiring a

material with very high failure elongation and low yield stress, in order to keep transmitted forces low.

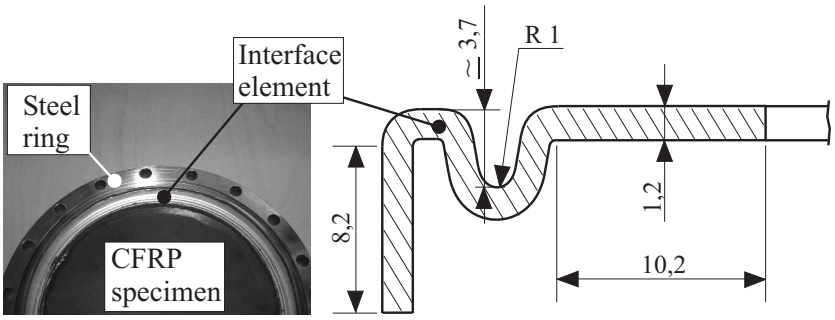


Figure 32: Interface element and its section. Bulged section contributes to keep stresses low while allowing deformation.

### 7.1.8 Permeability test specimen

Leakage specimen is shown in figure 5 together with a quarter CAD model, while geometric parameters are summed up in table 17. Two regions can be identified: a central bulged part and an outer flat flange. The two are connected through a radius (R1 in figure 5) which provides a smooth transition. The central bulged part is the actual test article, because it is the place where thermomechanical loads are supposed to produce cracks and where the state of stress better represents that of a sphere. The double cambered form has been chosen because of axial symmetry of the pressure chamber and its double curvature is kept moderate because of the need to apply prepreg technology for manufacturing the test article.

| $\Phi_1[mm]$ | $L_1[mm]$ | $R_m[mm]$ | $R_1[mm]$ |
|---|---|---|---|
| 156 | 10 | 450 | 10 |

Table 17: Geometric parameters of the permeation specimen and values chosen after trade off analysis.

A moderate curvature also represents an effective mean to help generating a state of stress which shall approximate that of a sphere as much as possible, as described in the following sections. The flat outer ring is used to bond the specimen to the interface element. Bonding length, $L_1$ in table 17 and figure 33, is constrained by the need to have a central bulged part as big as

possible and the outer dimension of available round bars used for the pressure chamber.

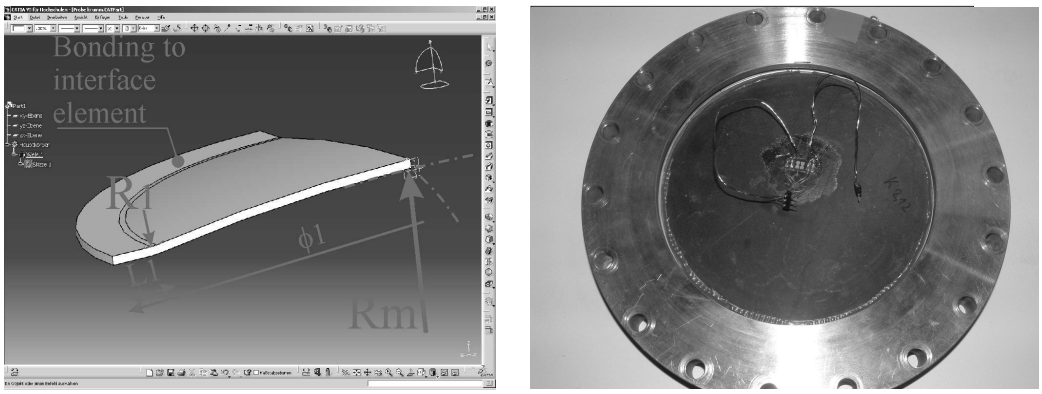


Figure 33: CAD quarter model and picture of the bulged specimen for permeation tests.

Specimen form has been chosen with the aim to produce a tensile state of stress by means of test gas pressure in the pressure chamber. According to equation 24 ($\sigma = \frac{PR}{2t}$) of chapter 9, the highest stress in the specimen is proportional to bulk radius and inner pressure, while inversely proportional to specimen thickness. Thus these three parameters have to be appropriately chosen in order to get stress states comparable to those occurring in tanks. Specimen thickness is to be chosen in a reasonable range of values: too thin specimens are not tank wall representative, while a too thick one would necessitate a too high gas pressure in the pressure chamber. Thus a design value of 1 millimeter well fits the purpose, representing a reasonable value for a CFRP tank. Gas pressure is constrained by two considerations: it affects system components costs, in that pressure pipes and valves have to be stressed for the chosen operating pressure. On the operating side a high pressure is desired, because specimen bulk radius may be kept low while high stresses occur in its wall. Anyway safety reasons induced to renounce too high pressures and a good compromise has been found by choosing a design value of 10-12 bar. Concerning specimen bulk radius, it has an almost proportional influence on ply stresses, and thus it should be as big as possible. A second point to be discussed is the effect which bulk radius has on bending stresses, which arises due to stiffness differences among pressure chamber wall and CFRP specimen. These bending can not be neglected unless the whole pressure chamber is made of the same material. Stress dependence on specimen radius in the specimen central portion is shown in figure 34:

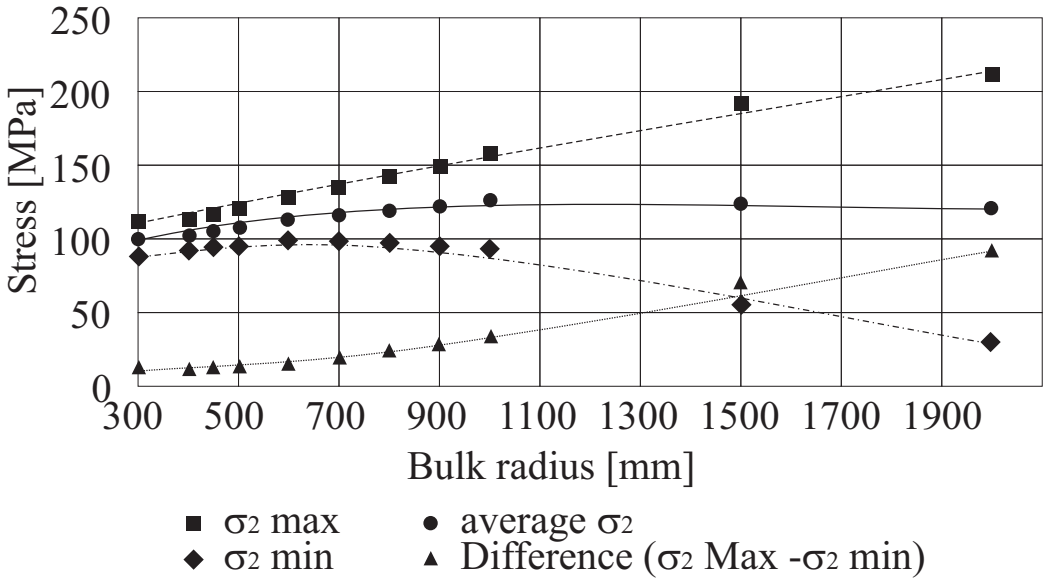


Figure 34: Stresses in the central portion of the CFRP permeability specimen in dependence on its bulk radius, for a 10 bar test pressure. The maximum and minimum stresses are respectively $\sigma_2$ stress components of the last (top) and first (bottom) layers. "Difference" is the difference between these two values due to bending and increases as bulk radius increases.

The stress state in the specimen under gas pressure and cryogenic temperature is due to the superposition of a membrane and a bending load. Bending stress represents a deviation from the ideal stress state which occurs in a sphere of same radius than the specimen and increases as specimen bulk radius is increased (flatter specimen). This bending component produces a stress difference between the inner and the outer specimen facesheet plies, which is shown as "Difference" line in figure 34. Membrane stress, on the contrary, decreases as specimen radius is increased. In the extreme case of a flat specimen, not shown in figure 34, no membrane stress is produced by gas pressure and stress distribution along specimen thickness is characterized by a change of sign, so that compression (negative) stresses are produced on one specimen surface having the same absolute value than tensions on the other surface. Furthermore, the stress state in the permeability specimen has another degree of inhomogeneity, namely it changes from the boundary, where specimen is bonded to the interface element, to the centre. This distribution is again generated by bending stresses which are bigger in the nearby of the boundary region (where specimen is bonded to the interface

element) and decrease toward the specimen centre. The bulk radius has an influence on the gradient of the bending stresses, so that they extend on a bigger specimen portion as the bulk radius increases. Figure 35 shows the influence of the bulk radius on stress distribution in the two facesheet plies. The region having stress component $\sigma_2$ bigger than 75 MPa extends from the centre outwards to the boundary. As figure 35 shows, the region of high tension stress reduces its extension as bulk radius increases. Thus bending damps farther from specimen centre when the bulk radius is smaller and, as figure 34 shows, this results in a smaller difference between stresses in the two opposite face sheets.

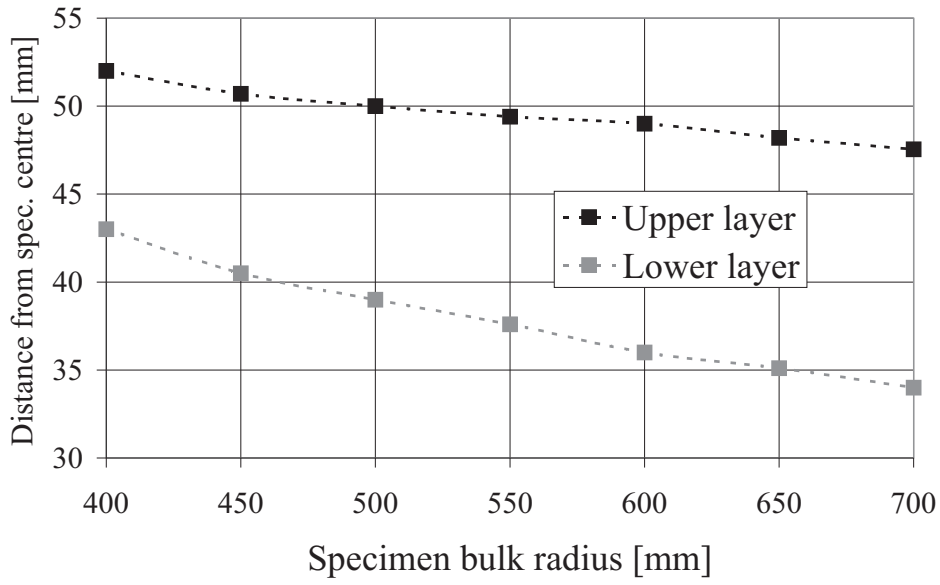


Figure 35: Extension from specimen centre of the region having stress component $\sigma_2$ bigger than 75 MPa as function of specimen bulk radius.

Compression stress components, arising when bending superimposes tension, are responsible for closing layers cracks and thus possible leak paths. As result, the measured permeability could be much lower than in the case of the whole tension stress state, where stress components are only positive and open cracks, as they form. For that reason stress state distribution in the specimen should be characterized by an extended central portion having high degree of constancy through the thickness and in which the average $\sigma_2$ is positive and as big as possible, at least bigger than the UD ply failure value at liquid nitrogen temperature. The last requirement affecting the choice

of the bulk radius is related to manufacturing aspects: because specimen has to be manufactured by standard prepreg and autoclave technology, the bulk radius should be kept as big as possible. These conflicting objectives have led to the compromise bulk radius of 450 millimeter. This value allows application of prepreg technology, while stress state through the thickness is enough homogeneous to assure a high $\sigma_2$ component in all plies on an extended central portion of the test article. A two layer stepped doubler has additionally been placed in the outer region of the specimen with the aim to further reduce stresses outside the central portion and thus help forcing highest stresses in the specimen centre.

### 7.1.9 Test setup qualification

Because the purpose of the test setup is to measure CFRP cryogenic helium permeability, it has been necessary to assess overall leak rate of the several junctions and sealing in operational conditions in order to verify:

1. If thermo mechanical load do not cause failure of the assembly or of one of its parts

2. If leakage through bonding and metal gaskets is negligible, compared to the expected values for CFRP.

Qualification tests have been carried out first using a steel cap to close the pressure chamber and then a 4 millimeters thick CFRP flat specimen in place of the bulged one. Results shown in figure 36 and 37 and following discussed. Figure 36 shows the room and cryogenic temperature helium permeability of the whole test setup when the pressure chamber is closed by a steel cap. The use of the steel cap assures complete thermal matching between the two parts of the chamber, thus provides the best performance of the indium seal. As figure shows, the leakage signal is approximately hundred times smaller at CT than at RT. Reason for that is mainly due to two factors: first, as temperature diminishes vacuum quality inside the vacuum chamber improves, leading to lower free molecules and thus a less intense signal. Second, metallic gaskets improve their effectiveness as steel parts contracts under thermal gradient, tightening the Indium seals.

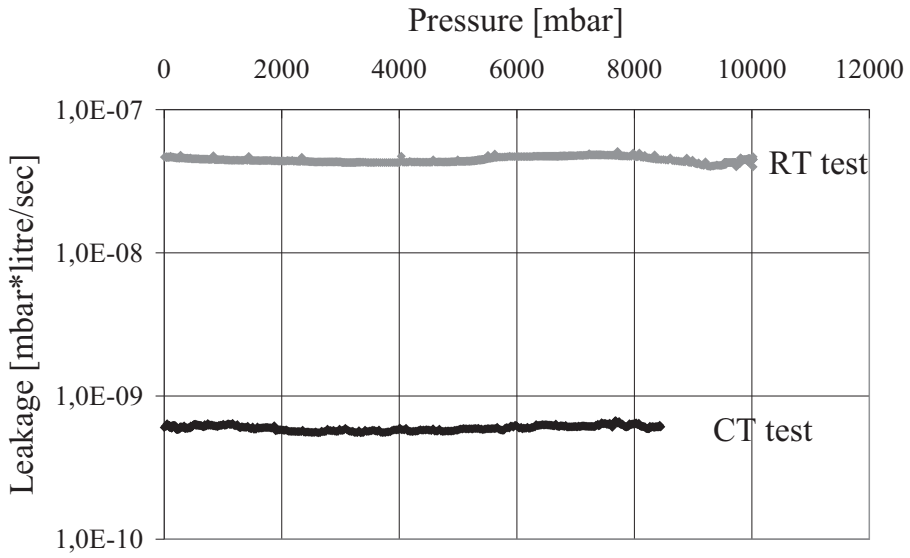


Figure 36: Relation among pressure and leakage at RT and CT with steel cap at the place of the specimen

A qualification test has been conducted with a CFRP specimen in order to test the aluminium interface element. The very thick (4 millimeters) CFRP disk, used in this test, produces a more severe load on the interface element than the foreseen 1 millimeter thick permeability specimens, when the test setup is cooled down to cryogenic permeability. Test results are shown in figure 37 (upper diagramm). Here the progressive reduction in leakage signal as temperature reduces is clearly visible in the upper diagram. After about 50 minutes in liquid nitrogen, leakage stabilizes to its final value, amounting to about $2,5 - 6 \cdot 10^{-10}$ $\frac{mbar \cdot litre}{sec}$, although the temperature has not yet reached 77 Kelvin. Four episodes of sudden leakage increase and immediate decrease occurred during the test. Their cause can be identified in a same number of particle releases from the inner steel walls into the vacuum chamber (outgassing). After each of them, leakage signal returned to the same value of $2.5 - 6 \cdot 10^{-10}$ $\frac{mbar \cdot litre}{sec}$. After leak and temperature had stabilized, pressure has been built up into the pressure chamber by one bar steps up to six bar. Each pressure step has been kept for 15 minutes without any detectable influence on the leakage signal. As last part of the test a dynamic pressure load has been applied to the pressure chamber by carrying out 10 pressure cycles, each of which having pressure extremes of

one and six bars. Load was applied with 1/30 bar/second slope. Even this load case did not have influence on the leakage signal.
The lower diagram in figure 37 shows the response of a defective bonding. The bonding did not provide a sufficient barrier to helium molecules and a clear relation between gas pressure and leakage was detected as typically when mechanical leak path occur.

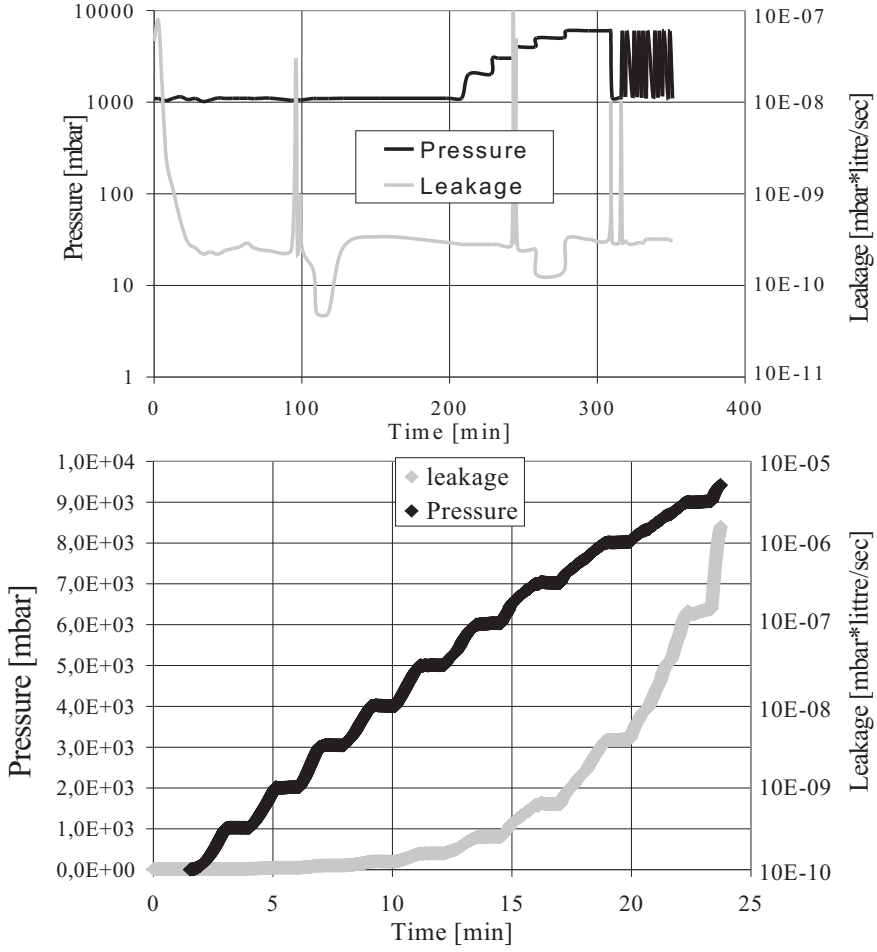


Figure 37: Test setup qualification. The signal from 4 millimeter thick specimen is shown in the upper diagram, while the lower one shows leakage signal through a defective bonding.

## 7.2 Permeation tests result and discussion

The permeability of IM7/8552 1 millimeter thick bulged specimens has been measured under a helium pressure from 0 up to 11,5 bar. The following tests have been carried out in order to investigate the suitability of this material to cryogenic containment:

1. Short duration leak detection in function of helium gas pressure at room and cryogenic temperatures
2. Leak detection in function of the number of thermal cycles (RT $->$ 77K $->$ RT)
3. Long duration leak test (10 hours under 10 bar pressure) at RT and CT

Test results are discussed in the following sections.

### 7.2.1 Leakage - gas pressure relation

Figure 38 shows the leakage signal at room and cryogenic temperature for the 1 millimeter thick CFRP specimen and the signal produced during the qualification test as reference (steel plug). Both at room and cryogenic temperatures there is no relation among helium gas pressure and leakage, for the whole duration of the test.

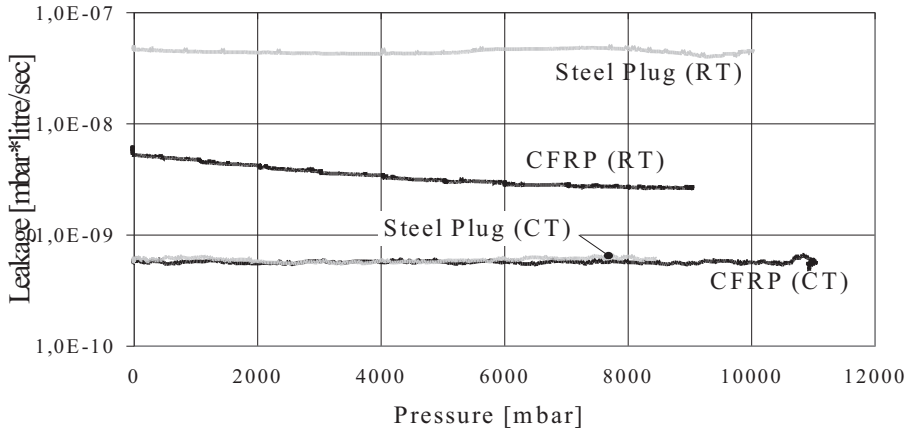


Figure 38: Leakage signal as function of gas pressure at room and cryogenic temperature

This means that if cracks occur, as pressure is risen up to 11 bar, no full leakage paths form through the thickness. Room temperature leakage, measured when the CFRP specimen is mounted, is lower than that measured with the steel plug. This means that the indium sealing worked better during the tests with the specimen and the measured signal was generated by helium penetrating the sealing or by free gas molecules in the vacuum chamber. This is confirmed at cryogenic temperature, where leakage with CFRP and with steel plug are equal. the consequence of this fact is that the measured signal is always generated by the sealing or by free molecules moving in the vacuum chamber, that is, the CFRP specimen has far higher impermeability. This partially agrees with the CFRP permeability values available in the literature and will be discussed below.

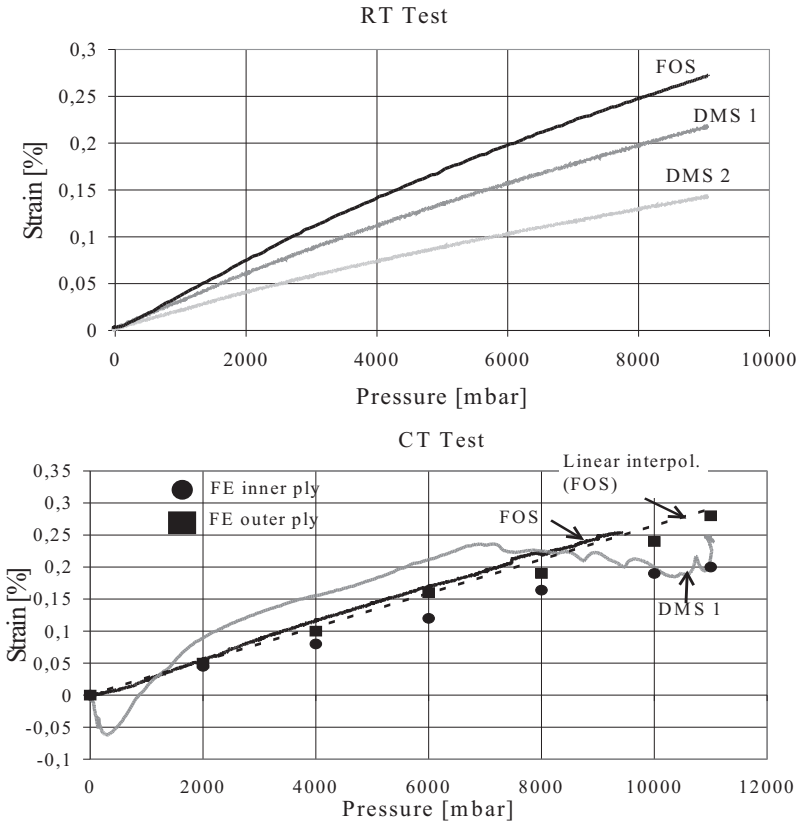


Figure 39: Strain measurements on the permeation specimen. DMS stands for resistive strain gauge, while FOS for Fibre Optic Sensor

Strain measurements have been carried out with strain gauges applied on the top and bottom of the CFRP specimen. Measured strain amounted to 0.23% - 0.25% on the outer side and 0.144% on the inner side of the specimen at room temperature and 9 bar pressure. The two different measurements on the outer side of the specimen are due to two different strain gauges: the higher signal was achieved by a fibre optic sensor, which was bonded on the specimen, while the lower by a conventional resistive strain gauge. At cryogenic temperature strain amounted to 0.25% on the outer side and 9 bar pressure. A measurement on the inner side was not possible because the combination of high pressure and thermal load destroyed the bonding between strain gauge and specimen. An extrapolation of the measured signal to 11 bar pressure led to strains up to 0.27% at CT on the outer side, which was also achieved by the FE simulation (see figure 39 for comparison). If the bending ratio is equal to that at RT the strain of the bottom layer shall reach 0.16% (which is a little bit lower than the 0.2% resulting from FE simulation) and the laminate average 0.2125% (0.235% from FE simulation). These differences may be caused by two factors: the different dimensions of the optic fibre sensor compared to the resistive strain gauge and the different adhesive used. The optic fibre is much more compact and thus able to measure punctual strains, while the resistive strain gauge could measure average strains over its not negligible surface. Second, because of its extension, it is more difficult to exactly place the resistive strain gauge, than it is for the optic fibre. The adhesive used for curing the optic fibre is stiffer than that used for the other sensor. This choice was driven by the need not to exceed $+85^oC$ during curing in order to avoid damages to the resistive strain gauge. An estimation of the CFRP permeability can be obtained from the measured leak rate:

$$P(T) = 10^{-1} \cdot \frac{Q \cdot t}{\Delta P \cdot A} \tag{7}$$

where: $P$ = permeability $[\frac{m^2}{sec}]$, $Q$ = leakage $[\frac{mbar \cdot liter}{sec}]$, $\Delta P$ = pressure difference $[\frac{N}{m^2}]$, $t$ = specimen thickness $[m]$ and $A$ = specimen area $[m^2]$. Coefficient $10^{-1}$ is needed to convert $[\frac{mbar \cdot liter}{sec}]$ into $[\frac{Pascal \cdot m^3}{sec}]$.
Equation 7 leads to the following two values respectively for room and cryogenic temperature permeability:

$$P(RT) = 1,877 \cdot 10^{-16}\ [\frac{m^2}{sec}]$$

and

$P(CT) = 3,13 \cdot 10^{-18}\ [\frac{m^2}{sec}]$

While the cryogenic permeability well fits the extension of the curve measured by Humpenöder in reference [18], the RT value is 1000 times lower than his measurements.
Comparison with measurements carried out by Yokozeki and Ishikawa [21] exhibit a still bigger discrepancy. In their permeability test setup they used IM6 intermediate modulus carbon fibres together with #133 toughened epoxy. Specimen geometry was tubular having a 0,01885 $m^2$ gauge area and 0,9 millimeter thickness, which is comparable to the LLB specimens (0,0145 $m^2$ and 1 millimeter). Despite material similarity, they measure a far higher leak rate at CT than done at LLB. Even when applying no mechanical strain, the leak rate they measured lies in the best case around $0,1 \cdot 10^{-5}\ [\frac{Pascal \cdot m^3}{sec}]$ ($0,1 \cdot 10^{-4}\ [\frac{mbar \cdot liter}{sec}]$). If the measured permeability is compared, the LLB measurement results $6.78 \cdot 10^4$ times smaller. Results at room temperature are also very different: LLB measurements give a 1000 times lower permeability than the Japanese specimen without mechanical strain.
This result may be due to the fabrication method: being the tubular specimens probably filament wound (but no indication are given by the authors) while the LLB curved specimen a prepreg lay up. This argument would also be consistent with results achieved by Shimoda and Cantoni [1] and by Murhpy and Wilkerson [2] who manufactured and tested filament wound tanks: in both cases considerable leakage was measured even at RT.
According to the results achieved at LLB, the X-33 tank failure (reference [4]) is also not clearly explicable. According to NASA final report, the cause of the X-33 hydrogen tank failure is the occurrence of micro cracks in the face sheets as mechanical strain reached 0,2% at cryogenic temperature. But no change in cryogenic leak rate, that could produce a sudden pressure increase in a tank core like that of the X-33, was detected during LLB measurements with strains up to 0.27%.

### 7.2.2 Leakage - Thermal cycles relation

The influence of thermal cycles on material permeability has been investigated. Specimens have been subjected to 100 thermal cycles (temperature extremes: 293 Kelvin and 77 Kelvin) and then placed into the permeability test setup. Results are reported in figure 40. No relation among number of cycles and leakage can be identified both at room and cryogenic temperature: either no cracks form after 100 thermal cycles, or they do not significatively affect permeability. The hundred times cycled specimen even

produced smaller leak than the one without cycles. This must again be attributed to the better indium sealing and underlines the fact that real CFRP permeability, even after thermal cycles, is far lower than test setup sensitivity. Actually in some cases, during the whole test program, a leak signal under the detection limit of the leak detector was measured.

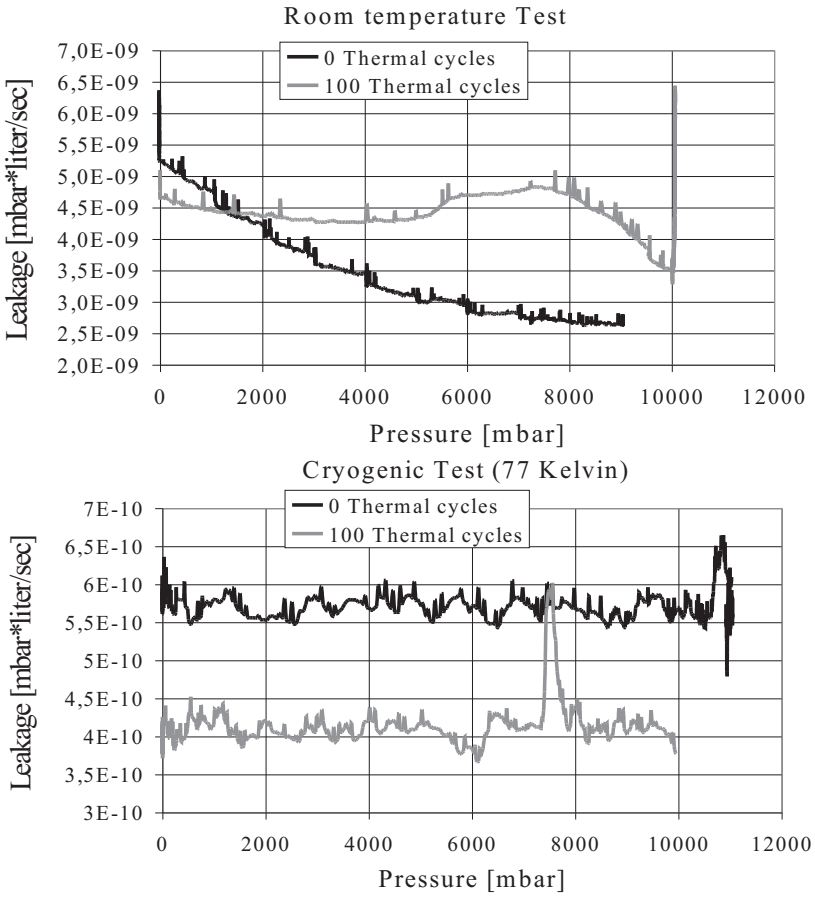


Figure 40: Leakage signal as function of gas pressure for thermally cycled specimens (RT - 77 kelvin - RT)

### 7.2.3 Leakage - Time relation

Specimens have been subjected to a long duration leakage test at room and cryogenic temperature. Permeation measurements have been carried out at a gas pressure of 10 bar, which has been kept for 10 hours. Results are shown in figure 41.

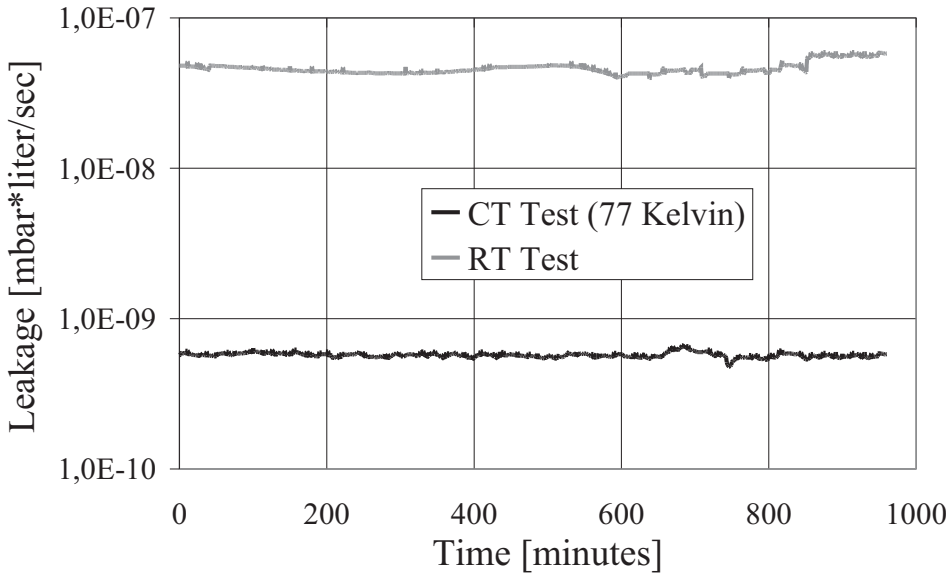


Figure 41: Leakage signal as function of time (gas pressure 10 bar)

The time trend shows no permeability increase during the whole test, both at room and cryogenic temperatures. This result has two main consequences:

- If cracking phenomenon proceeds with time under constant load, its slope is so small that after 10 hours no leakage paths form through the specimen thickness, at least for strains up to 0.25% - 0.27%
- If permeation through CFRPs occurs according to a transient law, that is molecules are progressively adsorbed, diffuse in the specimen and are released in the vacuum on the other side of the specimen, either the steady state leakage is negligible or the phenomenon has much bigger setting time than ten hours.

### 7.2.4 Conclusions

Permeability tests carried out at LLB showed a very promising behaviour of CFRPs for application in pressurised containment of cryogenic fluids:

- No relation has been found among gas pressure, from 0 up to 11 bar, and leakage both at room and cryogenic temperature. As consequence no micro cracking phenomenon could be identified for the range of mechanical strains up to 0.25% - 0.27% (corresponding to 11 bar pressure).
- Thermal cycles from room temperature down to 77 Kelvin did not result in changes in leakage signal through the specimen both at room and cryogenic temperature.
- Long exposition to gas pressure and cryogenic environment did not cause changes in leakage signal.
- Tests, carried out with a metal cap at the place of the specimen in order to qualify the test setup, resulted in the same level of permeability that was later measured with 1 millimeter thick CFRPs specimens.

Consequence of short and long duration tests, as well as of the qualification test with the steel plug, is that material permeability lies far below the detection limit of the test setup. Micro cracking are either absent or do not affect permeability, that is, no full leak paths form for strains up to 0.25% -0.27%. This conclusion is also consistent with material tests on tensile specimens, which showed no cracks in laminates with thin layers for mechanical strains below 0.4%.
A comparison among LLB experimental results and calculated requirements (see chapter 3) can be done if the leak rate requirements of section 3.3.2 are multiplied by the area ratio between test specimen and the unitary area considered there. Table 18 reports the modified requirements and the experimental measurement.

| (Modified) Requirement $[\frac{mbar \cdot liter}{sec}]$ | | | Measurement $[\frac{mbar \cdot liter}{sec}]$ | |
|---|---|---|---|---|
| Automotive | Commercial aeroplane | RLV | RT | CT |
| $4,9 \cdot 10^{-13}$ | $1,3 \cdot 10^{-11}$ | $4,3 \cdot 10^{-10}$ | $5 \cdot 10^{-9}$ - $5 \cdot 10^{-8}$ | $5 \cdot 10^{-11}$ - $6 \cdot 10^{-10}$ |

Table 18: Comparison among calculated permeability requirements and measured permeability

All requirements, with the exception of the RLV case, lie 10 to 100 times below the measured values. But because LLB results were mainly influenced by gas flowing through the sealing, the possibility to reach these stringent values in a CFRP tank may not be excluded.
Comparison of LLB tests with the literature shows that past tanks failures may be due either to poor tank design, not satisfactorily material choice or both causes. From the point of view of material choice the right combination of fibre and toughened epoxy may not be a trivial issue, as indicated by results achieved with IM6/#133 or even those with IM7/977-2 in comparison to those achieved at LLB with IM7/8552. From the point of view of the manufacturing technique, filament winding could not be the most appropriate choice for the purpose, because in no cases filament wound tanks or specimens have achieved comparable impermeability to those manufactured by prepreg and autoclave technology.
A final point of major importance for cryogenic tanks is the attitude epoxies have to outgas, that is to release gas molecules in vacuum. During the experiments it was simply not possible to discern between epoxy outgassing and release of gas molecules from the inner walls of the steel chambers or through the indium sealing. The same phenomenon has occurred when the steel plug was mounted at the place of the CFRP specimen, thus if outgassing occurs its intensity must also be at least one order of magnitude lower than the measured signal.

# 8 Failure models and analysis - test correlation

## 8.1 Failure criteria for laminate analysis

Research on failure criteria for FRPs has not yet resulted in a definitive model able to exhaustively describe FRPs failure behaviour (Manne and Henriksen, [44]). Several criteria have been proposed for FRPs and can be divided into four main categories: classical criteria, like the maximum stress and the maximum strain, quadratic criteria, like Tsai-Hill and Tsai- Wu, physical criteria, to which the Puck's and fracture mechanics criteria belong. Because of the nature and multiplicity of aspects concerning failure phenomena in fibre reinforced composites, development trends in criteria conceived to describe them has been characterized by an increasing complexity as more aspects have been included in the models. Thus, starting with classical criteria, these are easy to use but have the major disadvantage of treating each stress component separately and compare it to the respective allowable. In case more components act together, interaction phenomena may lead to failure, even if each of the stress components is smaller than its allowable. In case of contemporary presence of several stress components, like for example $\sigma_2$ and $\tau_{12}$, quadratic criteria have interaction coefficients which take into account these synergetic effects and thus they lead to more accurate results. Anyway the correctness of predictions relies upon material parameters which have to be estimated through complicated tests which give substantially unreliable and unrepeatable results, as well as being expensive. In some cases, like the Tsai- Hill, it is worth noticing that a ductile material criterion is commonly applied to model the essentially brittle inter fibre failure of reinforced composites, which represents a basic inconsistency ([44]).
Physical criteria have this name because they are driven by the physics of failure. Based on that, two main failure modes have been identified, namely fibre failure (FF) and inter fibre failure (IFF). Interactions between these two forms of failure can be generally neglected and arise only when both stresses in the two directions ($\sigma_1$ and $\sigma_2$) are near the respective failure values. Thus while a combination of tensile stresses in and perpendicular to fibres having a value of 0,8 times the respective failure strains, results probably safe according to physical based criteria, it is not when quadratic criteria are applied ([44]). At still higher strains, for examples 0.99% the respective failure strains, even physical criteria predict failure. The reason for that limited interaction in the nearby of fibre and inter fibre failure stresses is the strain experienced by the matrix when load is applied in fibre direction and whose

effect on strength perpendicular to fibres is as much important as lower matrix failure strain is. This issue could gain major importance at cryogenic temperatures, because both thermoplastics and thermosets are much more sensitive to thermal effects than fibres and show a more pronounced reduction in failure strain at cryogenic temperatures, even if relative values are considered. As consequence interaction between fibre and inter fibre strains may lead to failure even at smaller mechanical strains than it does at room temperature. Puck's criterion models this sort of interaction phenomena, but complexity and number of parameters to be estimated has been further increased (see Puck, [46] and [47]).
Based on this introduction some remarks has to be made regarding the choice of a suitable failure criterion and in consideration of the kind of load which is modelled and expected failure modes: as indicated in chapter 5, the combination of mechanical loads and thermal ones are expected to result in very high tensile $\sigma_2$ stresses and relative low $\sigma_1$, compared to the respective failure values. Thus priority in detecting failure shall be focused on inter- fibre failure modes and particularly on interaction phenomena between in- plane shear ($\tau_{12}$) and tension perpendicular to fibre direction ($\sigma_2$). Further, prediction of several failure criteria (where interaction is considered) has shown their fairly good agreement for the typical stress distribution occurring in laminates, due to high thermal loads and mechanical two- axial tension as shown in figure 42.

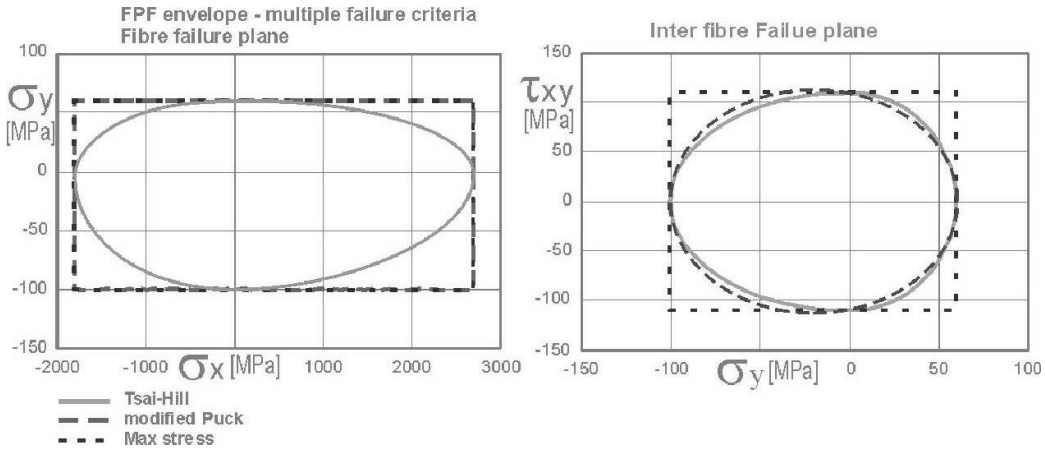


Figure 42: Comparison of several failure criteria belonging to the three categories on the IFF and on the FF planes (X and Y are respectively fibre and in plane perpendicular to fibre directions).

### 8.1.1 Maximum strain criterion

The max Strain criterion represents, together with that of max stress, the classic criteria. Here failure occurs when one or more strain components reach the respective allowable. The failure surface is a polygon because no interaction between strain components is considered (see figure 42. This criterion can be applied to the single ply as well as to the entire lamiate. In this second case, it is necessary to specify what is meant as "laminate failure", that is onset of cracks or final failure.

### 8.1.2 Fracture mechanics criteria

The fracture mechanical approach is based on the concept that a new crack builds up in the laminate when it is physically possible and energetically favorable. The energetic balance is based on the difference between the work done by external loads and the change in elastic energy stored in the material when a crack increases in size:

$$\Delta W - \Delta U \geq f(G_{IC}, G_{IIC}, G_{IIIC}) \tag{8}$$

where $\Delta W$ is the work done by external forces, $\Delta U$ the change in stored elastic energy, $G_{IC}$, $G_{IIC}$ and $G_{IIIC}$ are the energy release rates for crack opening modes I, II and III.
The expression of the change in elastic energy depends on stress distribution before and after cracks have formed, thus on laminate parameters like materials, elastic constants, laminate lay up, geometric parameters.
Central point in stress state modelling is the load transmission in the crack region from the damaged ply to the undamaged constraining ply. This task is fulfilled by two possible approaches: the shear lag approach and the variational approach. According to the shear lag model, stress is transferred by a thin matrix sheet placed between the two CFRP plies. This sheet has negligible tensile stiffness in comparison to the reinforced plies, thus transfer mechanism is occurs through shear stress.
The variational approach attempts to find an approximation of the state of stress by the theorem of the minimum complementary energy. Among all state of stress that satisfy the boundary conditions, the effective one will also provide a minimum of the complementary energy in the laminate (see Brown [35]). Further approximations of the state of stress consist in neglecting any dependence of the distribution of the stress components on the Z coordinate (t.i. the normal to laminate plane). However it includes the z- components of the stress tensor, thus giving a more precise approximation of the state of stress.

Both models offer advantages and disadvantages: the shear lag Model is simpler and can be applied to a wider category of laminates than the variational approach. On the other side the variational approach gives a better representation of the real stress distribution.
In case of the shear lag solution for $[0_m/90_n]_S$ laminates, the cross ply onset strain has the following expression according to Parvizi et al. [50]:

$$\epsilon_{\perp,F} = \sqrt{\frac{b \cdot E_0 \cdot G_{23} \cdot G_{IC}^2}{(b+d) \cdot d^2 \cdot E_X \cdot E_2^3}} \tag{9}$$

where:

b = thickness of the $0^0$ ply
d = half thickness of the cross ply
$E_0$ = stiffness of the constraining plies
$E_X$ = total laminate stiffness in load direction
$E_2$ = cross ply stiffness
$G_{23}$ = cross ply shear modulus
$G_{IC}$ = critical energy release rate for opening mode I

This relation is able to model the delaying effect due to the presence of stiff $0^0$ plies and the dependence of the crack onset strain on plies thickness ratio.
However both approaches are still far from providing correct estimation of failure loads for all possible type of laminates and external loads.

### 8.1.3 Strain invariants criterion

A new strain criterium has been recently proposed by Gosse and Christensen [52], based on the determination of the equivalent and hydrostatic strains in the epoxy matrix of a CFRP laminate. This failure criterion is based on the assumption that IF cracks develop either when the first or second invariant of the strain tensor in the matrix reaches a limit value.
A constant value of the first tensor invariant, $I_1$, represents an deviatoric plane, while a fixed value of the second, $I_2$, a cylinder parallel to the hydrostatic axis.

$$I_1 = \epsilon_1 + \epsilon_2 + \epsilon_3 = K_1 \tag{10}$$

$$I_2 = (\epsilon_1 - \epsilon_2)^2 + (\epsilon_2 - \epsilon_3)^2 + (\epsilon_3 - \epsilon_1)^2 = K_2 \tag{11}$$

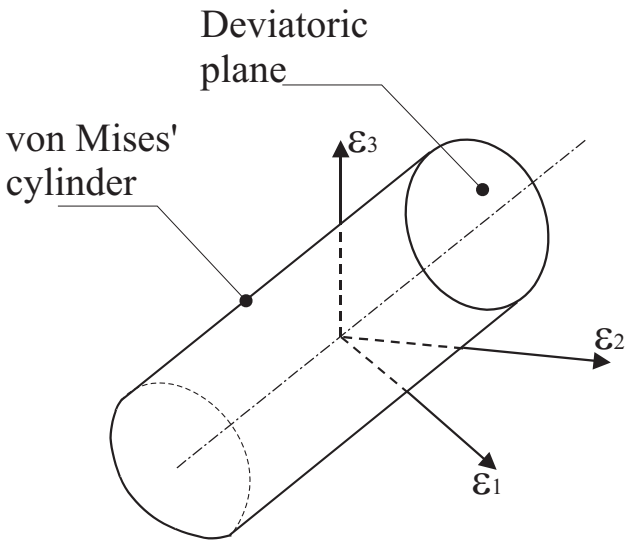


Figure 43: Strain failure surface for matrix failure in CFRPs.

In other words, failure occurs when the strain vector exceeds the closed surface identified by the von Mises cylinder delimited by two deviatoric planes like shown in figure 43.
Matrix failure is brittle because the presence of surrounding fibres prevents the development of extended plastification zones.
Calculation of precise matrix strain tensor requires a three dimensional micromechanics approach and is carried out as following explained:

1. The three dimensional strain state due to external mechanical load is calculated in each ply by means of a macroscopic FE model

2. The three dimensional strain state due to thermal load is calculated in each ply by means of a macroscopic FE model

3. The micromechanical thermal strain in the matrix is calculated by means of an FE micromechanical model

4. Mechanical strain intensification factors are calculated by the micromechanical model.

5. Each component of the macroscopic mechanical strain is multiplied by the respective intensification factor in order to get the total mechanical strain in the matrix

6. The microscopic thermal strain is added to the macroscopic strain in order to get the total thermal strain in the matrix

7. Total thermal and mechanical strains are added one to the other and the total strain state is so calculated

8. The first and second invariants of the total strain are calculated.

This procedure requires a remarkable calculation effort because micro- and macromecanical FE models must provide the necessary resolution of ply and matrix stresses. Despite the necessary effort, this failure criterion promises to be able to represent actual composite failure behaviour because it is based on material failure properties which are material dependent, and on an accurate stress distribution, which is laminate and load dependent, thus able to take into account constraining effects.

## 8.2 Analysis test correlation

The experimental results on tensile specimens (see chapter 6) have been used to study the correlation among failure criteria and real CFRP behaviour. Several quadratic together with strain and fracture mechanics failure criteria have been considered.

### 8.2.1 Quadratic and physical based criteria

The following table 19 shows comparison among three criteria, namely the Tsai-Hill, Tsai-Wu and Puck criteria, and room temperature experimental results determined during the UD test campaign (see chapter 6).

The comparison shows a remarkable difference among failure prediction and measurement. For all laminates effective load capability exceeds the theoretical value, according to most used failure criteria. This difference remains in case of cryogenic tests, not reported here: while according to failure criteria cracks should appear already during cooling down, they appear at cryogenic temperature only after a significant mechanical strain amounting at least to 0,13% (but up to 0,62% in the constrained plies of laminate 2) has been applied.
Calculation of failure strains without taking into account thermal loads in laminates shows a better agreement with the experimental data for thin inner angle plies (laminates 1,2 and 5).

| Laminate | Laminate strain $\epsilon_0$ [%] | | | | |
|---|---|---|---|---|---|
| | Numerical results (RT) | | | Experimental results (RT) | |
| | Tsai-Hill | Tsai-Wu | Puck | Outer ply | inner ply |
| 1 | 0,188 | 0,168 | 0,188 | 0,588-0,688 | $> 0,988$ |
| 2 | 0,262 | 0,225 | 0,259 | 0,719-0,868 | 0,868-1,016 |
| 3 | 0,831 | 0,821 | 0,774 | $> 0,85$ | $> 0,85$ |
| Laminate | Numerical results (without thermal loads) | | | Experimental results (CT) | |
| 1 | 0,52 | 0,52 | 0,52 | 0,128-0,228 | 0,478-0,628 |
| 2 | 0,58 | 0,585 | 0,565 | 0,176-0,326 | 0,623-0,772 |
| 4 | 0,52 | 0,52 | 0,52 | 0,265-0,365 | 0,265-0,365 |
| 5 | 0,52 | 0,52 | 0,52 | | 0,413-0,513 |

Table 19: Comparison between room temperature measured and calculated first ply failure strains

### 8.2.2 Shear Lag criterion

Comparison between the shear lag model and the experiment is shown separately for the inner plies of the tested laminates in table 20 .

| | Laminate 1 | Laminate 2 | Laminate 4 | Laminate 5 |
|---|---|---|---|---|
| $\epsilon_\perp$ [%] (computed) | 1,79 | 1,61 | 1,02 | 1,44 |
| $\epsilon_\perp$ [%] (measured) | $> 1,40$ | 1,00 - 1,1 | 1,00 - 1,1 | $> 1,2$ |

Table 20: Comparison between room temperature measured and calculated constrained ply failure strains, according to the shear lag model.

More accurate than the failure model previously examined, the shear lag model is able to give a reasonable prediction of the failure strain when angle ply is laminated at $90^0$ (cross ply). On the contrary prediction is far below the measured value for laminate 2, in which angle ply lies at $60^0$.
The shear lag model is used here somewhat outside its field of validity, because it is applied to laminates which geometry differ from the $[0^0_m/90^0_n]_S$, but it still gives reasonable predictions. In case a significative shear component is present, as in case of laminate 2, the model produces non conservative results, because crack formation is ascribed only to opening mode I, while the effect of shear is not modelled. Crack opening mode II and related toughness,

$G_{IIC}$, should be included.

### 8.2.3 Strain invariants criterion

A test of the strain criterion from Gosse and Christensen [52] has been carried out by following the procedure described in section 8.1.3. A macroscopic half model of laminate 1 and a micromechanical model have been implemented in ANSYS 8.1. in order to calculate micromechanical and macroscopic thermal and mechanical strain tensors for the $90^0$ layers. Cross plies are modelled by 12 quadratic elements along the thickness in the macroscopic model, in order to achieve a good approximation of all strain components. The macroscopic model provides macroscopic thermal and mechanical strains.
The micromechanical model has cubic geometry and it is composed of 16 fibre segments imbedded into the matrix. It is used to calculate mechanical strain amplification coefficients and micromechanical thermal strains.

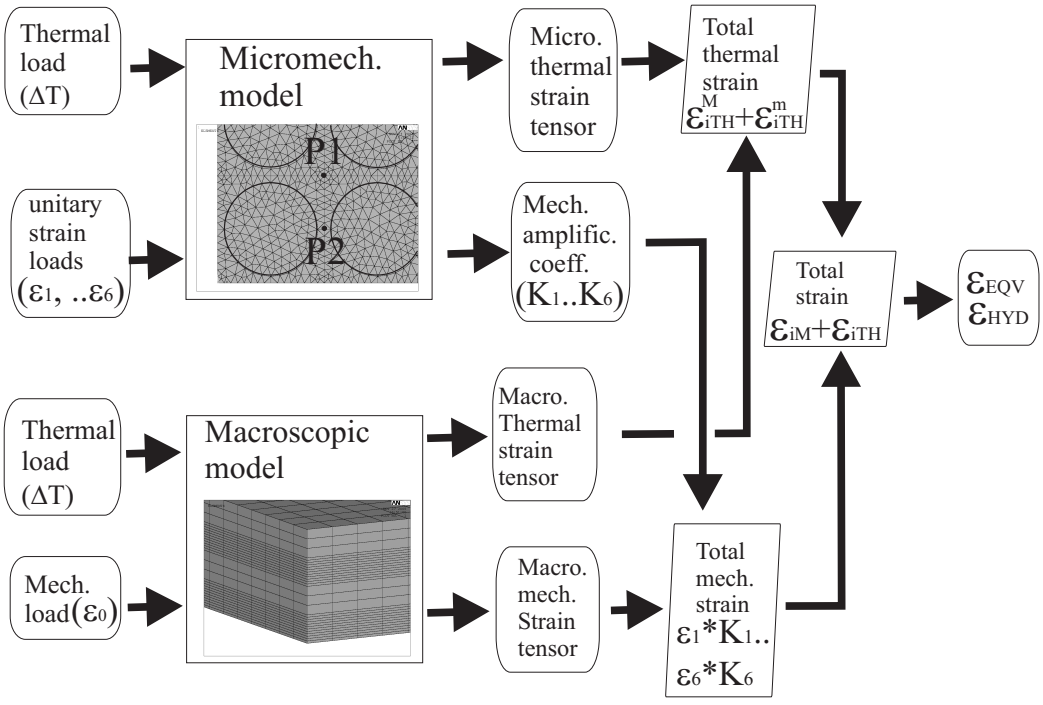


Figure 44: Flow chart for the implementation of the strain criterion

These values are computed in the two points indicated as $P_1$ and $P_2$ in figure 44 and the point giving the biggest value is then chosen (Point 2 has always

revealed the one giving the highest values for amplification factors and thermal strains). After turning the micromechanical results into the macroscopic reference system, the solutions are combined to get the total strain. Three results are computed for each load case: the average strain tensor in the cross plies (average on the nodes), the tensor in correspondence of the node where the highest equivalent strain occurs and that in correspondence of the node where the maximal hydrostatic strain occurs. Micromechanical corrections are then added to these three tensors and the equivalent and hydrostatic strains are calculated. Figure 45 shows the results for laminate 1.
The three following issues can be derived from the graphs in figure 45:

- Equivalent and Hydrostatic strains (the latter when averaged over the whole ply) have in the outer and inner ply the same value
- The equivalent strain decreases as the laminate strain is increased
- When maximum values are chosen as terms of comparison, the hydrostatic strain in the inner ply is bigger than or equal to that in the outer ply, for the whole laminate strain interval

As consequence it is not possible to identify a particular value of the strain invariants at which the onset of cracks in the $90^o$ plies occurs.
The reducing value of the second strain invariant, $I_2$, as mechanical tensile strain in the specimen is increased is due to the contribution of the micro- and macromechanical thermal strains. As explained in section 8.1.3, this are fixed terms which superimpose on the increasing mechanical term. Because the thermal load is negative, several components of the thermal strains are also negative. At the same time, the components of the mechanical strain have opposite signs than those of the thermal strain tensor and increase in module when the mechanical load is increased. Thus the linear combination of the dominating thermal strains with the smaller mechanical strains leads to the behaviour shown in figure 45. The most important issue in the computation of this strain criterion is that the macroscopic components, both of the mechanical and thermal strains, show little difference in case of the inner and outer plies.

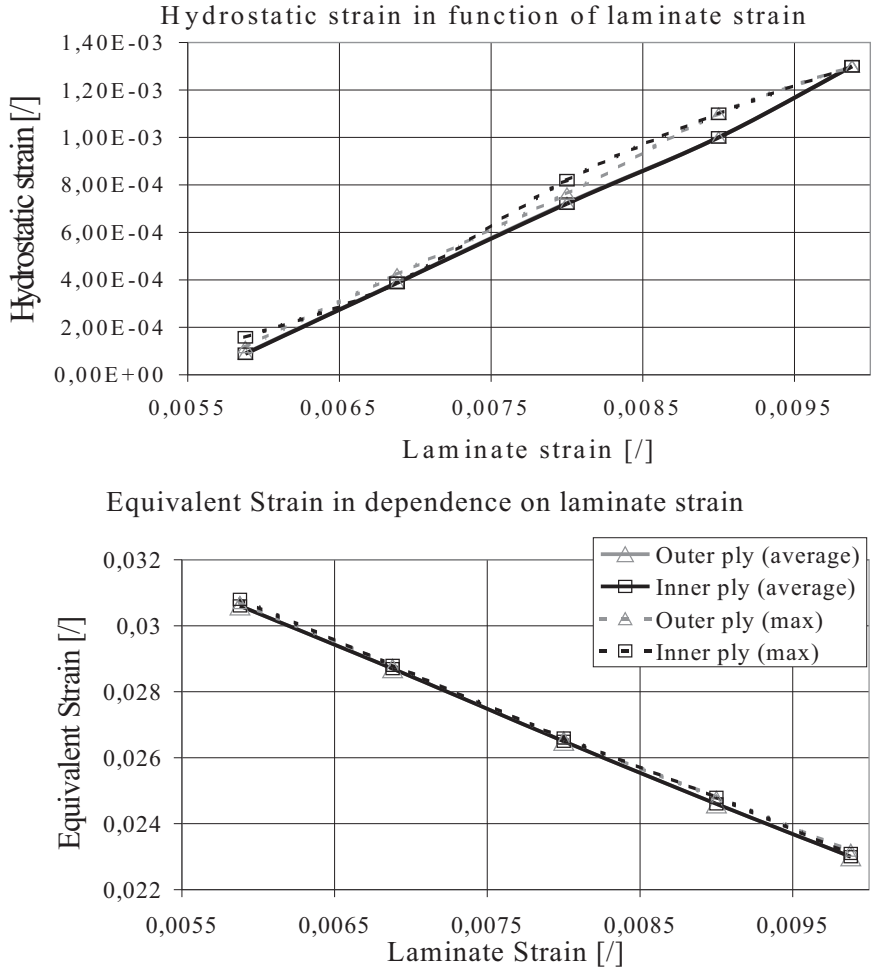


Figure 45: Relation among inner and outer equivalent strain, hydrostatic strain and laminate load (laminate strain)

This leads to equal total strains and thus equal strain invariants which do not agree with the different experimentally determined crack onset strains. Table 21 shows the values of both the micro- and macromechanical thermal strains, of the mechanical intensification factors and of the macromechanical strains for the inner and outer plies at two different laminate mechanical strain. Here is shown that the mechanical macroscopic strain tensors for the inner and outer plies differ only starting from the seventh decimal digit (the fifth decimal digit when strain is in percentage).

| | | Component | | | | | |
|---|---|---|---|---|---|---|---|
| | | X | Y | Z | XY | XZ | YZ |
| Micromechanical thermal strain [%] | | 1,08 | -1,73 | 1,01 | -0,0038 | 0 | 0 |
| Micromechanical intensification factor | | 1,3 | 1,02 | 0,96 | 2,54 | 0,039 | 0,47 |
| Outer ply (macroscopic results) | Thermal strain [%] | -0,43 | 0,005 | -0,43 | 0 | 0 | 0 |
| | Mechanical strain [%] ($\epsilon_0 = 0,588$ %) | 0,588 | -0,0191 | -0,2309 | 0 | 0 | 0 |
| | Mechanical strain [%] ($\epsilon_0 = 0,688$ %) | 0,688 | -0,02238 | -0,27 | 0 | 0 | 0 |
| Inner ply (macroscopic results) | thermal strain [%] | -0,43 | 0,005 | -0,43 | 0 | 0 | 0 |
| | mechanical strain [%] ($\epsilon_0 = 0,588$ %) | 0,588 | -0,0191 | -0,2309 | 0 | 0 | 0 |
| | Mechanical strain [%] ($\epsilon_0 = 0,688$ %) | 0,688 | -0,022393 | -0,27 | 0 | 0 | 0 |

Table 21: Calculated strain components in the cross ply laminate inner and outer $90^o$ plies

## 8.3 Numerical simulation of adhesively bonded joints

### 8.3.1 Introduction

Together with the need for measuring adhesive bonded joints properties at cryogenic temperature for design purposes, a research of the possibility of simulating material behaviour by use of available software for structural analysis has been carried out. Modern FE software environments allow reproducing the behaviour of complex geometries and load combinations, thus they are a powerful and in many cases the only mean for executing parametric analysis and optimization of a structure. One condition for their successful application is the existence of adequate material models able to reproduce the behaviour of a complex combination like that of a bonded joint. In order to investigate that availability, the EA9361 5 millimeter OL bonded joints have been simulated up to failure by exploiting non linear material models

and geometries. Numeric results have then been compared to the test at room temperature and at 203 Kelvin.
The simulation environment was ANSYS 8.1 which provides mainly material laws developed for metallic materials (both isotropic and non isotropic). Thus a brief discussion of the assumptions made for these material will follow.

### 8.3.2 Material models

Materials like many metallic alloys and plastics react elastically under stress up to a certain critical value, which depends on the material, and, beyond that, experience a plastic deformation. Plastic behaviour is characterized by non linear stress- strain relation and residual deformations when the external load is removed. In the space of the principal stress components, $\sigma_1$, $\sigma_2$, $\sigma_3$, the two distinct behaviours correspond to two subspaces, which union gives the whole space. The limit of the elastic subspace is called yield function. One state of stress whose vector lies inside the space delimited by the yield function (point P in figure 46) is an elastic one, while one lying on the surface (like Q in figure 46) describes a combination of stresses which induces yielding. Starting from the unloaded state and loading progressively the material, the state of stress will initially be elastic and thus lie inside the yield function. As the norm of the stress vector increases it reaches the yield surface producing yielding.

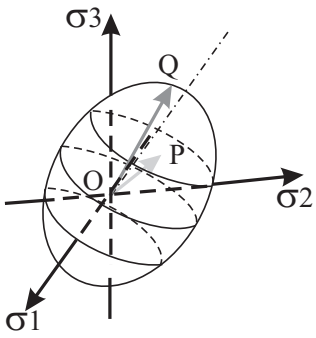


Figure 46: Representation of a possible yield surface in the space of the principal stress components.

Further increase in the stress vector produces a displacement of the stress point, which drags the yield surface. In other words, since the stress points has reached the yield surface further increase of its intensity will change the yield surface itself. The yield surface of an isotropic material must satisfy

some symmetry features. With reference to figure 47 left, let plane p be the deviatoric plane, that is the plane perpendicular to the hydrostatic axis in the space of the principal stresses. The hydrostatic axis has equation:

$$\sigma_1 = \sigma_2 = \sigma_3 = \sigma_0 \tag{12}$$

while one plane perpendicular to this axis is identified by the following equation 13:

$$\sigma_1 + \sigma_2 + \sigma_3 = \sigma_0 \tag{13}$$

These are called deviatoric planes. For k=0 equation 13 describes the deviatoric plane containing the origin. Figure 47 (right) shows the intersection of the yield function with the deviatoric plane. Because yielding of an isotropic material can depend only on the values of the principal stresses, but not on their direction, if (p, q, r) is a state of stress which induces yielding, than (p, r, q) must also induce yielding. This implies that the yield locus is symmetric about the projection of $\sigma 1$ axis and, because it is function of stress invariants, also about those of the other two axes.

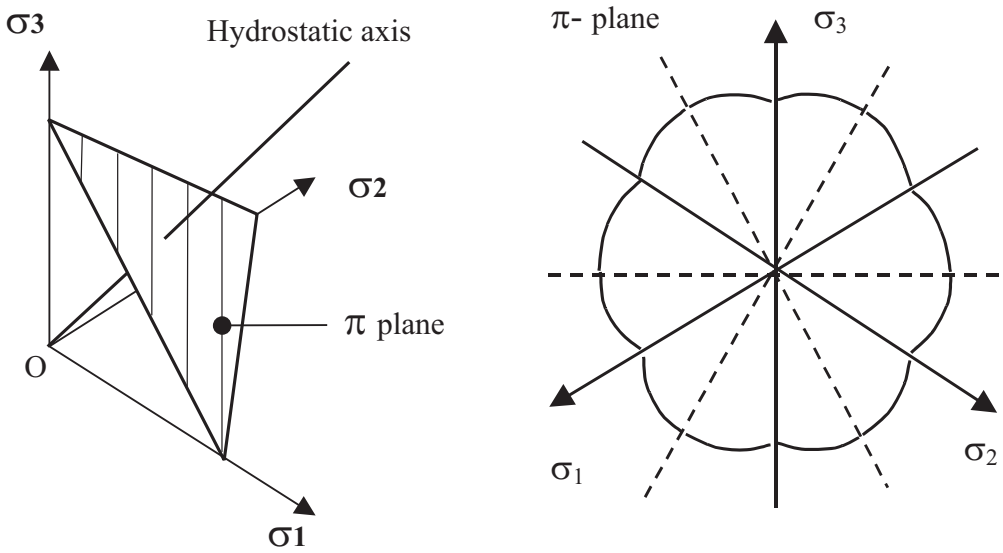


Figure 47: $\pi$ (deviatoric) plane and hydrostatic axis (left) and shape of the intersection of a possible yield function with the $\pi$- plane (right)

### 8.3.3 Material models for metals

Some hypotheses concerning metals and metallic alloys are listed below. Most of them derive from experimental observations or metal behaviour

1. Yielding of a metal is unaffected by a moderate hydrostatic stress state.
2. The magnitude of the yield stress is the same in tension and compression
3. After yielding isotropy is preserved
4. The yield surface is a function only of the final applied stress (although this is not exactly true also for metals)
5. During progressive plastic deformation, the yield surface increases in size but keeps the same form
6. Changes in volume during plastic deformation are elastic
7. Final yield locus depends only on the total plastic work done ( and, therefore, it is independent on the strain path).

Consequence of hypothesis 1 is that the yield locus must be an open surface parallel to the hydrostatic axis, because a hydrostatic state of stress shall not intersect the surface. Hypothesis 2 leads to the fact that if (p, q, r) is a plastic state of stress than (-p, -q, -r) must also lay on the yield surface, thus this must be symmetric about the hatched lines. It is not necessary to investigate the whole stress state space in order to determine the yield surface. Parallelism to the hydrostatic axis has as consequence that all intersections between the yield surface and one deviatoric plane are equal. Furthermore because of symmetry of the intersection curve it is necessary to investigate only all stress points between one of the hatched lines and one of the adjacent principal axes projection (see figure 48). This can be rigorously expressed by the following:

$$f(J_2, J_3) = const \tag{14}$$

where $J_2$ and $J_3$ are respectively the second and third invariants of the deviatoric stress, and f is an even function of $J_3$
Starting with a pure tensile state of stress and adding progressively a shear it is possible to cover the hole space delimited by the two lines of figure 48. Pure tension corresponds to the following stress vector:

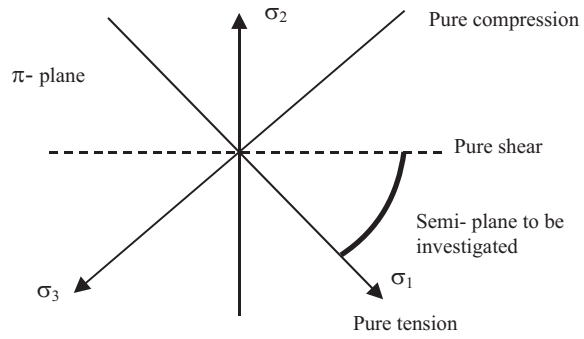


Figure 48: Sector of the space of principal stresses to be investigated to determine the yield locus of a ductile metal.

$$\{\sigma\} = \begin{Bmatrix} \sigma_0 \\ 0 \\ 0 \end{Bmatrix} = \begin{Bmatrix} \frac{\sigma_0}{3} \\ \frac{\sigma_0}{3} \\ \frac{\sigma_0}{3} \end{Bmatrix} + \begin{Bmatrix} \frac{2\cdot\sigma_0}{3} \\ \frac{-\sigma_0}{3} \\ \frac{-\sigma_0}{3} \end{Bmatrix} \tag{15}$$

where the first term on the right represents the hydrostatic part and the second the deviatoric one.
Pure shear can be expressed by the following:

$$\{\sigma\} = \begin{Bmatrix} \sigma_0 \\ -\sigma_0 \\ 0 \end{Bmatrix} \tag{16}$$

which has no hydrostatic component and a maximum shear equal to $\tau = \sigma_0$. Equation 15 shows us that the application of a pure tension generates a hydrostatic component, which has no effect on metals. In case of a material which yielding depends on the hydrostatic component as well as from the deviatoric one it is necessary to investigate the effects of both separated and together. That is the simple one dimensional tension plus superimposed shear load does not suffices.

### 8.3.4 Von Mises, Tresca and Hill's Yield criteria

The three yield surfaces having the best agreement with the experimental behaviour of metals are Tresca and von Mises laws. Tresca suggested that yielding occurs when the maximum shear stress reaches a critical value. Von Mises' criterion states that yielding is related to the value of the second invariant of the deviatoric stress, $J_2$. The two yield loci are shown in figures 49 and 50. The Tresca locus is piecewise linear in the space of the principal stresses and represents a cylinder having hexagonal base. In the semi-plane delimited by the positive $\sigma_1$ and the negative $\sigma_3$ axis projections Tresca locus is analytically described by the following:

$$\sigma_1 - \sigma_3 = 2 \cdot K \tag{17}$$

Von Mises yield locus represents a circle on the deviatoric plane ($\pi$- plane), which equation is given by substituting equation 13 into the following:

$$(\sigma_1 - \sigma_2)^2 + (\sigma_2 - \sigma_3)^2 + (\sigma_3 - \sigma_1)^2 = 2 \cdot k^2 \tag{18}$$

note that the constant k of equation 13 is different from K of equation 18. The Hill's criterion represents an adaptation of von Mises' criterion to non-isotropic metals.

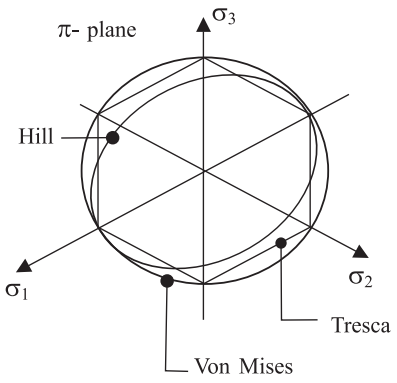


Figure 49: Tresca, Mises and Hill yield loci projected on $\pi$-plane.

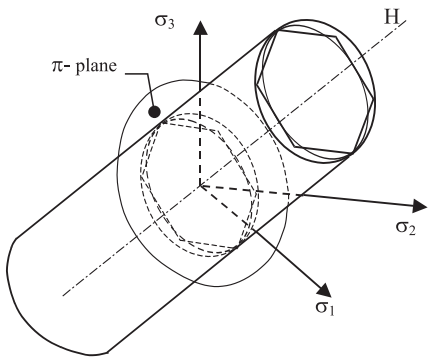


Figure 50: Tresca, Mises and Hill yield surfaces.

Basic thought is still that hydrostatic stress does not influence yielding, but, because of anisotropy arising from previous yielding (i.e. plastic deformation) the yield locus is not anymore circular, but elliptic. As results this criterion

represents a cylinder having axis parallel to the hydrostatic one and elliptic normal section (see figure 49). The equation of the surface is as follows:

$$H \cdot (\sigma_1 - \sigma_2)^2 + F \cdot (\sigma_2 - \sigma_3)^2 + G \cdot (\sigma_3 - \sigma_1)^2 = 1 \tag{19}$$

where H, F, and G are coefficient related to tensile failure stresses in the three principal directions according to the following equations:

$$H = G = \frac{1}{2 \cdot \sigma_{1U}^2} + \frac{1}{2 \cdot \sigma_{2U}^2} - \frac{1}{2 \cdot \sigma_{3U}^2} \tag{20}$$

$$F = -\frac{1}{2 \cdot \sigma_{1U}^2} + \frac{1}{2 \cdot \sigma_{2U}^2} + \frac{1}{2 \cdot \sigma_{3U}^2} \tag{21}$$

When the three coefficients are equal, the yield surface reduces to that of von Mises.

### 8.3.5 Yield criteria for polymers

Since the beginning of the seventies it has been clear that polymers do not generally yield according to the Mieses' surface. Most of the assumptions on which the theory of yielding for metals is based are simply not true for them. Among them, the most important are:

1. Yielding is affected by hydrostatic stress, that is plastic changes of volume occur

2. Absolute value of compressive and tensile yielding stresses generally differ

The first assertion is referred with certainty to materials like PE, PVC, PS, PMMA [69]. Nevertheless the difference in compression and tension yielding behaviour of epoxies is well documented. This second feature is itself a proof for the first one, in case of isotropic materials. In fact, because of isotropy, the deviatoric stress leading to yielding can not change on a deviatoric plane. Thus if there are differences among deviatoric stress at yielding in a compression and tension state, this can only be caused by the hydrostatic components, which is positive in one case and negative in the other. The same consideration is valid when the deviatoric stress at yielding varies between a case of pure tension and pure shear, for an isotropic material. Because of these reasons, all proposed yield surfaces for plastic materials are dependent of hydrostatic stress. In one secular paper ([71]), Raghava, Caddel and Yeh, propose a yield surface in which deviatoric stress has a linear dependence on hydrostatic stress:

$$(\sigma_1-\sigma_2)^2+(\sigma_2-\sigma_3)^2+(\sigma_3-\sigma_1)^2+2\cdot(C-T)\cdot(\sigma_1+\sigma_2+\sigma_3)=2\cdot C\cdot T \quad (22)$$

where: $C=|\sigma_{UC}|$ and $T=|\sigma_{UT}|$
The dependence on hydrostatic stress is linked to the difference between the absolute value of compression and tension yield stresses, so that the yield surface becomes the von Mises cylinder when the two values are equal. A more general theory of yielding and failure for isotropic materials is developed in [72]. Here a yield criterion, in which a linear dependence on hydrostatic stress appears, is proposed as well:

$$\frac{\zeta\cdot K}{\sqrt{3}}\cdot\sigma_{ii}+\frac{1}{2}\cdot(1+\alpha)\cdot(\sigma_{ij}\cdot\sigma_{ij}-\frac{1}{3}\cdot\sigma_{ii}^2)\leq K^2 \quad (23)$$

where the compact notation is used (whenever a letter appears twice within the same term a summation is implied over the range of the index). The first term of the equation represents the hydrostatic stress, while the second distortion energy (t.i. von Mises cylinder). The criterion is general in the sense that parameters $\alpha$ and $\zeta$ allow to change the form from that of cylinder ($\alpha$, $\zeta=0$) to that of cohesionless solids ($\alpha$, $\zeta$ very big), while Parameter K represents a scaling factor. Values of $\alpha$, $\zeta$ and K can be determined when the three yield stresses (uniaxial tension, compression and shear) are known. Based on the values for epoxy EP 5 in paper [64], for which the ration between shear and tensile yield stresses is 1.6, and taken a typical value for the ratio between tensile and compression yield stresses (for example 2) the resulting values are $\alpha=20$ and $\zeta=1,94$.

## 8.4 Test simulation and discussion

### 8.4.1 FE Model

A simulation of single lap shear specimens has been carried out in ANSYS 8.1 environment. ANSYS offers principally the von Mises, Hill and Drucker-Prager yield criteria together with several work hardening rules. The last one is the only criterion in which deviatoric stress depends on the hydrostatic one at yielding. Indeed, it is offered together with the elastic - ideal plastic body, in which after yielding no hardening takes place.
A 2D and a 3D models of the 5 mm OL specimen have been used for the simulation with substantially equal results. The 2D FE model is shown in figure 51. The adhesive region has been modelled by 10 elements in the thickness, 100 in the width and the spacing has been set in order to have smaller elements at the corners, where bigger stress components are expected

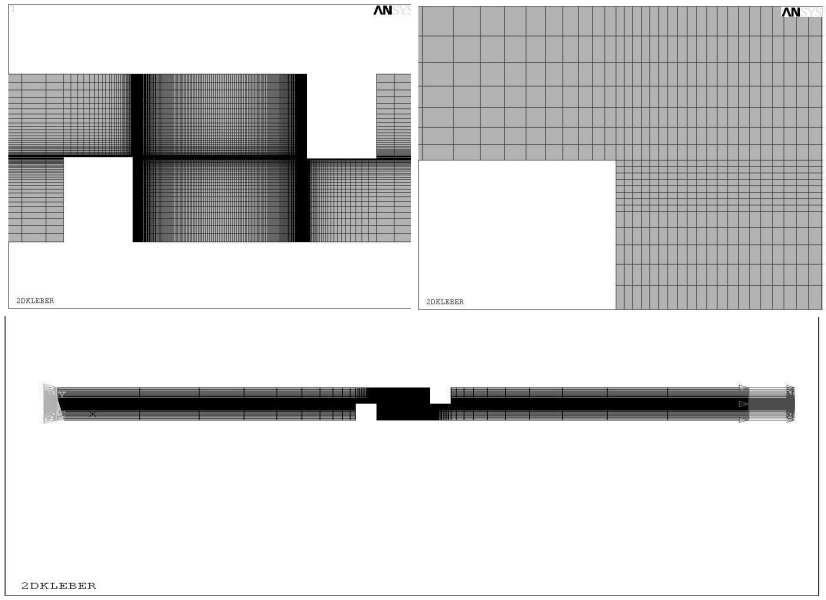


Figure 51: 2D FE model used for the simulation of the bonded joint.

to arise. The modelled portion of the aluminium adherends reaches the point in the real specimen where the bolts begin. Here simply support constraints are placed both in and perpendicular to the load direction (respectively X and Y axis) and in direction perpendicular to the plane of the specimen (Z) on one side, while only in Y and Z directions on the other side, where the tension load acts. This leads to the fact that the typical setting effect of the bolt (knee in conjunction to the origin of the load - deformation diagram, as shown in figure 52) does not appear in the simulation. The non linear behaviour of the aluminium adherend was also modelled and non linear geometric deformations were also computed.

### 8.4.2 Simulation results and comparison to the experiment

An initial calculation has been attempted by using the implementation of the von Mises criterion, but without being able to reproduce the experimental curve: an apparent to high strain in adhesive corner elements forced the simulation to stop
at an average shear stress of about 12-13 MPa (see figure 52). At even smaller shear stresses the slope of the simulated stress-strain curve already deviated from the experimental results because yielding occurred on almost the whole adhesive length. Better results have been achieved by the Hill criterion, as

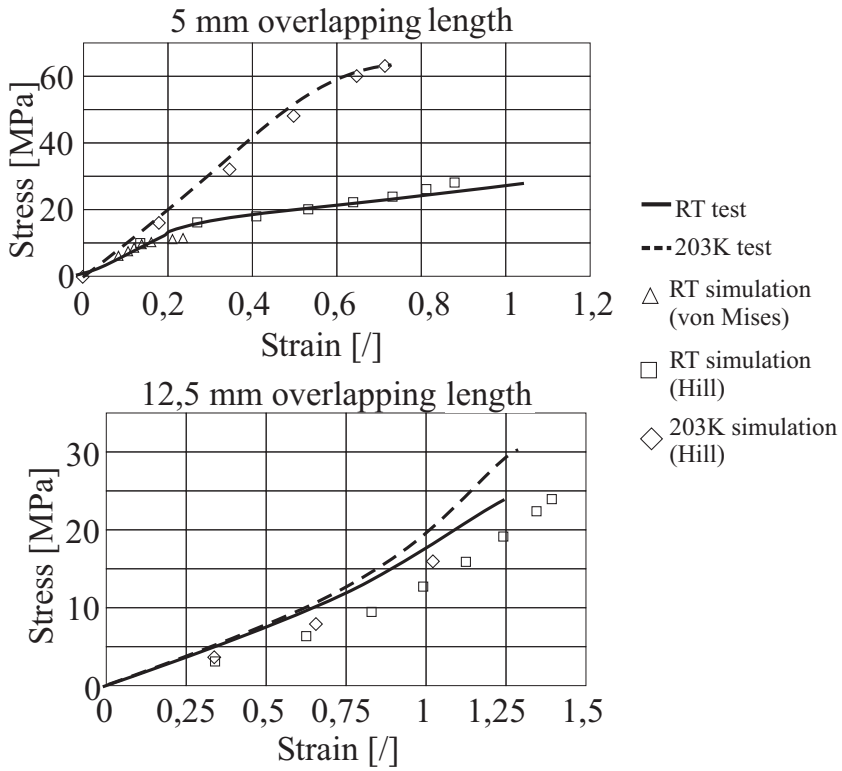


Figure 52: Simulation of the 5 and 12,5 millimeter overlapping length specimens at RT and 203 K temperatures.

figure 52 shows. Simulation of the short overlapped specimen well agrees with the experiment. In case of the 12,5 millimeter the simulated stress strain curve could not reproduce the tests. As already said, the relatively good results achieved by the Hill criterion for the 5 millimeter overlapping lengths appear in this case a contradiction, because a yield criterion developed for non isotropic materials is applied to an isotropic one. The reason for that is probably that the 5 millimeter overlapped specimens, being very stiff and having a short bonding length, develop a high shear on the whole bonding length. This leads to an average stress which is shear dominated and relative constant then peel stresses develop only at the edges. In case of the other bonding lengths, this statement can not be done: shear stress is mainly elastic in the centre of the bonding line and reaches the yield value only at the edges, where peel stress has much bigger amplitudes. The joint gives no decided signs of yielding on a macroscopic scale, but plastification at the edges is driven by the peel stresses. Taken as reference figure 48, the behaviour of

the short and stiff specimen is closer to the pure shear line than that of longer bonding lines and thinner adherends.

## 8.5 Conclusions

The first (trivial) conclusion that can be taken, according to the literature and to this work, is that in no case the behaviour of an epoxy adhesive can be modelled by von Mises yield criterion. As several papers report, plastic materials show a dependence of the deviatoric stress on the hydrostatic stress at yielding. Yielding surfaces capable of describing this behaviour need the determination of the yielding behaviour in case of pure tension, pure compression and, in some cases, also of pure shear, because a number of adjusting parameters must be determined. The experimental work needed to investigate the suitability of other yielding surfaces required an effort which was not justified in this research project. On the side of the simulation, ANSYS did not offer the possibility to model such yielding behaviour. The implementation in ANSYS of a yielding surface available in the literature was also not possible for the same reasons discusses here above. Application of the Drucker - Prager yield criterion did not give good results, because ANSYS does not provides a hardening rule for it, but only the ideal perfectly elastic - perfectly plastic behaviour, which leads to extremely high plastic strains at the bonding edges. The partial success achieved by the Hill yield theory is justified because of the differences in the stress state among short and long overlapping lengths, but not because of its suitability for adhesive materials. A final remark on the behaviour at failure of the adhesive should be made. In all tested configurations, except from the short overlapping lengths, joint failure occurred suddenly without any macroscopic sign of yielding (i.e. reduction in joint shear modulus) as could be expected for a material undergoing marked plastification. This results in the impossibility to foresee joint failure by means of FE simulation, except for the 5 mm OL for which after an initial slope, plastification occurs and the average stress strain curve follows a second (apparent) shear modulus (see figure 52).

# 9 Laminate analysis

## 9.1 Introduction

A numeric laminate analysis, under thermal and mechanical loads has been carried out with the aim to investigate the potential of FRPs in cryogenic containment. The response of several base materials and their combination has been computed and compared to that of metals and to test results on thermo- mechanically shocked specimens. Results from several failure theories are also shown and compared.

## 9.2 Modelling thermomechanical loads

In addition to mechanical loads, i.e. inner pressure and inertial loads, cryogenic structures can be affected by thermal loads, depending on several features, among which, material combination and joint types among several parts of the structure. Material combinations are responsible for thermal loads because of differences in thermal expansion coefficients (CTE).
Among them and as a particular case (as discussed in chapter 5), are orthotropic materials, like fibre reinforced plastics, in which the same thermal loads may occur in laminates, due to the difference in CTE between fibre and normal to fibre directions. More in depth, thermal loads in cryogenic structures have a stationary component and a transient one: a dynamic thermal field, arising during cooling down, generates transient loads in the structures, which may exceed the stationary value, as demonstrated for cross ply laminates in [32]. These transient effects, though not to be neglected, have in FRPs cross ply laminates a main influence on stress in fibre direction, which results in no lost of permeability, until overall failure of the tank structure occurs. Major concerns arise from stresses perpendicular to fibres, but whose maximal value is reached only after transient phenomena has declined (Baier and Haberle, [38]). Based on these considerations and taking into account the primary purpose of assessing the overall suitability of composite materials for cryogenic tank applications, non stationary effects have been neglected and a simple stationary temperature load has been considered. Mechanical

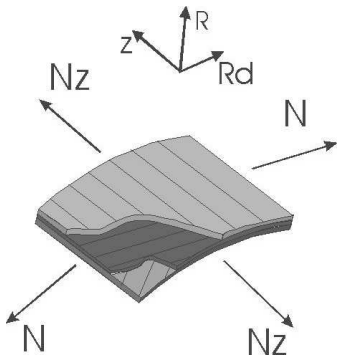


Figure 53: Representation of typical mechanical load (due to inner pressure) in tank structures.

loads modelling may be carried out through geometrical assumptions, which, though not affecting general validity of the results, allow an easy correlation among geometric parameters, cryogenic liquid pressure and resulting loads on the tank structure. Following this approach, two geometries are investigated: cylinder and sphere. For these two configurations mechanical tension due to inner pressure is given by the well known relations:

for a sphere

$$N_Z = N_\phi = \frac{P \cdot R}{2} \tag{24}$$

for a cylinder

$$N_Z = \frac{N_\phi}{2} = \frac{P \cdot R}{2} \tag{25}$$

Where P is the cryogenic fluid pressure and R represents curvature radius of the structure. By means of this assumptions it is possible to identify a merit parameter, i.e. the $P \cdot R$ product, to evaluate and compare the overall performance of several materials / material combinations. If considered as separated load cases, thermal and mechanical loads have completely different effects on optimal laminate layout. For the mechanical load case, fibres shall be in the load directions and thus a cross ply laminate is the best choice. In case of thermal load, orthotropicity of fibre reinforced plastics, produces increasing stresses perpendicular to fibres, as ply angle increases. Thermal stress is computed by means of the CLT, for a symmetric laminate and shown in figure 54, in which it is clearly pointed out that stress perpendicular to fibres ($\sigma_2$) in the cross ply configuration, reaches the UD ply failure value, or in the best case it approaches it, as just thermal load is applied, leaving no room for additional mechanical loads. In addition, shear stress, begins to increase for very low ply angles and, though it does not approach its failure value, it may add its effect to promote inter fibre failure in correspondence to relative low $\sigma_2$ values. Effects due to inertial loads comprise, among others, local stresses at load introduction points and effects related to global geometry, like buckling, both of which can not be

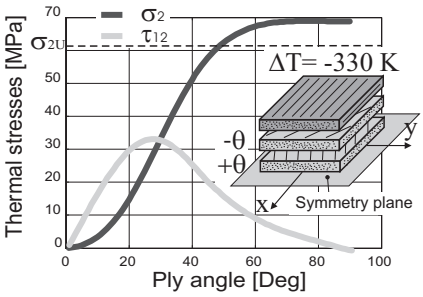


Figure 54: Thermal stresses contributing to IFF in CFRP $[0/ \pm \theta]_S$ laminates, due to thermal loads.

treated without assumptions on the global vehicle architecture and mission profile. Thus they will not be considered in this work.

## 9.3 Load scaling factor

An essential point for the study of tank structures, particularly in consideration of the reduction of development costs, is the identification of scaling factors for the loads affecting the tank. As for the previous paragraph, inertial loads can not be treated separately for tank and rest of the vehicle, and thus no possibility arises to treat the problem from a general point of view. On the contrary, this possibility exists for the case of thermal loads and inner pressure, at least when the analysis is restricted to the two geometries indicated above, as far as wall thickness can be neglected respect to the radius of curvature (thin wall). This is the case of typical laminates for tank structures, where the value of the radius is in the order of 500 millimeter, or more, and laminate thickness range in the order of 5- 10 millimeter or less. In this condition membrane stresses at locations far from the end domes are still given by preceding equations 25. Starting from that, if a radius $R_1$, and pressure $P_1$ produce a state of stress $N_Z$ and $N_\Phi$ in the vessel, the same stress is produced by a radius $R_2$, smaller than $R_1$ and pressure:

$$P_2 = P_1 \cdot \frac{R_1}{R_2} \tag{26}$$

Based on these considerations, a small cylindrical or spherical structure of radius R2 can be tested to gain information on the behaviour in the full scale structure.

## 9.4 Numerical Design of laminates for cryogenic tanks

The numerical analysis has been conducted taking as geometry an infinite cylinder, for which the circumferential load, $N_\Phi$, amounts to two times the axial load. Thus a symmetrical laminate, having four layers in axial and eight in circumferential direction has been chosen, as starting configuration. Layer angles have been parameterized, but the overall symmetry and balanced lay-up of the laminate has been kept during the simulation in order to avoid tension - bending coupling effects, which is a usual goal in real laminates. Aim of the simulation is to find the combination of laminate angles which provides the highest load capability for each of the considered materials. A further comparison to metallic materials has also been performed to investigate if FRPs may offer real weight saving in cryogenic tank structures. Constraining effects have been taken into account inasmuch, even if

they may occur only for inner plies, a full leak path forms only when all plies in the laminate have developed cracks. The dependence of plies real IFF from the stiffness of the rest of the laminate, and thus from the orientation of surrounding plies, has also been neglected. Thus a ply strain allowable amounting to $\epsilon_2 = 1.4\%$ and a laminate strain allowable amounting to 0.4% have been considered, according to the one which occurs for first. This further assumption means that achieved results represent an upper boundary for the load carrying capability of the laminate, which can be approached only if the majority of its plies fail as the constrained failure strain has been reached and not for lower values. In the real laminate, outer plies will develop micro cracks already at lower strains, thus the influence of these cracks on laminate fatigue life should be investigated.
A lower value of the load capability has been calculated by using UD failure figures, that is, neglecting all constraining effects. As results a range of loads is produced in which the real capability of the laminate must lie. Together with the mechanical load a thermal load has been applied, consisting of the difference between $LH_2$ and curing temperatures, so it varies according to the resin system. This approach represents the inverse of the laminate design problem and had to be adopted in order to minimise the number of parameters in the simulation, which could not be managed manually. An automatic approach has been attempted, by exploiting genetic optimization methods, but did not conduct to useful results. Reason for that has to be attributed to the particular effects of the load case on laminate stress distribution: because applied load is a tension and laminate is symmetric, ply stacking sequence has only a secondary effect on ply stresses, so that the genetic algorithm could not retrieve useful improvements in laminate performances after several generations. Results of the analysis are normalized respect to the product between laminate thickness and material density. This results in a figure, the specific load capability (SLC), giving the amount of pressure load, P, in a given tank radius, R, that can be carried by a unitary weight of material:

$$SLC = \frac{P \cdot R}{\rho \cdot t} \tag{27}$$

In fact weight of a laminate is proportional to the volume and density. Thus, if laminate surface is taken unitary, weight will depend only on density and thickness. A first analysis has been done by considering only FRPs in order to rank the several non metallic materials available on the market. The material giving the best performances has been used as term of comparison to conventional metallic materials, like 2219-T87 alloy, and new generation ones, like the 2195-T6 aluminium lithium alloy.

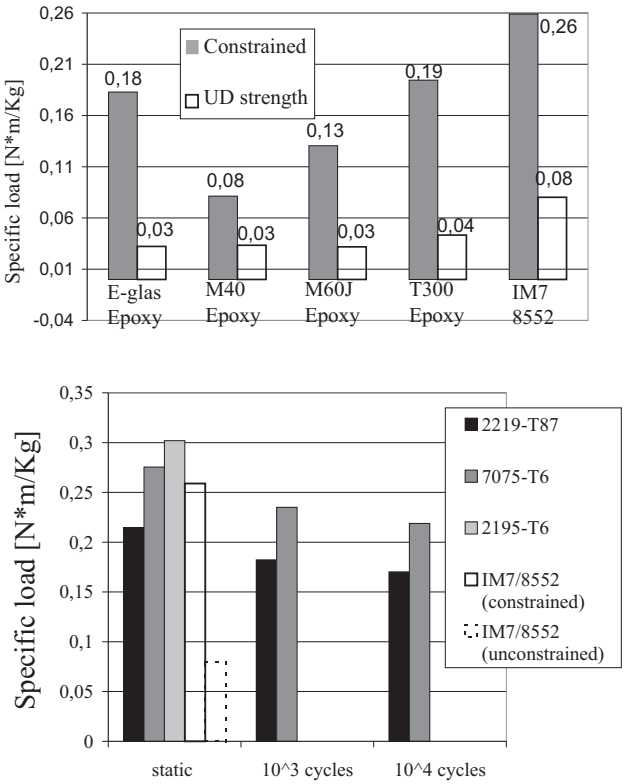


Figure 55: Results of the thermomechanical analysis. Specific load is shown for several FRP materials (left). Right, comparison among $IM7/8552$ and metallic materials Show the preponderant effect of thermal load on FRPs.

Figure 55 shows numerical results. The specific load capability of reinforced plastics is strongly conditioned by the chosen strength: simulation using constrained data results in load carrying capability which is more than two times that of unconstrained plies for all considered materials. The reason for this difference is that thermal loads alone produce ply stresses which approach UD strengths in angle ply laminates, as shown in figure 53. Thus constrained strength, if fully taking place, provides a remarkable additional capability. On the plane of single materials, behaviours of HM carbon fibres is worse than that of HT and IM ones, because the combination of the high module and high (negative) CTE leads to higher thermal loads than for the other ones. Even glass fibres show in this respect a better behaviour than HM carbon fibres, but for the opposite reason that they have very low stiffness and high CTE in fibre direction which minimizes mismatch

with the direction perpendicular to fibres. Noteworthy is that stress for all plies in the analysed laminate is characterized by a $\sigma_2$ component which approaches the failure value, that is at maximum load all ply develop inter fibre microcracks, thus a leakage path through the thickness. Analysis on 8-ply $[\beta/-\beta/\theta/-\theta]_s$ laminate resulted in similar specific load capability that by the 12- ply laminate (0.26 and 0.08 for the $IM7/8552$ with constrained and UD strength respectively).

### 9.4.1 Discrete gradient materials

The term "gradient material" identifies a material in which one or several properties change along one or more spacial directions, like for example the thickness. A change in mechanical properties can be achieved in FRPs when for example fibre percentage changes along the thickness.

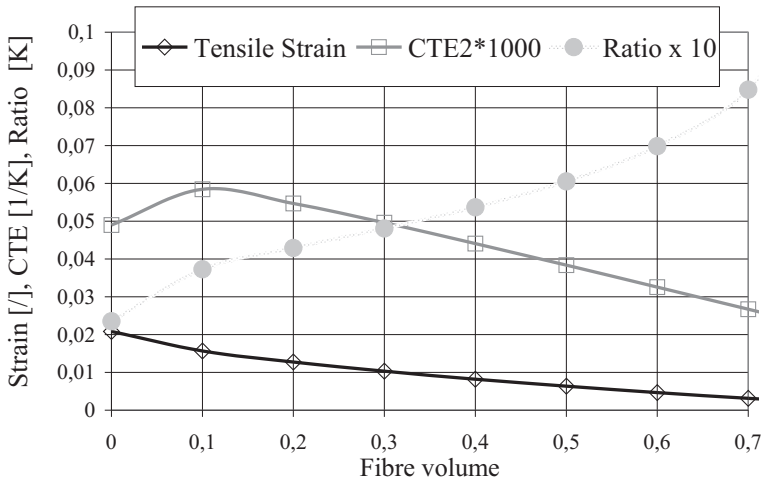


Figure 56: Dependence of tensile strain and CTE both perpendicular to fibre on fibre percentage. Their ratio $\frac{CTE}{eps_T}$ is also shown

Another way is that of laminating plies composed of different fibres or even when a homogeneous material is laminated together with FRPs. According to this definition even usual CFRP laminates, when composed of plies laminated with different angles, can be considered discrete gradient materials.
Application of gradient materials in order to increase composite tank load capability has been considered here. Purpose of the investigation, carried out in the form of a numeric optimization, was to design a laminate lay up composed of some load bearing layers, in which micro cracks are tolerated,

and of some other layers, free from micro cracks, which provide a gas barrier. These barrier layers should be less stiff than the those carrying the load, but have a higher failure strain in order to follow laminate deformations imposed by the external load.
Determination of ply properties for fibre percentage different from the usual values available on the market has been carried out by semi-empirical relations taken from Herrmann (reference [53]). According to these relations, CTE in direction perpendicular to fibre depends on fibre percentage as shown in figure 56. In case of failure stresses, no semi- empirical relations were available thus the values for intermediate fibre volumes were gained by linear interpolation starting from those for pure matrix and those for usual fibre volumes (typical $V_f$=60%). Thus Failure stress in and perpendicular to fibres for $Vf = 30\%$ results from the following:

$$\sigma_{30\%} = \sigma_M + \frac{\sigma_{60\%} - \sigma_M}{0.6} \cdot 0.3 \tag{28}$$

Where $\sigma_M$ is the property for the pure matrix and $\sigma_{60\%}$ that corresponding to 60% fibre percentage.
As fibre percentage is reduced, UD failure strain and CTE perpendicular to fibre direction increase, but as their ratio show, CTE undergoes smaller relative increments than failure strain. This characteristic could help the layer with small fibre percentage to resist the high thermal and mechanical strains without that inter fibre cracks develop.
The failure criterion previously used for normal CFRPs has not been applied in this case because cracks were tolerated in the laminate, but the barrier layers. Thus Puck criterion and UD allowables were applied to determine failure of gas barrier plies.
The inverse of Specific Load Capability, as defined in equation 27, has been chosen as object function, while design variables were material type, fibre percentage and ply angle, while number of plies was fixed and equal to 10. Thickness was given as parameter: for usual fibre percentage the ply thickness of the prepregs available on the market was chosen, while for lower fibre percentages the fixed value 0.1 millimeters was chosen. The optimization has been carried out by the GAME algorithm developed at the Chair for Lightweight Structures. Initial population amounting to 500 individuals and 100 generations were calculated. Figure 57 shows the change in objective function within the optimization. The final laminate is shown in table 22. This final laminate achieves a SLC equal to 0,476, much higher than that achieved by $IM7/8552$ or aluminium. Nevertheless the laminate not symmetric, thus subject to several drawbacks. A second optimization has been carried out with a 10 layer laminate, in which layup have been kept symmet-

ric except for the two central plies (ply 5 and 6). In this case the final SLC was 0,28, value under that achieved with aluminium 2195.

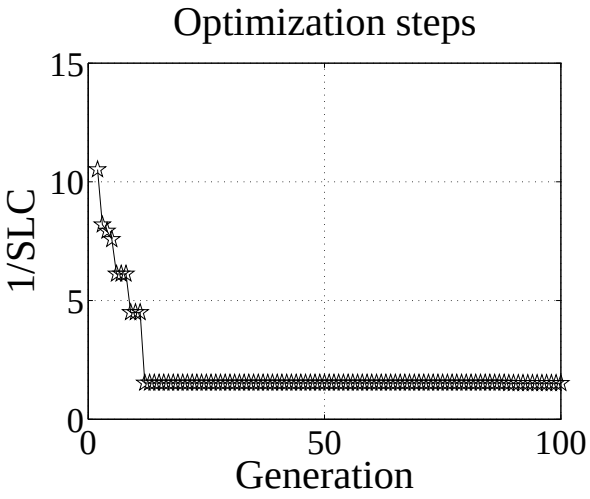


Figure 57: Object function change in dependence of the generation number. Very steep changes are initially achieved, but than the load carrying capability does not significantly change.

If these values are compared to the 0.26 achieved by standard $IM7/8552$, they are very competitive. Nevertheless two issues must be briefly discussed. First, the calculation does not make use of any degradation model to compute load redistribution as one ply fails in direction perpendicular to fibres. Second, if cracks are tolerated and impermeability is achieved by means of a liner, than the standard $IM7/8552$ has far higher capabilities than those shown in figure 55. In fact a 13 layers symmetric cross ply laminate with a strain allowable of 0.8% (which an in- laminated aluminium sheet would stand at cryogenic temperature without fail, as seen in chapter 5) would reach an SLC of 0,585. At a laminate strain equal to 0.8% fibres are less stressed than in case of the laminate resulting from the optimization, in which the Puck index for fibre failure of 4 plies is around 1 (see table 22). Again the point to be clarified is actually the effect of micro cracks when repeated load cycles are considered.

| Ply Number | Material | Vf [%] | Angle [deg] | Thickness [mm] | Puck index | |
|---|---|---|---|---|---|---|
| | | | | | (fibre) | (Matrix) |
| 1 | T300/Epoxy | 60 | 90 | 0,23 | 0,91 | 1,00 |
| 2 | T300/Epoxy | 27 | -26 | 0,1 | 0,23 | 2,46 |
| 3 | M40/Epoxy | 60 | -16 | 0,203 | 0,99 | 4,27 |
| 4 | M40/Epoxy | 60 | 26 | 0,203 | 1,02 | 4,72 |
| 5 | IM7/8552 | 60 | 90 | 0,125 | 0,26 | 6,91 |
| 6 | T300/Epoxy | 60 | -46 | 0,23 | 0,56 | 3,37 |
| 7 | T300/Epoxy | 60 | 79 | 0,23 | 0,93 | 3,45 |
| 8 | Glass/Epoxy | 25 | 90 | 0,1 | 0,37 | 5,58 |
| 9 | Glass/Epoxy | 34 | -84 | 0,1 | 0,3 | 7,14 |
| 10 | T300/Epoxy | 60 | -79 | 0,23 | 0,56 | 4,92 |

Table 22: 10 layer laminate resulting from the optimization

## 9.5 Conclusions

An attempt to foresee the load capability of FRPs in unlinered tanks has been done by applying analytic means. As first step, the available failure criteria have been tested in order to understand if and which one is able to make predictions close to the reality. For that purpose tensile specimens have been manufactured and tested under room and cryogenic conditions and laminate failure strains have been calculated by the several known failure criteria. A comparison has shown marked divergence among prediction and reality when quadratic and some physical criteria are applied. When thermal loads are included in the simulation Tsai-Hill, Tsai-Wu and Puck criteria underestimate the real failure load in such a manner that their predictions may be too conservative for design purposes.
The following step has been to choose a suitable failure criterium which could provide credible predictions for the laminate design. As possible solution a mixed criterium consisting of two failure conditions has been adopted. The first one being maximum laminate strain and the second one maximum layer strain perpendicular to fibres. The values 0.4% and 1.4% respectively have been taken as allowables for the two strains. Laminates have been considered to fail when one of the two conditions is verified, that is laminate and/or ply strain exceeds the allowable. The practice of taking laminate strain allowables is common in the design of composite structures, while a second condition on ply failure strain is needed because of the very high thermal strains at ply level due to the thermal load. This ply failure strain represents

a realistic crack onset value even when constraining effect are considered, while it is an overestimation of the crack onset strain for facesheet plies, in which no constraining effect takes place.
Based on these considerations the laminate specific load for several CFRP materials has been calculated and compared to that of conventional and new aluminium alloys. When repeated load cycles are not considered, the specific load capability of metallic alloys is superior to that of CFRPs (although the influences of different joining and technological characteristics could not be included in the evaluation). This comparison showed that metallic alloys possess higher potential in cryogenic lightweight structures, when yield stresses are used as allowables. In case the effect of repeated load cycles is considered, the progressive reduction of stress allowable of metallic alloys can be estimated by means of simple Whöler curves. In case of CFRPs the effect of micro cracks and their propagation can not be estimated with analytical methods if adequate experimental results are not available. These cracks form in the facesheet plies of composite laminates when they are loaded with mechanical strains reaching 0.4% at cryogenic temperatures (as seen in chapter 6). If micro cracks can be tolerated, at least for limited numbers of load cycles, than the lightweight potential of CFRPs is far superior to those aluminium alloys provide. This could be the case of expendable, or even reusable launchers, which in any case would experience a relative low number of missions. In any case a gas barrier is needed to prevent gas from penetrating the tank wall through the cracks and thus escape as in the case of the X-33 hydrogen tank. In that respect the analysis carried out on gradient materials did not show competitive potential in comparison to a metallic barrier in the form of an aluminium sheet. Two reasons can be used to argument this statement:

- In order to avoid crack occurrence at least in one ply, the laminate must be stressed for lower mechanical strains than in case an aluminium layer is foreseen
- A metallic liner provides a higher impermeability than a CFRP ply having small fibre percentage. This is particularly true at room temperature

# 10 Summary and outlook

Some aspects of composite materials application to cryogenic tanks have been investigated in this work, both from a numerical and experimental point of view, including CFRPs suitability to cryogenic environment, manufacturing and joining techniques. From the point of view of the material the main question, which this work answers, arises from inter fibre (IF) cracks, also known as microcracks, that may form within the laminate due to the significant thermal load under which the composite is subjected. These cracks, spreading within a ply in fibre direction, do not significantly alter composite characteristics and strength, which are dominated by fibres. Nevertheless they may build leak paths which definitely degrade tank impermeability.
The task of predicting crack onset by means of numerical analysis has been discussed in chapter 8. Major inaccuracies arise when UD ply failure criteria together with the Classical Lamination Theory are used. Prediction based on classic, quadratic and physical based failure criteria are too conservative even at room temperature. At cryogenic temperatures thermal load suffices to produce cracks, according to failure criteria, while in the reality a significant mechanical load is needed. Criteria based on fracture mechanics can predict layer failure with more accuracy but their application is limited to a small class of laminates and one dimensional load cases. Thus a laminate max strain failure criterion revealed the most appropriate choice for failure predictions. Based on this criterion an estimation of laminate load capability and a comparison with lightweight alloys showed equivalent potential between the latter and CFRPs. A greater lightweight potential can be achieved by today's CFRPs only if inter fibre cracks are tolerated in the tank wall. This can be done only if further gas barriers are used to avoid leakage through the laminate. In that respect, the most appropriate choice seems to be a thin aluminium sheet, because it can work in the plastic region an thus follow the deformation imposed by CFRPs without giving origin to high stresses. At the same time it offers high hydrogen impermeability both at room and cryogenic temperatures.
Experimental activity focused on measurement of crack onset strains in tensile specimens and measurement of CFRPs gas permeability, both at cryogenic temperatures. A test setup for cryogenic permeability testing ("tank simulator") has been developed at LLB with the purpose of investigate occurrence and effects of micro cracks on tank-wall-shaped specimens. Bulged specimens are loaded by a gas pressure so that a two dimensional tensile strain originates and opens micro cracks if they form. Test results on $IM7/8552$ specimens (chapter 7) showed no micro crack occurrence for two dimensional mechanical strains averaging 0.22% - 0.235% (corresponding to a 11 bar gas

pressure) at cryogenic temperatures. During the test campaign specimens were cryo- cycled (100 times) and even long duration tests were carried out, but no changes in leakage signal were measured. These results are opposite to those achieved by Yokozeki, Aoki and Ishikawa ([21]) and NASA X-33 hydrogen tank testing ([4]). They confirm that CFRPs, if the right fibre/matrix combination chosen, can withstand a significative mechanical strain at cryogenic temperatures without occurrence of micro cracks, but are far from assessing CFRPs superiority to metallic alloys for cryogenic fluid containment. For that purpose more thorough investigations are needed, which should include:

1. Mechanical strains up to 0.6%
2. A higher number of thermomechanical cycles (in the order of 4000)
3. The sensitivity of the test setup should be increased, in order to Measure cryogenic and room intrinsic material adsorption and diffusion properties
4. Use of other leakage gases in order to investigate the effect of chemical reactions with CFRPs.

Goals 1 to 3 may be achieved by a major redesign of the test setup, relying upon the experience currently gained. Increase of specimen radius and a refined design of the metallic sealing could significantly increase sensitivity and allow higher mechanical strains.
From the point of view of joining techniques, bonding is the one which provides impermeability characteristics necessary to cryogenic tanks. Experimental investigation on the effect of cryogenic environment on bonding strength showed a considerable influence of thermal load on joint strength. After an initial increase at temperatures slight under $0^oC$, due to increase in adhesive intrinsic strength, bonded joint strength significantly decreases at very low temperatures and becomes more sensitive to peel stresses. These act together with thermal stresses and cause adhesion failure at the interface between adhesive and assembly part.
Numerical analysis of bonding strength and stiffness was attempted in ANSYS, with little success. Highly non linear short overlapped joints can not be successfully simulated by usual material laws. Specimens with longer overlapping length fail without reduction in the slope of the average stress - strain curve, as could be expected if a big portion of the adhesive would yield. Thus an FE analysis can not help predict their strength.

# References

[1] T. Shimoda, T. Morino and Y. Morino
NASDA, Ibaraki, Japan
T. Ishikawa
NAL, Tokyo, Japan
S. Cantoni, G. Di Vita and G. Totaro
CIRA, Caserta, Italy
"Study of CFRP Application to the Cryogenic Propellant Tank of Reusable Launch Vehicle"
AIAA 2001-1598

[2] A.W. Murphy, R. E. Lake and C. Wilkerson
"Unlined Reusable Filament Wound Composite Cryogenic Tank Testing"
NASA/TM-1999-209039

[3] Tom Kooij, Oscar van der Jagt and Adrian Beukers
"A Full Composite LOX Fuel Tank for a Hybrid Rocket"
Proceedings of the European Conference on Space Structures, Materials and Mechanical Testing
Noordwijk, The Netherlands
Nov. Dec. 2000

[4] "Final Report of the X-33 Liquid Hydrogen Tank Test Investigation Team"
Marshall space Flight Center
May 2000

[5] G. Vendroux, M. Auberon, J. Dessaut
"Cryogenic Composite Tanks: Structural Analysis and Manufacturing Concepts"
42nd International SAMPE Symposium
May 1997

[6] T. W. Reynolds
"Aircraft-fuel-Tank Design for Liquid Hydrogen"

NACA RM E55F22

[7] M. Desloire
"Le Lanceur ARIANNE choix des matriaux et problmes associs"
CNES
October 1979

[8] D. Lestrat, Y. Prel
"Evolution et Choix Technologique pour les Rservoirs des Lanceurs ARIANE "
Centre National D' tudes Spatiales
Proceeding of the Int. Symp. On Advanced Materials for Lightweight Structures
March 1994

[9] "LH2 Fuel Tank Design for SSTO Vehicle"
Vanderbilt University
N95-26309

[10] A. Denaro, D. Dosio, J. Antonenko
"Design and Technology development of a reusable Cryogenic Tank"
Conference on Spacecraft structures, Materials and Mechanical Testing
Noordwijk, The Netherlands
1996

[11] B.W. Grimsley, R. J. Cano and N. J. Johnston
NASA Langley research Center, Hampton, VA
A. C. Loos
Virginia Polytechnic Institute and State University, Blacksburg, VA
W. M. McMahon
NASA Marshall space Flight Center, Huntsville, Alabama
"Hybrid Composites for LH2 Fuel Tank Structure"
SAMPE Technical Conference, Seattle, Washington
November 4-8, 2001

[12] M. Bittner, D. Bittner
"Entwicklung und Fertigung von Barriereschichten auf CFK fr den

Einsatz in Kryotanks"
Frderkennzeichen: 13N6317/7
1996

[13] H. M. Herring
"Characterisation of Thin Film Polymers Through Dynamic Mechanical Analysis Permeation"
NASA/CR-2003-212422

[14] T. Aoki, H. Kumazawa, I. Susuki, T. Ishikawa
"Modeling of Propellant Leakage through Laminated structures"
AIAA 2001-1217

[15] H. Estrada, S. Smeltzer
"Design and development of a Composite Dome for Experimental characterisation of Material Permeability"
1999 ASME Pressure Vessel and Piping Conference

[16] D. Evans and J. T. Morgan
"The Permeability of Composite Materials to Hydrogen and Helium Gas"
Advances in Cryogenic Engineering N. 34

[17] T. Okada, S. Nishijma, K. Fujioka, Y. Kuraoka
"Gas Permeation and Performance of an FRP Cryostat"
Advances in Cryogenic Engineering N. 34

[18] J. Humpenöder
"Gaspermeation von Faserverbunden mit Polymermatrices"
Forschungszentrum Karlsruhe
ISSN 0947-8620

[19] H. K: Rivers, J. G. Sikora, S. N. Sankaran
"Detection of Micro- Leaks through Complex Geometries under Mechanical Load and at Cryogenic Temperature"

AIAA 2001-1218

[20] Klaus Kutze
"Dichtheitsprfungen und Lecksuche mit dem Helium- Leckdetektor"
ISBN 3-8169-0822-5

[21] T. Yokozeki, T. Aoki, T. Ishikawa
"Experimental cryogenic Gas Leakage Through Damaged Composite Laminates for Propellant Tank Application"
Journal of Spacecraft and rockets
Vol. 42, 2005

[22] H. Eggers, W. Hartung and S. Knaak
"Damage in carbon fibre reinforced epoxy after thermal cycling and T-fatigue loading"
Cryogenics, Vol. 31, 1991

[23] K. Pannkoke, H. J. Wagner
"Fatigue properties of unidirectional carbon fibre composites at cryogenic temperatures"
Cryogenics, Vol. 31, 1991

[24] S. Kessler, T. Matuszeski, H. McManus
"Cryocycling and Mechanical Testing of CFRP for X-33 Liquid H2 Fuel Tank Structure"
NASA/TM-1999-209560

[25] B. Z. Jang, Y. S. Chang, L. R. Hwang
"Cryogenic Failure Mechanism of Fiber- Epoxy Composites for Energy Applications"
Polymer Composites, Vol. 8 No3, 1987

[26] Klaus Ahlborn
"Das Ermdungsverhalten von Kohlefaserkunststoff- Verbunden und Harzmatrix bei tiefen Temperaturen"
Vortrag auf der 16 Jahrestagung der GUS

Mrz 1987

[27] G. Hartwig
"Polymer Properties at Room and Cryogenic Temperatures"
ISBN 0-306-44987-0

[28] "Cryogenic Material Data Handbook"
US Department of Commerce
ML-TDR-64-280

[29] L. Boniface, P. A. Smith, M.G. Bader
"Transverse Ply cracking in Cross-Ply CFRP Laminates- Initiation or Propagation Controlled?"
Journal of Composite Materials, Vol. 31, No. 11
1997

[30] j. G. Weisend II
"Handbook of Cryogenic engineering"
ISBN 1-56032-332-9

[31] G. Childs
"Thermal Conductivity of Solids at room temperature and Below"
US Department of Commerce
1973

[32] T. Haberle
"Thermodynamik werkstoffhybrider, faserverstrkter Schichtverbunde und Bauteile bei Tieftemperatur"
PH. D. Thesis
TU- Mnchen
2001

[33] T. Aoki, T. Ishikawa, H. Kumazawa, Y. Morino
"Mechanical Behaviour of CF/Polymer Composite Laminates under cryogenic Environment"

[34] R. Hübner
"Zug- und Schereigenschaften von Kreuzverbunden aus Kohlenstoffaferverstrkten Polymeren bei tiefen Temperaturen"
Forschungszentrum Karlsruhe
FZKA 5694
1996

[35] T. L. Brown
"The effect of Long-Term Thermal Cycling on the Microcracking Behaviour and Dimensional Stability of Composite Materials"
Virginia Polytechnic Institute and State University
1997

[36] Alexander Popp
"Auslegung einer CFK-Tankwand unter Bercksichtigung der Brucheigenschaften von Laminaten bei Raum- und Tieftemperatur"
TUM-MW65/0522-SA
2005

[37] H. Y. Yeh, L. Kilfoy
"A Simple Comparison of Macroscopic Failure Criteria for Advanced Fiber Reinforced Composites"
Journal of Reinforced Plastics and Composites, Vol. 17, No 5/1998

[38] T. Haberle, H. Baier
"Rechnerische und Experimentelle Untersuchung zur Auslegung Werkstoffhybrider Faserverbundbauteile bei Kryogenen Temperaturen"
DGLR-JT99-014

[39] R. Jones
"Mechanics of composites Structures"
ISBN 0-07-032790-4

[40] K. Reifsnider
"Fatigue of Composite Materials"

ISBN 0-444-70507-4

[41] Ramesh Talreja
"Fatigue of Composite Materials"
ISBN No. 87762-516-6

[42] H. Baier
"Faserverbundwerkstoffe Skript zur Vorlesung"
Technische Universitt Mnchen

[43] A. Puck
"Festigkeitsanalyse von Faser- Matrix Laminaten, Modelle fr die Praxis"
Carl Hanser Verlag
1996
ISBN: 3-446-18194-6

[44] P. M. Manne, T. K. Henriksen
"Composites Failure Criteria for Industrial Applications"
Proceedings of the European Conference on Spacecraft Structures, Materials and Mechanical Testing
1998

[45] H. Schrmann
"Konstruiren mit Faserverbundwerkstoffe"
Springer Verlag Berlin Heidelberg New York
ISBN: 3-540-40283-7

[46] A. Puck and H. Schrmann
"Failure analysis of FRP laminates by means of physically based phenomenological models"
Science Composites and Technology
Vol. 58, Issue 7, July 1998

[47] A. Puck, J. Kopp, M. Knops
"Guidelines for the determination of the parameters in Puck's action plane strength criterion"

Composites Science and Technology
Vol. 62, Issue 3, February- March 2001

[48] Wilhelm Flgge
"Statik und Dynamik der Schalen"
Springer-Verlag Berlin Heidelberg New York
1981
ISBN: 3-540-02815-3

[49] G. A. Schoeppner, R. Kim, S. L. Donaldson
"Steady State Cracking of PMCS at Cryogenic Temperatures"
AIAA- 2001- 1216

[50] A. Parvizi, K. W. Garrett, J. E. Bailey
"Constrained cracking in glass fibre- reinforced epoxy cross ply laminates"
Journal of Materials Sciences, N. 13, 1978

[51] S. G. Lim, C. S. Hong
"Prediction of Transverse Cracking and Stiffness Reduction in Cross-Ply Laminated Composites"
Journal of Composite Materials, Vol.23, July 1989

[52] J. G. Gosse, S. Christensen
"Strain Invariant Failure Criteria for Polymers in Composite Materials"
AIAA2001-1184

[53] A.S. Herrmann
"Mechanik der Faserverbundwerkstoffe I und II"
DLR Braunschweig
1999

[54] R. D. McCarty
"Hydrogen Properties"
CRC Press

[55] B. I. Verkin
"Handbook of Properties of condensed Phases of Hydrogen and Oxygen"
ISBN 0-89116-714-5

[56] R. D. McCarty
"Thermophysical Properties of Helium-4 from 2 to 1500 K with Pressures to 1000 Atmospheres"
National Bureau of Standards
US Department of Commerce
1972

[57] W. Peschka
"Liquid Hydrogen Fuel of the Future"
ISBN 3-211-81795-6

[58] J. Ziemann, N. Rostek
"Key elements of a Hydrogen Aircraft Fuel System and Powerplant"
Paper No. 4 - 8
12th World Hydrogen Energy Conference, Buenos Aires, Argentina
1998

[59] G. D. Brewer
"Hydrogen Aircraft Technology"
CRC Press

[60] H. Pfeffer
"Towards reusable Launchers - A widening Perspective"
Internet document (http://esapub.esrin.esa.it/bulletin/bullet87/pfeffe87.htm)
17.12.2004

[61] R. Hill
"The mathematical theory of plasticity"
The Oxford Engineering science Series
1956
ISBN 0 19 856162 8

[62] A. A. Becker
"Understanding Non- Linear Finite Element analysis"
ISBN 1 874376 35 2

[63] R. D. Adams, J. Coppendale, V. Mallick, H. Al-Hamdan
"The effect of temperature on the strength of adhesive joints"
Int. Journal Adhesion and Adhesives
Vol. 12, 1992

[64] J. Bornemann
"Kennwertermittlung und mechanische Modellbildung zur Berechnung geklebter Verbindungen"
20th CAD-FEM User Meeting
2002

[65] "Standard Test Method for Apparent Shear Strength of Single-Lap-Joint Adhesively Boned Metal specimens by Tension Loading (Metal-to-Metal)"
ASTM D 1002-01

[66] M. Fischer, R. Schmidt
"Die Eigenschaften des Klebstoffs und die Festigkeit der Verklebung"
Adhsion 1979, Heft 12

[67] K. Matsui
"Effects of curing conditions and test temperatures on the strength of adhesive-bonded joints"
Int. J. Adhesion and Adhesives, Vol. 10 No. 4, October 1990

[68] Loctite Corporation
"Hysol EA9361 Data Sheet"
Online document

[69] Gerd Habenicht
"Kleben"
Springer Verlag, Berlin, Heidelberg, New York Tokyo

ISBN: 3-540-15893-6
1986

[70] [70] Helmut Wehlan
"Untersuchung neuer Klebstoffe zur anwendung im Flugzeuginnenbereich"
TUM Diplomarbeit
2004

[71] R. Ragawa, R. M. Caddell, G. S. Y. Yeh
"The macroscopic yield behaviour of polymers"
Journal of Materials and Science, 8, 1973

[72] R. M. Christensen
"Yield function / failure criteria for isotropic materials"
Proc. Roy. Society of London, N.453, 1473-1491
1997